MINISTÈRE DE L'ENSEIGNEMENT SUPÉRIEUR ET DE LA RECHERCHE SCIENTIFIQUE

Université des Frères Mentouri (Constantine 1)

Faculty of Exact Science

Department of Chemistry

N° d'ordre: 43/D3c/2018

Série: 09/CH/2018

A thesis submitted in conformity with the requirements for the degree of

« Degree *Doctor LMD*» In inorganic chemistry

« Study of the properties of heterostructures based on semiconductor metal oxides obtained by electrochemical deposition »

By

Halla Lahmar

Defended in January before the examination board:

H. Merazig	Pr. U. Constantine-1	Président
F. Setifi	Pr. U. Sétif -1	Rapporteur
A. Azizi	Pr. U. Sétif -1	Co-Rapporteur
A. Beghidja	Pr. U. Constantine-1	Examinateur
B. Boudine	Pr. U. Constantine-1	Examinateur
H.M. Benia	Dir.Rech. URNN Sétif	Examinateur

Soutenue le : 10/05/2018

DEDICATION

*This thesis is dedicated to my **beloved family** and to **Rohingya***

***Muslims** who are facing outright genocide in **Burma**.*

Acknowledgements

All the praises and thanks be to Allah, the most beneficent and merciful, for giving me this opportunity to increase my knowledge, the strength, and the patience to complete my thesis after all the challenges and difficulties.

The works in this thesis have been carried out at the Laboratory of Chemistry, Molecular Engineering and Nanostructures (LCMEN), University Ferhat Abbas-Setif 1. I would like to thank the laboratory director my co-supervisor, **Pr. Amor Azizi**, for his patience, support and for sharing me his time and guiding me through every step of my work. His confidence in my work inspired me.

I am extremely thankful to my supervisor **Pr. Fatima Setifi** for her support and for accepting my request to work in LCMEN laboratory.

Sincere thanks to **Dr. Hocine Merazig**, **Dr. Adel Beghidja**, **Dr. Boubekeur Boudine** and **Rech. Dir. Hadj Mohamed Benia** for agreeing to be the examiners for my thesis presentation.

Special thanks to the LCMEN members **Dr. Khaladi Mohamed Ridha** and **Dr. Measoudi Yazid** for their operation of the MFP-3D Asylum Research AFM, this made it possible to achieve more detailed pictures, increasing the knowledge of the samples. I also like to thank **Dr. Djamel Hamza** who is always ready to help whenever I have technical difficulties.

Special thanks to **Dr. Mohamad Salah Aida** and his Ph.D. student **Ms. Fatima Zohra Boutebakh** from the Laboratory of thin films and Interfaces, University Freres Mentouri-Constantine1, for their technical assistance in the DC reactive sputtering of the top electrode and the electrical measurements. Without this setup, it wouldn't have been possible to get the conclusions about the photocurrent in this thesis.

I would give my special thanks to **Ing. Guy Schmerber** and **Dr. Aziz Dinia** from the Institute of Physics and Chemistry of Materials of Strasbourg (IPCMS), University of Strasbourg for their technical assistance with many measurements in the first part of this study. Without their help, the amount of research would have been significantly less.

I would like to give my special thanks to **Pr. Thomas Hanapel** for accepting me as visitor student in the Photovoltaic department in Ilmenau University, Germany. Special thanks to his team members for their technical assistance with many measurements.

I am deeply thankful to **Dr. Kamel Lahmar** University Ferhat Abbas-Setif 2, I benefited from his kind guidance to improve my English language, his linguistic critical help in improving the quality of my manuscript writing.

I am thankful to my colleagues in LCMEN laboratory **Mr. Abdelmadjid Herbadji**, **Mr. Ibrahim Yaacoub Bouderbala** for their help and encouragement during my studies.

I owe my warmest thanks to my friends and colleagues, **Meriam Aloui**, **Rayhana Bengas**, **Khadidja Daideche** for encouraging me in pursuing my dream helping me and creating such a pleasant accompany during my studies. Which made it possible for me to spend a precious time in LCIMN laboratory.

Words won't be enough to thank my beloved PARENTS for their endless love, effort, and prayers, thanks to my dearest Mum **Nadia Ghozlane** who sacrificed her careers to paved the way for me and my brothers and sisters to outshine in life with proud and zeal. Thanks to my dad **Kamel Lahmar** who has been a source of inspiration to me, his encouragement have given me strength and helped me to improve myself.

I also like to convey many thanks to my entire family including, my dear aunt like friend **Nassira Ghozlane** for her never-ending love, support and for her refreshing accompany during my stay in Germany. Thanks to our family friend **Regine Petit** for her sincerity, love, and help in my hard days in Germany. My endless gratitude goes to my beloved sisters and brothers **Mohamed, Loubaba**, **Omama**, **Thouaiba**, and **Ouais** for cheering me all my life and especially during my hard times as a Ph.D. student. Your moral support, good wishes and nice accompany will remind me of these unforgettable days.

Certainly, the completion of this thesis could not be achieved without the help and encouragement of many other peoples to whom I am very grateful for.

I hope this Ph.D. thesis will not be the end of my journey in seeking for more knowledge.

TABLE OF CONTENTS

LIST OF ILLUSTRATIONS

LIST OF TABLES

Preface

Since the solar energy is unlimited and environmentally friendly, direct conversion of solar energy into electric energy using photovoltaic devices is considered as an ideal solution to the growing demand for energy supply. Thin film solar cells based on metal oxide semiconductors are promising for renewable energy, owing to their non-toxicity and abundance. So far, zinc oxide (ZnO) and cuprous oxide (Cu_2O) are considered as very interesting candidates in this respect, as they are inexpensive, abundant and have good optoelectronic properties. Since the ZnO is usually an intrinsic n-type semiconductor with a wide band gap energy (3.4 eV), it can be used as the transparent conducting window layer in solar cells. On the other hand, the synthesized Cu_2O is usually a p-type semiconductor with a band gap of 2.17 eV and have a large absorption coefficient (10^5 cm^{-1}), thus, it has been considered as a potential material for the light absorbing layer in solar cells. Due to the difficulties in doping ZnO to p-type semiconductor or doping Cu_2O to n-type semiconductor, putting ZnO in heterojunction with Cu_2O (Cu_2O/ZnO) is the common approach to construct PV device.

The methods most commonly used in depositing Cu_2O/ZnO heterojunctions are not only complicated and involve expensive processing but also use high temperature, in contrast, electrochemical (ECD) deposition has a number of attractive features, such as a low-cost, low-temperature fabrication procedure, direct control of the film thickness, simplicity of the process, and the potential for large-scale production. Despite this large advantage spectrum, there are few reports on the deposition of ZnO/Cu_2O thin film heterojunctions using entirely an ECD approach.

The theoretical conversion efficiency of ZnO/Cu_2O solar cell is expected to reach 20 %. However, the highest conversion efficiency reported to date was 8.1 %, obtained for MgF_2/ZnO:Al/$Zn_{0.38}Ge_{0.62}O$/Cu_2O:Na device deposited in vacuum by pulsed laser deposition (PLD). Actually, this efficiency is far below the theoretical limit, which is mainly due to the poor quality of the ZnO/Cu_2O interface and the poor minority carrier transport. Thus, to improve the performance of ZnO/Cu_2O heterojunction it is necessary to overcome those two challenges.

In this Ph.D. research, we focus on improving the performance of Cu_2O/ZnO formed by electrochemical deposition. In order to achieve this goal, we implemented many strategies Firstly, we employed two different windows layers, ZnO and Al-doped ZnO (AZO), Cu_2O/ZnO

and Cu_2O/Al:ZnO heterojunctions were deposited on FTO under optimal deposition conditions by two steps electrodeposition. The structural, optical, morphological and electrical proprieties of the two junctions were investigated in details. The Cu_2O/ZnO device shows better performance than Cu_2O/AZO heterojunction due to the high mismatch between AZO and Cu_2O that creates more recombination sites at the interface of p-Cu_2O/n-AZO heterojunction.

Secondly, we expanded the research on Cu_2O/AZO heterojunction, we introduced ZnO buffer layer with a different thickness between Cu_2O and Al:ZnO layers for engineering the heterointerface. The Cu_2O/ZnO/AZO heterojunction was formed by electrodeposition and the proprieties of the tri-layer heterojunction was studied in detail. We demonstrated that the performance of Cu_2O/ZnO/AZO heterojunction enhanced by increasing ZnO thickness. The best performance was obtained for 200 nm ZnO buffer layer as optimal thickness. This buffer layer decreases the band offset between AZO and Cu_2O layers, which facilitate the electrons transport in the junction.

Thirdly, we optimized Cu_2O properties by increasing the deposition pH to improve carrier transport in the absorber layer. The Cu_2O was deposited from a strongly alkaline solution of two different pH values and with different thickness. Changing the deposition pH enhanced the carrier concentration and improved the photo-response of Cu_2O layer. The effect of Cu_2O layer properties on the structural, morphological, optical and electrical properties of Cu_2O/ZnO heterojunction was carefully examined. The Cu_2O/ZnO heterojunction with 500 nm Cu_2O deposited at pH 12 shows the best performance due to the low valence band offset of 1.8 eV in this device.

Finally, we applied back surface field architecture to improve the light absorbance and carrier collection length. The Cu_2O^+/Cu_2O/ZnO device was prepared by three steps electrodeposition where Cu_2O layer was coated with a thin Cu_2O^+ layer (of a carrier concentration higher by two orders than Cu_2O) deposited from strong alkaline solution (pH 12). The effect of Cu_2O and Cu_2O^+ layers thickness on the structural, morphological, optical and electrical properties of the heterojunction was studied in details. We confirmed that the deposition of the Cu_2O^+ layer on Cu_2O layer tuned the absorption and improved the morphology of the absorber layer especially the 150 nm Cu_2O^+/300 nm Cu_2O. Moreover, Cu_2O^+/Cu_2O/ZnO device with 150 nm Cu_2O^+/300 nm Cu_2O structure as absorber shows the best performance due to the low band valence offset (ΔE_v) between 150 nm Cu_2O^+/300 nm Cu_2O structure and ZnO layer. The results of this study provide many strategies to improve the performance of ZnO/ Cu_2O photovoltaic devices prepared by electrochemical deposition.

Chapter 1

Background and literature review

Chapter 1: Background and literature review

1.1 Introduction

In the modern society, the consumption of energy is raising enormously year by year, due to the demands of comfort and the growing world population and economy [1]. Up to now, fossil fuels and nuclear fission fuels are playing the lead role to meet the energy demand (Figure1.1), with about 78.4 % come from the fossil fuels (oil, coal and natural gas) and 2.3% from nuclear power [2]. However, the availability and the pollution remains the major problems of the energy conventional sources. Now, it is well established that those sources are limited and they could be exhausted within one or two generations. Moreover, the fossil fuels burning produces many dangerous pollutants, such as carbon dioxide. As well, there is common concern about the safety of the nuclear energy technologies, especially the long-term storage of radioactive waste products. Therefore, it is necessary to increase the renewable energy contribution to the energy mix. Currently, the share of the renewable energy is only 19.3 % of the global consumption [2].

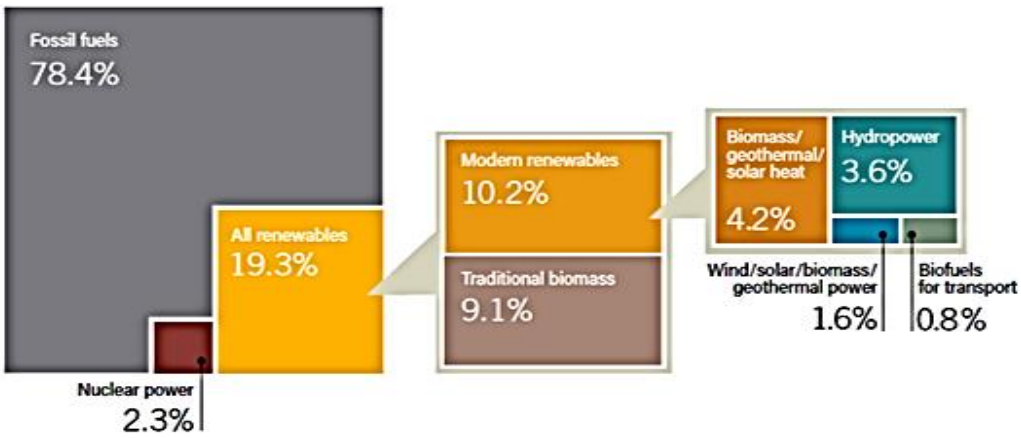

Fig. 1.1. *Estimated Renewable Energy Share of Total Final Energy Consumption, 2015 [2].*

Of the wide range of renewable energy sources, the solar energy has a good potential to meet the global energy demand due to several reasons:

(i) It is a long-term natural resource and the most abundant energy source, where, the solar energy received by the earth is ~10,000 times greater than the worldwide energy consumption [3].

(ii) It is significant cost reduction; in the past decades, the solar industry has relied on improving the production process and increasing the conversion efficiency to reduce the cost.

(iii) It is beneficial for the society, as it has the potential to improve the health and can be available even for the poorest world's population.

According to Intergovernmental Panel on Climate Change report, solar energy is abundant and offers significant potential for near-term (2020) and long-term (2050) climate change mitigation [4]. To make the solar energy competitive with fossil fuels, it is necessary to lower the cost and increase the efficiency.

There are several thermodynamic pathways to convert the solar energy into a usable form of energy such as heat, kinetic energy, electric energy and chemical energy. Among these, as noted above, the cleanest and most direct and efficient mode is the conversion of light to electrical power with the help of photovoltaic (PV) or solar cell devices. In principle, a photovoltaic cell is an electrical device that converts the light energy directly into electricity by the photovoltaic effect.

1.2 Photovoltaic device

The solar cell (or photovoltaic device) is one of the technologies that allow us to convert the enormous amount of solar energy directly into electricity. Therefore, the solar cell acts like a diode in dark and generates photo-voltage under illumination without the influence of any external voltage source. In principle, a solar cell is a junction device obtained by placing two electronically different materials together with a thin electronic barrier in between, to separate charges [5]. The photovoltaic conversion occurs under the light through three successive processes [6]:

(1) The semiconductor absorbs the light and converts the photons to electron-hole pairs.

(2) The collection and the separation of these carriers by an internal electric field (p-n junction).

(3) The distribution of electricity to an external load.

Based on the nature of the photovoltaic phenomena, for efficient photovoltaic energy conversion, semiconductor materials in the form of a *p-n* junction are essential. Up to now, the research has tended to focus on improving the conversion efficiency and reducing the costs of both fabrication process and material by the development of solar cells based on alternative materials. Therefore, the solar cells are classified into three main categories: Silicon solar cells, inorganic compound solar cells, and organic solar cells. The various types of solar cells and

their advantages and disadvantages are summarized in table 1.1. The inorganic compound solar cells mentioned in table 1.1 are the mass-produced ones only.

Table 1.1. *The main categories of solar cells.*

Category	Type	Advantage	Disadvantage
Silicon solar cells	Crystalline Si	High conversion efficiency	High production cost
	Amorphous Si	Low production cost	Low conversion efficiency
Inorganic compound solar cells	Chalcopyrite Semi-conductor (CIS, CIGS)	High absorption coefficient and high conversion efficiency	Long-term instability
	II-VI Semiconductor (CdTe)	High efficiency and low cost	Toxicity of Cd
	III-V Semiconductor (GaAs)	High conversion efficiency	Expansive materials
Organic solar cells	Pentancene	low cost	Poor stability

Among those categories, the compound semiconductor solar cells seem to be the promising one, since the thin films give more possibilities of designing devices and has the potential for commercial feasibility due to the low costs of both the fabrication processing and the used materials. Thus, thin film compound solar cells will be an important alternative for Si-based devices in the future.

1.3 Thin film solar cells

Generally, thin film solar cells (TFSC) works based on p-n junctions; thus, they have been fabricated by successive deposition of many semiconductor layers. Usually, they contain substrate, transparent conducting oxide (TCO), window layer (p-type or n-type), an absorber layer (*i*-type or p-type) and a contact layer. The general structure of TFSC is presented in figure 1.2. The performance of this device depends on the physical and chemical properties of each layer. Hence, a good understanding of the behavior of these individual layers is essential for designing an effective PV device. In the following section, we presented a brief review of each layer of the TFSC; also, we limited the discussion and examples to the thin film solar cells based on Cu_2O/ZnO inorganic heterojunction.

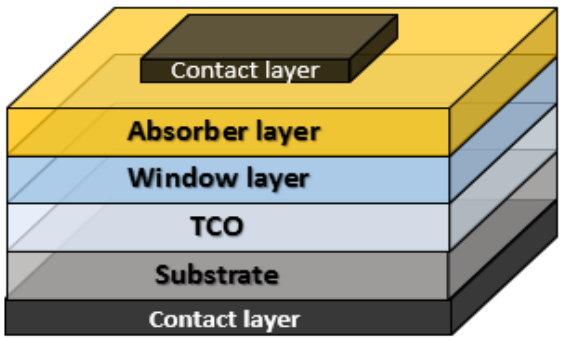

Fig. 1.2. *General structure of thin film photovoltaic devices.*

1.3.1. Substrate

In the PV device configuration the substrate is an inactive constituent, thus, it is required to be mechanically stable and inert during the device fabrication. Based on those standards, suitable substrates can be selected for different processes of deposition. Therefore, expensive and rigid substrates such as ceramics or high-temperature glass are generally required for deposition at high-temperature, while, the low-temperature process allows the usage of less expensive and flexible substrates. TFSC devices have been classified depending on the substrate into super-straight type and substrate type structures [5]. In super-straight type configuration, the substrate is transparent and the conducting oxide coating on the substrate made the contact. In substrate type configuration, the substrate is metal or metallic coating on a glass (or polymer) substrate, which also acts as the contact.

Currently, both substrate type and super-straight type configurations are used for Cu_2O/ZnO PV device fabrication [7-10]. For the super-straight configuration, the Cu_2O/ZnO junction was deposited on a transparent conductive window layer coated on a glass substrate. Whereas, in the substrate type configuration, the n-ZnO transparent conductive window layer was deposited on Cu_2O layer formed by thermal oxidation of metallic Cu sheets. Concerning Cu_2O/ZnO PV device conversion efficiency, the substrate appears to play an active role in improving the photovoltaic performance by affecting the absorber material (Cu_2O) properties. Since the Cu_2O prepared in super straight configuration presents a polycrystalline structure with random orientation and contains some impurities, the device performance deteriorate. Hence, the best efficiency reported for super-straight type device with $Zn_{0.79}$ $Mg_{0.21}O$ buffer layer was 2.2 % [11]. On the other hand, the high-temperature processes used in the construction of the substrate type devices allow the formation of high quality layer of Cu_2O, which ameliorate the

device performance. Thus, best conversion efficiency obtained from substrate type device with zinc–germanium-oxide ($Zn_{1-x}Ge_x$-O) window layer was 8.1 % [12].

1.3.2. Transparent conducting oxide (TCO)

Generally, the TCOs are n-type degenerate semiconductors with two critical characteristics. First, a high transparency in the visible spectrum to ensure the transmission of the incident light to the absorber layer and second, good electrical conductivity to form a low-resistance contact to the device. Other than the optoelectronic properties, the mechanical, thermal, chemical, plasma-exposure stability and passivity [13] of TCOs have great importance for high PV performance. Major et al. [14] have reported that ZnO-based materials are the only TCOs that can withstand H-bearing plasma; also, they are stable up to 800 K. Thus, ZnO-based materials were increasingly used in thin film solar cell technologies [5].

Since controlling the characteristic of p-type Cu_2O deposited onto n-type ZnO is very difficult at high-temperature processes, the super-straight type Cu_2O/ZnO devices could be fabricated only by electrochemical deposition (ECD), which requires a conducting substrate. Hence, a transparent Tin oxide doped Fluor (F:SnO_2; FTO) or doped indium (In:SnO_2; ITO) coating glass substrates were used as TCO layer in super-straight type Cu_2O/ZnO devices.

1.3.3. Window layer

Usually, the window layer has two main roles in the TFSC device. One is to form a junction with the absorber layer and the other is admitting a maximum amount of light to the absorber layer and the junction region. Hence, there is no generation of photocurrent in the window layer [15]. The window layer should be as thin as possible (to maintain low series resistance) and it should have large bandgap [5] to guarantee a high optical output with a minimal resistive loss. Moreover, to ensure an optimal minority carrier transport through the heterojunction, it is necessary to minimize any potential spike in the conduction band at the window layer/absorbent layer heterojunction and consider the lattice mismatch between window layer and the absorber layer. Briefly, to ensure high performance of the PV device the band gap of the window layer, the lattice mismatch and the band alignment at the window layer/absorbent layer junction interface should be optimized.

In Cu_2O-based solar cells, many n-type semiconductors were employed as a window layer, such as ZnO [10, 16], CdO [17], TiO_2 [18-20] and Ga_2O_3 [21]. Among them, the ZnO was the best match for Cu_2O as typical n-type window layer of large band gap [22]. The ZnO have hexagonal structure (Figure 1.3a) with lattice constant of (a = 3.250 Å, c = 5.207 Å) [23],

while the Cu_2O have cubic structure (Figure 1.3b) with a lattice constant of 4.2696 Å [24]. Therefore, when forming ZnO/Cu_2O heterojunction solar cells it is important to reduce the lattice mismatch between ZnO and Cu_2O to the minimal to prevent the recombination of the generated electrons at the interface.

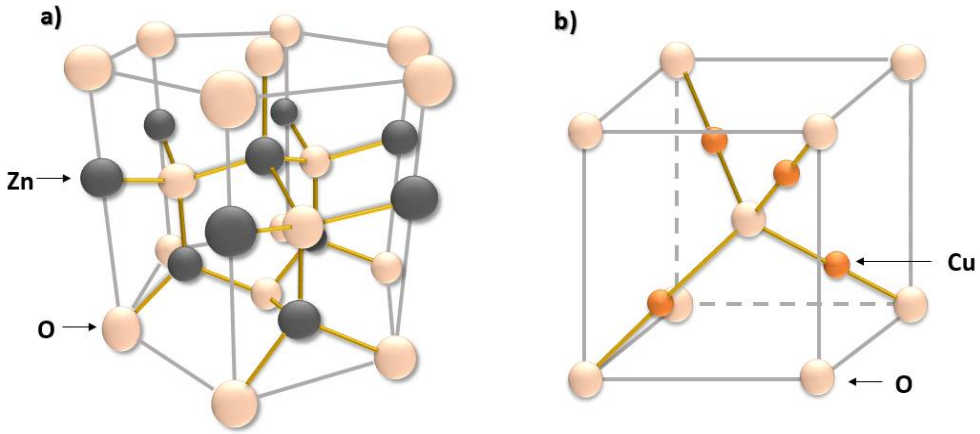

Fig. 1.3.a) *The hexagonal wurtzite structure of ZnO,* ***b)*** *The cubic structure of Cu_2O.*

Accordingly, Akimoto et al. [25] have proved that Cu_2O(111)/ZnO(0001) heterojunction exhibits a good performance compared to ZnO/Cu_2O solar cell with other orientations of Cu_2O. This is due to the good lattice match between the ZnO (0001) plane and Cu_2O (111) plane, which exhibits a hexagonal atomic arrangement at the interface with a small lattice mismatch of only 7.1 % [26, 27]. This allowed the Cu_2O-(111) film to grow epitaxially on ZnO (0001) and improve the device performance.

1.3.4. Absorber layer

The Absorber layer mainly consists of a photovoltaic material that absorbs effectively the sunlight. Since the majority of the sunlight energy is in the visible region (Figure 1.4), the band gap of the absorber layer should be of ~1.5 eV. In selecting an absorber material that ensures the capture of all available photons, many parameters should be considered, such as, the wide availability of the absorber material, the direct bandgap, high solar absorption, long diffusion length of minority carrier and low recombination rate.

Although, the Silicon (Si) dominates 90 % of the solar cells market [28], being an indirect bandgap material (gap energy of 1.1 eV) the Si is by no means an ideal PV material. Therefore, for an effective solar absorption, the thickness of Si wafers should be at least 250–300 µm. Which is the main reason behind the high cost of Si-based solar cells that prevents a large- scale household commercialization of Si-based solar cells. This problem was recognized right from the beginning, thus, the researcher attention is shifted to the photovoltaic materials that respond

to the commercial needs i.e. that satisfy the constraints for minimizing the thickness and the wide availability. One of the promising candidates is the Cu_2O, as a direct bandgap material with a high absorption coefficient. To date, the Cu_2O is widely used as an absorber layer in solar cells such as Cu_2O/ZnO heterojunction solar cells.

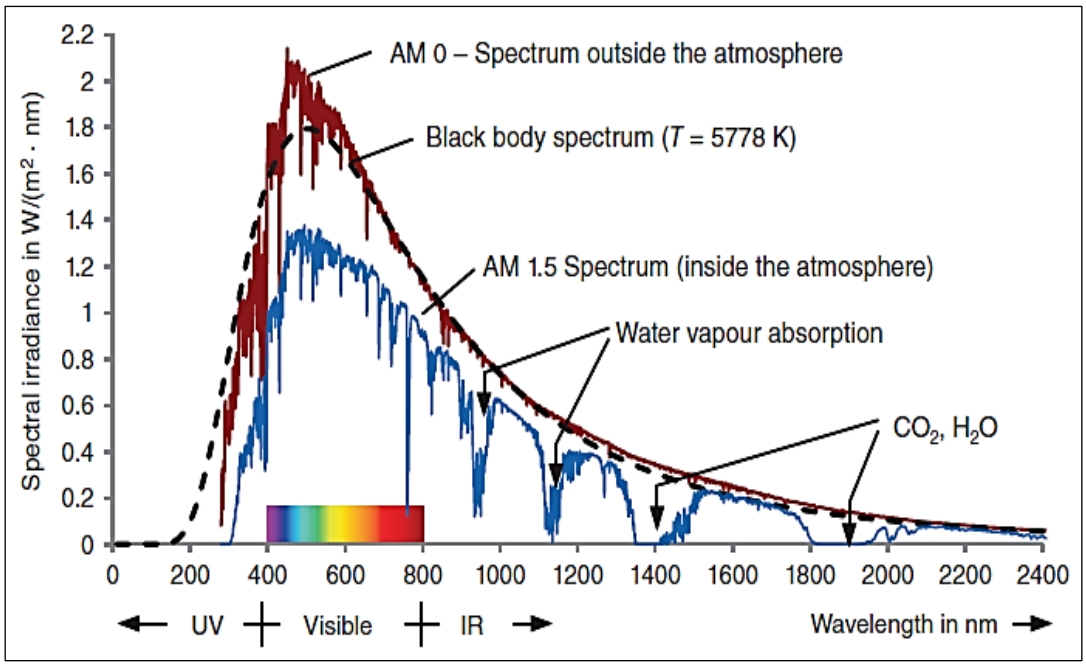

Fig. 1.4. *Solar spectrum outside and inside the atmosphere [29].*

1.3.5. Contact layer

The principal role of the contact layer is to form a perfect Ohmic junction with the semiconductor to collect the resulting current. Therefore, the Ohmic junction with the p-type semiconductor act as the holes-collecting contact and that with n-type semiconductor act as the electrons-collecting contact. It is well known that choosing proper contact materials have a great effect on the overall efficiency of the solar cell. In theory, to form an Ohmic contact with a p-type semiconductor, the contact material should have a work function higher than the semiconductor to align the Fermi level of the contact material with the upper edge of the semiconductor valence band [30]. On the other hand, for n-type semiconductor Ohmic contact, the contact material should have smaller work function than the semiconductor. In practice, the interface metal/semiconductor may not behave as predicted due to the presence of interface states and defects. This imperfect Ohmic junction is one of the major limitations in the solar cell devices.

In the substrate type configuration of Cu_2O/ZnO solar cells, the substrate is a metal or a metallic coating (Au, Al) on a glass substrate, thus is act also as the back contact. Whereas in

the super-straight type configuration, the conducting oxide coating on the substrate (generally the commercially available ITO or FTO) made the back contact, while a metals of high work-function such as Au forms the top contact in most cases.

To date, thin film solar cells have been formed using various device configurations and employing different materials. Recently, there has been an increasing interest in solar cell devices composed of low cost, non-toxic and earth-abundant materials as an alternative clean energy. So far, zinc oxide (ZnO) and cuprous oxide (Cu_2O) have considered very interesting candidates in this respect. The following pages present a brief review of Cu_2O/ZnO heterojunctions solar cells.

1.4 Literature review of Cu_2O/ZnO heterojunction solar cells

In the past few years, the semiconductor nanostructured heterojunctions, consisting of two or more components have attracted considerable attention for their applications in several optoelectronic devices such as lasers, photodetectors and solar cells [31, 32]. Choosing materials that have proportioned properties is a primordial parameter for excellent performances of these structures. Over the years, ZnO and Cu_2O have received extensive attention since they are low cost, nontoxic and abundantly available on earth and present exceptional optical and electronic properties. The Cu_2O is one of the few oxides that naturally shows p-type conductivity [33], with band gap energy of 1.96 to 2.38 eV [34], large absorption coefficient (10^5 cm^{-1}) higher than the single crystalline Si [35, 36] and can be easily produced with a suitable minority carrier diffusion length [25, 37, 38]. Those properties meet the criterions for good absorber layer in solar cells. On the other hand, the ZnO is an n-type semiconductor with wide band gap energy of 3.37 eV [39], high charge carrier mobility [40], a large exciton binding energy of 60 meV at room temperature and it shows superior optical transparency in the visible region. For that reason, the ZnO have been widely used in solar cells as window layer [41].

Due to the difficulties in doping ZnO to p-type semiconductor or doping Cu_2O to n-type semiconductor, putting ZnO in heterojunction with Cu_2O (ZnO/Cu_2O) is the common approach to construct PV device. Especially as, the theoretical conversion efficiency of ZnO/Cu_2O heterojunction solar cell is around 18 % [42]. Effectively, a p-type Cu_2O junction with n-type ZnO was found to have excellent performances in photovoltaic applications [25, 37, 43]. A recent study [22] compared several TCO-Cu_2O heterojunctions, where various n-type semiconductors such as In_2O_3, ZnO, In_2O_3: Sn (ITO), Al: ZnO (AZO), were deposited by PLD on Cu_2O sheet. It was confirmed that ZnO-Cu_2O heterojunction shows better photovoltaic

properties than In_2O_3-Cu_2O and ITO-Cu_2O. In fact, many photovoltaic devices based on the p-Cu_2O/n-ZnO heterojunctions have been formed using different deposition method. Table 1.2 present the conversion efficiency obtained up to 2016 for Cu_2O/ZnO heterojunction solar cells formed by different deposition methods.

Table 1.2. *The development in Cu_2O/ZnO solar cells efficiency up to 2016.*

Heterojunction (The deposition occur on the last named semiconductor)	**Deposition method**	**PEC (%)**	**Ref.**
	In vacuum		
MgF_2/ZnO:Al/$Zn_{0.38}Ge_{0.62}O$/Cu_2O:Na	Pulsed Laser Deposition (PLD)	8.1	[12]
AZO/Al-Ga_2O_3/Na-Cu_2O	PLD	6.1	[44]
AZO/ Ga_2O_3/Cu_2O	PLD	5.38	[21]
AZO/ $Zn_{0.91}Mg_{0.09}O$/Cu_2O	PLD	4.31	[45]
AZO/ ZnO/Cu_2O	PLD	4.13	[46]
AZO/ Ga_2O_3/Cu_2O	Atomic Layer Deposition (ALD)	3.97	[47]
AZO/ ZnO/Cu_2O	PLD	3.83	[48]
AZO/ a-ZTO/Cu_2O	ALD	2.85	[49]
AZO/ a-ZTO/Cu_2O	ALD	2.65	[50]
AZO /Cu_2O	PLD	2.53	[21]
ITO/ZnO/Cu_2O	Ion Beam Sputtering (IBS)	2.01	[51]
ZnO :Ga /Cu_2O	Vacuum Arc Plasma Evaporation (VAPE)	1.52	[8]
AZO /Cu_2O	d.c. Magnetron Sputtering (dc-MSP)	1.39	[8]
AZO /Cu_2O	PLD	1.21	[52]
	Without vacuum		
Cu_2O/ZnO	Electrochemical deposition (ECD)	1.43	[9]
Cu_2O/ZnO	ECD	1.28	[10]
Cu_2O^+/Cu_2O/ZnO	ECD	0.9	[53]
Cu_2O/ZnO	ECD	0.47	[54]
Cu_2O/ZnO	ECD	0.41	[37]
ZnO/Cu_2O	Atmospheric ALD (AALD)	1.46	[11]
ITO/ $Zn_{0.79}Mg_{0.21}O$/Cu_2O	AALD	2.2	[11]

It is clear that the conversion efficiency is affected greatly by the deposition method, the Cu_2O/ZnO solar cells deposited in vacuum show better performance. The highest efficiency was 8.1 % obtained in vacuum by PLD, while the highest efficiency obtained at atmospheric condition was 2.2 % deposited by AALD. This is due to the presence of defects in the

polycrystalline Cu_2O deposited at the atmospheric condition and low temperature, which deteriorate the device performance.

Actually, the efficiency of these devices is far below the theoretical limit efficiency (18 %) which have hindered their practical application [55]. The main reasons of this limitation are: i) the presence of defect states in the polycrystalline Cu_2O thin films [56], ii) the poor interface quality [57], iii) and the poor minority carrier transport [54] that increase the recombination probabilities of photo-induced charge carriers. Consequently, improving the conversion efficiency requires the amelioration of ZnO and Cu_2O properties, as well as the ZnO/Cu_2O interface quality. To date, several methods have been applied to surpass those limitations, such as dye sensitization [58], doping [59] and engineering the heterostructure [60]. Among them, engineering and creating novel heterostructures are one of the potential methods to enhance the overall conversion efficiency of photovoltaic devices [61-63]. In the following section, we presented the major studies on the development of Cu_2O/ZnO solar cells performance.

1.5 Major studies on improving Cu_2O/ZnO heterojunction solar cells performance

1.5.1. Doping ZnO window layer

To date, incorporating impurities has been the main method to increase the bandgap and n-carrier concentration of ZnO and shift the transparency more to the visible region, thus, improving the conversion efficiency of Cu_2O/ZnO solar cell and add flexibility in device fabrication [64]. For ZnO n-type doping, group III elements such as gallium (Ga) or aluminum (Al) and group IV elements could be an extrinsic dopant for ZnO. Minami et al. [8] have reported that a high efficiency of 1.5 % and 1.42 % were obtained for Ga-doped ZnO (GZO)/Cu_2O and Al-doped ZnO (AZO)/Cu_2O heterojunction solar cell, respectively. In this study, high quality polycristallin of Cu_2O layer was deposited by oxidizing Cu sheets with heat treatment (1000 °C), then the n-type AZO and GZO thin films were deposited, at a substrate temperature around 200 °C, on Cu_2O layer (used as substrate) by PLD and vacuum arc plasma evaporation (VAPE), respectively. They mainly claimed that using damage free methods such as PLD or vacuum evaporation methods like VAPE to deposit n-type doped ZnO (AZO and GZO) on Cu_2O layer helps reducing the damage on Cu_2O surface i.e. prevents the reduction of Cu_2O to Cu at the interface. Which improve the overall performance of the device. In addition, depositing AZO at high temperature (200 °C) improve the film crystallinity, which reduce the defects near the interface AZO/Cu_2O and in the AZO film itself, thus, the device efficiency increased.

1.5.2. Inserting a buffer layer

The band alignment between the absorber layer and the window layer is of critical importance. Therefore, introducing a buffer layer between them, to reduce the interface defects and align the energy bands at the interface, will be necessary to improve the solar cells performance. A thin layer of non-doped ZnO with band gap and lattice constant between Cu_2O and AZO layer will be a good choice as a buffer layer in Cu_2O/AZO structure. Nishi et al. [46] have reported that inserting ZnO layer of 50 nm between AZO and Cu_2O layers improved the conversion efficiency of AZO/Cu_2O heterojunction solar cell significantly from 2.0 % to 4.13 %. Figure 1.5a presents schematic structures of AZO/Cu_2O and AZO/ZO/Cu_2O solar cells. The Cu_2O film was formed by oxidizing Cu sheets at a high temperature of 1000 °C, while the AZO and ZnO layers were deposited on Cu_2O by damage free method (PLD) to stabilized Cu_2O sheets surface. The efficiency improvement reported in this study have been attributed to the increase the barrier height as well as the width of the depletion layer in AZO/ZO/Cu_2O solar cell (Fig.1.5b) resulting from the insertion of ZnO buffer layer which functions as an n-type ZO layer as well as an active layer in AZO/ZO/Cu_2O heterojunction solar cells.

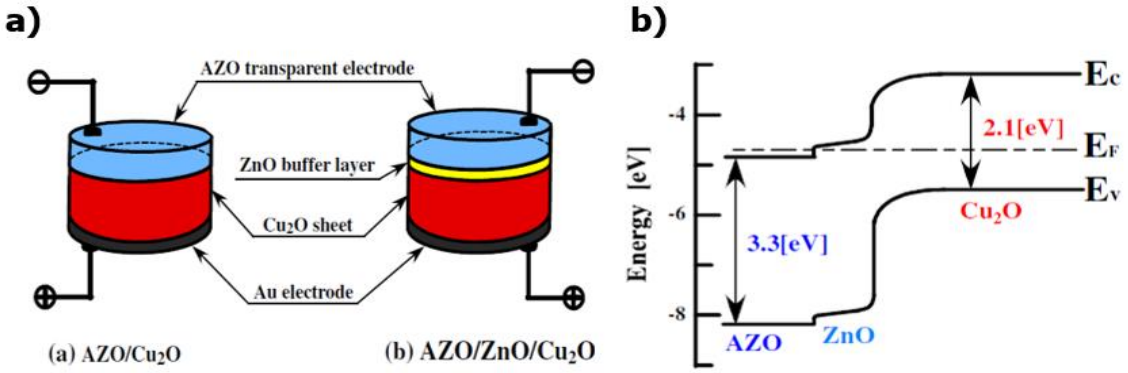

Fig. 1.5. a) *Schematic structures of the (a) AZO/Cu_2O and (b) AZO/ZO/Cu_2O solar cells.* ***b)*** *Energy band diagram of the AZO/ZO/Cu_2O heterojunction [46].*

Regardless of the high performance of the AZO/ZO/Cu_2O heterojunction solar cell, the open circuit voltage (0.72 V) and the fill factor (0.60) are too low. It is confirmed that the open circuit voltage dependents strongly on the kind of n-type semiconductor thin film used for forming the p-n heterojunction. In the AZO/ZO/Cu_2O heterojunction, the n-p junction of ZnO buffer layer and Cu_2O have a large cliff-type discontinuity of the conduction band i.e. high ΔE_C value because of the low electron affinity of Cu_2O compared to that of ZnO [65-67]. In this regard, Minami *et al.* [45] have reported that substituting ZnO buffer layer by $Zn_{1-x}Mg_xO$ layer to form AZO/ $Zn_{1-x}Mg_xO$ /Cu_2O heterojunction solar cell (Fig.1.6) have improved greatly the performance and the open circuit voltage. In this particular study, they confirmed that the

augmentation of Magnesium (Mg) content in ZnO increases the band gap of wurtzite $Zn_{1-X}Mg_XO$, which decreases the difference in electron affinity between p-Cu_2O and n-$Zn_{1-X}Mg_XO$. Thus, reducing the height of the cliff-type energy discontinuity of the conduction band (ΔE_C). Consequently, the photovoltaic properties of $Zn_{1-X}Mg_XO/Cu_2O$ heterojunction solar cells were improved and the highest efficiency (4.31 %) was obtained for AZO/50 nm $Zn_{0.91}Mg_{0.09}O/Cu_2O$ heterojunction solar cell fabricated by damage free method (PLD).

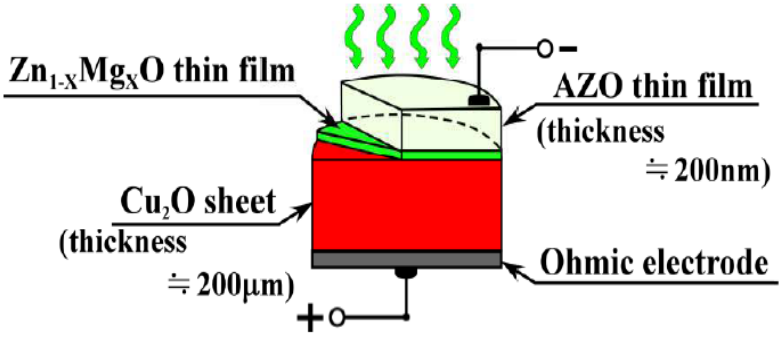

Fig. 1.6. *Schematic structure of an AZO/Zn_{1-X} Mg_XO/Cu_2O heterojunction solar cell [45].*

Overall, both studies proved the huge effect of the n-p junction interface quality and the band alignment between the n-type and p-type semiconductors on the photovoltaic properties of ZnO/Cu_2O based solar cells.

1.5.3. Improving the charge collection

The Cu_2O films deposited at low-temperature have a low holes concentration and low mobility (1.2 $cm^2.V^{-1}.S^{-1}$) compared to the thermally oxidized Cu_2O (90 $cm^2.V^{-1}.S^{-1}$) [35, 68-70]. Which produces recombination region far from the heterojunction interface (> 1.0 µm). As a result, the conversion efficiency of the PV device decreases due to the recombination of minority carrier before reaching the heterojunction interface. To improve the conversion efficiency we must ameliorate the charge collection in Cu_2O/ZnO solar cells. Musselman *et al.* [68] proposed a nanoscale structuring of the Cu_2O/ZnO interface to minimize the electron transport lengths, hence, increase the charge collection in Cu_2O/ZnO solar cells. In this study, a comparison was set between the nanostructured and bilayer architectures of ZnO/Cu_2O heterojunctions solar cells. The nanostructured architectures were constructed of ZnO Nano Wires (NWs) electrodeposited on ITO coated glass (with 50 nm Zn seed layer) followed by a galvanostatic deposition of Cu_2O layer on ZnO NWs. While, the bilayer heterojunction was constructed of 550 nm ZnO layer electrodeposited on ITO, followed by a galvanostatic deposition of Cu_2O. Figure 1.7 presents schematic structures of bilayer and NW Cu_2O-ZnO

solar cell architectures. Surprisingly, the conversion efficiency of NWs Cu_2O-ZnO solar cell (0.38 %) was significantly lower than that of bilayer Cu_2O-ZnO solar cell (0.85 %). According to these results, they claimed that the NWs architecture has increased the Cu_2O/ZnO interface area, however, it is insufficient to form Cu_2O depletion layer comparable to that in bilayer architectures. Which explains the low conversion efficiency of Cu_2O-ZnO NWs architecture.

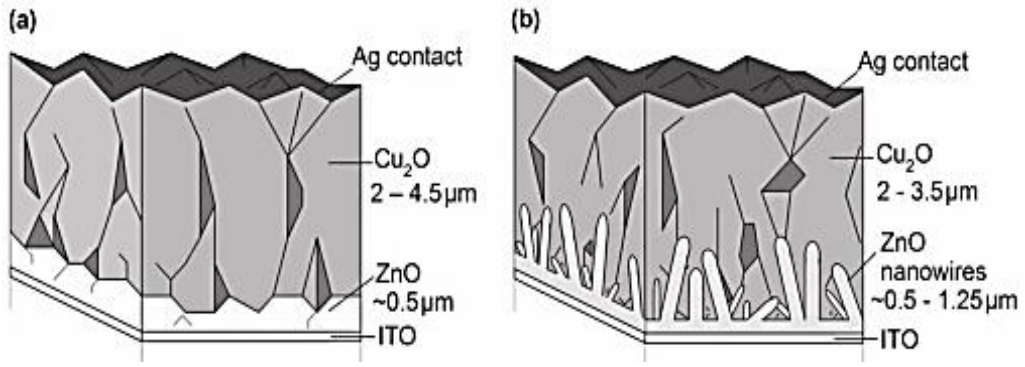

Fig. 1.7. *Schematic diagrams of bilayer (a) and NW (b) Cu_2O-ZnO solar cell architectures [68].*

Finally, this research suggests that the achievement of efficient charge collection and a high resistance to recombination, simultaneously, requires more improvements in the electrical and morphological properties of the nanostructured oxide materials.

Marin *et al.* [53] have proposed another solution to improve the charge collection in Cu_2O/ZnO solar cells by engineering Cu_2O^+/Cu_2O/ZnO back surface field device. Where the thickness of the absorber layer (Cu_2O) was reduced from 3.0 µm to 1.0 µm to meet the distance required for good charge collection in Cu_2O/ZnO solar cells while conserving the same activity as 3.0 µm thick Cu_2O. This new design was fabricated by the electrodeposition (ED) of 500 nm ZnO on ITO coating glass followed by a galvanostatic deposition of 1.0 µm Cu_2O layer coated with 200 nm Cu_2O^+ overlayer (has a higher carrier concentration than Cu_2O) grown by atmospheric atomic layer deposition (AALD). Figure 1.8 shows the cross-section SEM images of the AALD-enhanced cell (Cu_2O^+/Cu_2O/ZnO) and the fully-ED cell (Cu_2O/ZnO) used as a reference in this study.

They claimed that the 0.90 % conversion efficiency was achieved using Cu_2O^+/Cu_2O/ZnO cell, which is 28 % higher than the conversion efficiency of the fully-ED Cu_2O/ZnO used as a reference cell. This due to the effect of the high carrier concentration of Cu_2O^+ layer that allowed the depletion width to be achieved in the whole cell thickness appropriate with the minority carrier collection length.

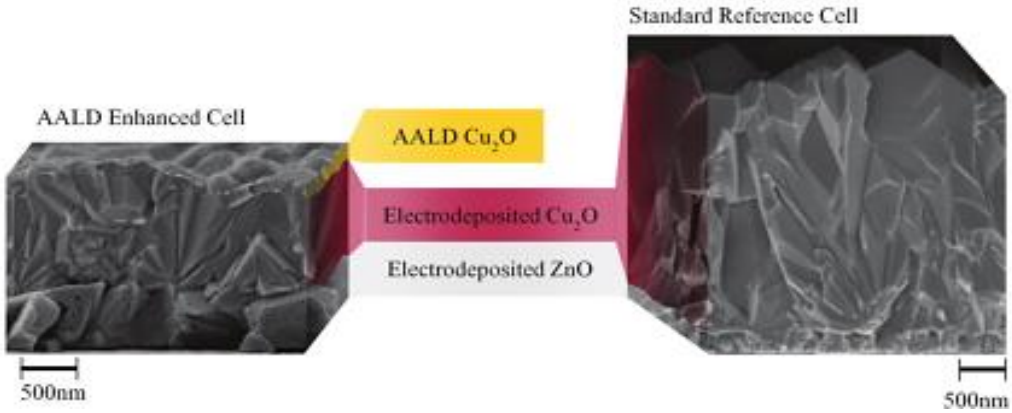

Fig. 1.8. *Cross-section SEM images of an AALD-enhanced cell (left) and fully-ED reference cell (right) [53].*

1.6 Electrochemical deposition (ECD)

The methods commonly used in depositing Cu_2O/ZnO heterojunctions solar cells were not only complicated and expensive processing but also uses high-temperature and vacuum. In such conditions, the metal (M)/semiconductor interface is very reactive and unstable at the initial stage of deposition in the vacuum; also, at high-temperature, metallic copper or copper-rich regions will be formed at the interface of Cu_2O/ZnO junction [46]. Therefore, it is important to choose a low energy and low damage deposition method to form a high quality interface. In contrast to vacuum-based deposition, electrodeposition is a non-equilibrium process, which could be controlled by various parameters such as the applied potential (or current), the pH of the aqueous electrolyte solution and the concentration of metal ions. Moreover, the electrodeposition has a number of attractive features, such as the low cost, the low-temperature fabrication procedure, a direct control of the film thickness and the simplicity of process with potential for large-scale production [47].

Experimentally, the ECD requires simple three electrodes cell with an electrolyte solution, containing the precursor ions, relied on a computer-controlled potentiostat/galvanostat as a potential (or current) source. Figure 1.9 shows the setup of electrochemical deposition. In this setup, the reference electrode is used to keep a stable potential at the working electrode. Hence, applying a fixed potential difference between the reference and the working electrodes attracts the ions to the working electrode surface and drives their electrochemical reaction to form the material film. On the other hand, the counter electrode balances the current produced at the working electrode.

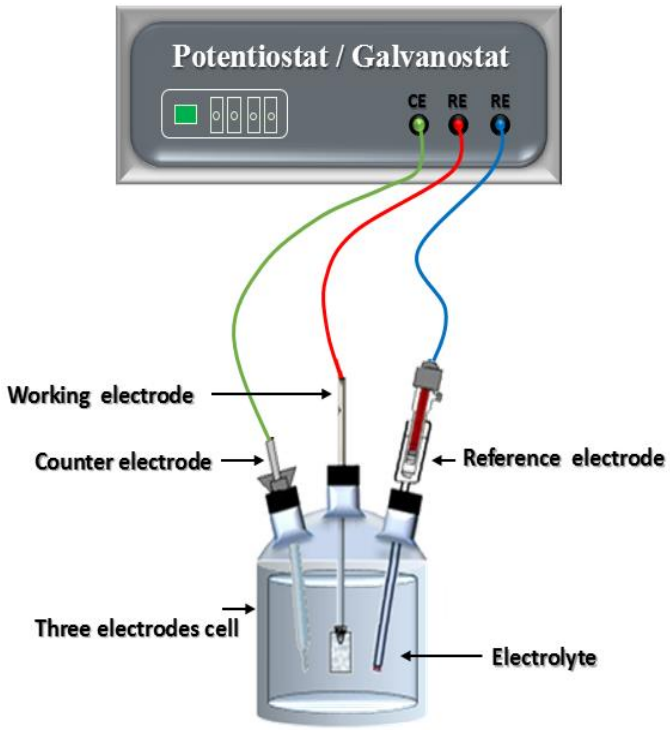

Fig. 1.9. *Schematic diagram of the electrochemical deposition setup.*

The properties of the electrodeposited materials could be easily controlled by monitoring the deposition parameters (applied potential, temperature, concentration, solution pH and the bath composition). To determine the preliminary condition of the electrodeposition, the cyclic voltammetry and Pourbaix diagram are commonly used, especially to identify the pH of the deposition bath and the deposition potential.

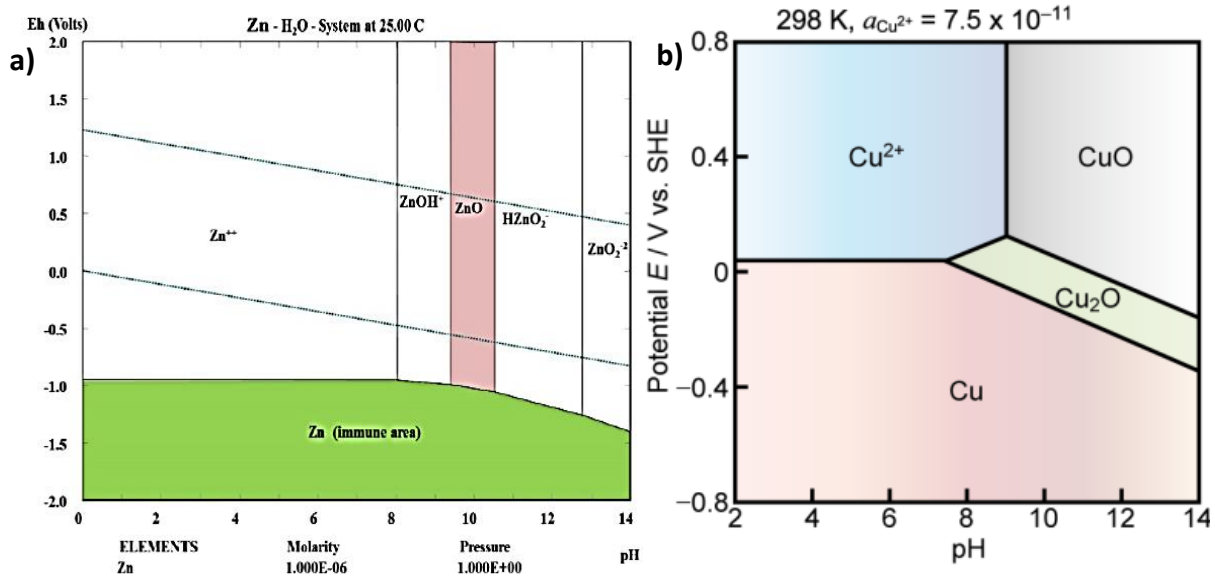

Fig. 1.10. *Pourbaix diagrams of:* ***a)*** *Zn-H_2O system calculated for Zn^{2+} concentration of 1.0×10^{-6} M at 25 °C [71],* ***b)*** *Cu-H_2O system calculated for Cu^{2+} activity of 7.5×10^{-11} at 25 °C [72].*

Figure 1.10 presents Pourbaix diagrams (Potential-pH) drown for Zn and Cu in solution at 25 °*C*. According to the diagram in Fig.1.10a, the deposition of ZnO is possible at pH higher than 8.0 at high temperature (as the desideration of Zn(OH) is easy at high temperature). These values are approximate and slightly different than other studies; for example, the E-pH diagram calculated by Wippermann et al [73] for higher Zn^{2+} concentration (10^{-4} M) shown that the deposition of ZnO is possible starting pH 7.5. On the other hand, the deposition of Cu_2O is possible at higher pH and potential (Fig.1.10b). Overall, Pourbaix diagrams give an estimated values of pH and potential that used as starting point in the electrodeposition, thus, the experimental values may differ than that in Potential-pH diagrams.

The electrodeposition process of ZnO and Cu_2O is well known; for ZnO film deposited from nitrate bath, the deposition occurs in three steps. Firstly, the applied potential (or current) drives the reduction of nitrate (NO_3^-) ions, presents in the deposition bath, to produce the nitrite (NO_2^-) and hydroxide (OH^-) ions on the substrate surface, which increases the local pH. Then, a chemical reaction occurs between the Zn^{2+} ions in the solution and the OH^- ions adsorbed on the substrate to form zinc hydroxide $Zn(OH)_2$. Finally, under the temperature effect, the $Zn(OH)_2$ dehydrated to form ZnO film. This electrodeposition mechanism is ascribed as follow [74]:

$$NO_3^- + H_2O + 2e^- \rightarrow NO_2^- + 2OH^- \quad (1.1)$$

$$Zn^{2+} + 2OH^- \rightarrow Zn(OH)_2 \quad (1.2)$$

$$Zn(OH)_2 \rightarrow ZnO + H_2O \quad (1.3)$$

On the other hand, the electrodeposition of high quality p-type Cu_2O requires an alkaline solution. The deposition occurs in two steps, the reduction of Cu^{2+} ions presents in the deposition bath to form Cu^+ ions, which reacts with the OH^- ions in the solution to form Cu_2O film on the substrate. As ascribed in the following reactions [75]:

$$Cu^{2+} + 1e^- \rightarrow Cu^+ \quad (1.4)$$

$$2Cu^+ + 2OH^- \rightarrow Cu_2O + H_2O \quad (1.5)$$

The ECD is based on the charge transfer, thus the deposition occurs only on conducting substrates, which is the main disadvantages of this method. In addition, most of the oxides films are electrodeposited from an aqueous solution, with distilled water as solvent, thus, the dissolved oxygen is incorporated unintentionally in the deposited films and the hydrogen reduction is inevitable reaction during the deposition.

1.7 Objective of this research

The main objectives of this thesis listed as follows:

1. The fabrication of non-toxic heterojunction (Cu_2O-ZnO) by cost-effective deposition technique (Electrochemical deposition).
2. Applied many strategies to improve the performance of Cu_2O-ZnO heterojunction, prepared by electrochemical deposition, such as:
   i) Substituted ZnO layer by Al-doped ZnO (AZO) as a window layer in Cu_2O/ZnO/FTO heterojunction solar cell.
   ii) Inserting ZnO buffer layer with a different thickness in Cu_2O/ZnO/AZO/FTO trilayer heterojunction.
   iii) Improving the carrier concentration of Cu_2O absorber layer by adjusting the bath pH.
   iv) Appling the back surface field architecture (Cu_2O^+/Cu_2O/ZnO/FTO) to improve the properties of the absorber layer.

1.8 Preview of the thesis

This study mainly aims to demonstrate many strategies for improving the performance of Cu_2O-ZnO heterojunction prepared by electrochemical deposition. This thesis has five chapters arranged as follows:

The first chapter presents an introduction to the development of the photovoltaic devices. In particular, a literature review on Cu_2O/ZnO heterojunction development limitation and ways of improvements. In addition, the electrodeposition principle is briefly explained.

In the second chapter, the Cu_2O/ZnO/FTO and Cu_2O/AZO/FTO heterojunctions were successfully fabricated by two steps electrochemical deposition under optimal deposition condition (concentration, temperature, potential…). To investigate the effect of the window layer material on the heterojunction, the structural, optical, morphological and electrical proprieties of the two heterojunctions were studied in details.

The third chapter investigates the effect of ZnO buffer layer insertion on the performance of Cu_2O/AZO heterojunction. Since the band offset was high in Cu_2O/AZO heterojunction, we inserted ZnO buffer layer with a different thickness in Cu_2O/AZO to facilitate the electrons transport in the heterojunction. The proprieties of the tri-layer heterojunction is studied in details and we demonstrated the effect of ZnO thickness on Cu_2O/ZnO/AZO heterojunction performance.

In the fourth chapter, we investigated the effect of the absorber layer (Cu_2O) properties on the performance of Cu_2O/ZnO heterojunction. The Cu_2O layer with different thickness was deposited in different alkaline solution (pH 11, 12) onto ZnO/FTO. The structural, optical, morphological and electrical proprieties of the heterojunctions were studied in details to demonstrate the effect of the solution pH on Cu_2O properties and on the heterojunctions properties.

In the fifth chapter, a Cu_2O^+ film of high carrier concentration was deposited, from an alkaline solution (pH 12), onto Cu_2O/ZnO heterojunction to improve its light absorbance and carrier collection length. The Cu_2O^+/Cu_2O/ZnO back surface field device was deposited with different thicknesses of Cu_2O and Cu_2O^+. The structural, optical, morphological and electrical proprieties of the device were studied in details.

Finally, *we* presented general conclusion for this study and suggestions for future research.

References

[1] B. Petroleum, *BP Statistical Review*, (2011).

[2] Renewable Energy Policy Network, *REN 21*, (2017).

[3] N. S. Lewis, *"Basic Research Needs for Solar Energy Utilization: Report on the Basic Energy Sciences Workshop on Solar Energy Utilization."* Argonne National Laboratory, (2005).

[4] E. H. Sims, *"Renewable Energy and Climate Change Mitigation: An Overview of the IPCC Special Report."* Weather Matters for Energy, (2014), pp. 91,

[5] K. L. Chopra, P. D. Paulson, V. Dutta, *Res. Appl.*, **12** (2004) 69.

[6] K. L. Chopra, S. R. Das. *" Thin Film Solar Cells."* Plenum Pr., (1983).

[7] A. Mittiga, E. Salza, F. Sarto, M. Tucci, R. Vasanthi, *Appl. Phys. Lett.*, **88** (2006) 163502.

[8] T. Minami, T. Miyata, K. Ihara, Y. Minamino, S. Tsukada, *Thin Solid Films*, **47** (2006) 494.

[9] K. Fujimoto, T, Oku, T. Akiyama, *Appl. Phys, Express*, **6** (2013) 086503.

[10] M. Izaki, T. Shinagawa, K. T. Mizuno, Y. Ida, M. Inaba, A. Tasaka, *J. Phys. D: Appl. Phys.*, **40** (2007) 3326.

[11] Y. Ievskaya , R.L.Z. Hoye, A. Sadhanala, K. P. Musselman, J. L. MacManus-Driscoll, *Solar Energy Materials & Solar Cells*, **43** (2015) 135.

[12] T. Minami, Y. Nishi, T. Miyata, *Appl. Phys, Express*, **9** (2016) 052301.

[13] S. Major, S. Kumar, M. Bhatnagar, K. L. Chopra, *Appl. Phys Lett.*, **49** (1986) 394.

[14] S. Major, K. L. Chopra, *Solar Energy Mater.*, **17(5)** (1988) 319.

[15] B.E McCandless, S.S Hegedus, *Proceedings of the 22th IEEE Photovoltaic Specialists Conference*, (1991) 967.

[16] K. P. Musselman, A. Marin, A. Wisnet, C. Scheu, J. L. MacManus-Driscoll, L. Schmidt-Mende, *Adv. Funct. Mater.*, **21** (2011) 573.

[17] Y. Hames S. E. San, *Sol. Energy*, **77** (2004) 291.

[18] D. Li, C. J. Chien, S. Deora, P. C. Chang, E. Moulin, J. G. Lu, *Chem. Phys. Lett.*, **501 (**2011**)** 446.

[19] A. R. Zainun, S. Tomoya, U. Mohd Noor, M. Rusop, I. Masaya, *Mater. Lett.*, **66**, (2012) 254.

[20] M. Wang, L. Sun, Z. Lin, J. Cai, K. Xie, C. Lin, *Energ. Environ. Sci.*, **6**, (2013) 1211.

[21] T. Minami, Y. Nishi, T. Miyata, *Appl. Phys. Express*, **6** (2013) 044101.

[22] H. Tanaka, T. Shimakawa, T. Miyata, H. Sato, T. Minami, *Thin Solid Films*, **80-85** (2004) 469.

[23] S. Desgreniers, *Phys. Rev.*, **B 58** (1998) 14102.

[24] P. Povarennykh, A. S.: Crystal Chem., *"Classification of Minerals"*, Plenum Press, New York, Vol.1, 1972.

[25] K. Akimoto, S. Ishizuka, M. Yanagita, Y. Nawa, G.K. Paul, T. Sakurai, *Solar Energy* **80** (2006) 715.

[26] S. Hussain, C. Cao, G. Nabi, W. S. Khan, Z. Usman, T. Mahmood, *Electrochim. Acta* **56** (2011) 8342.

[27] B. M. Fariza, J. Sasano, T. Shinagawa, S. Watase, and M. Izaki, *Thin Solid Films,* **520** (2012) 2261.

[28] P. Mints, Navigant consulting PV services program (2011)

[29] K. Mertens, *"Solar Radiation." PHOTOVOLTAICS: Fundamentals, Technology and Practice*, WILEY-BLACKWELL, 2014, p. 23.

[30] C. M. McShane, K. S. Choi, *Phys. Chem. Chem. Phys.*, **14 (**2012) 6112.

[31] Q. Shu, J. Wei, K. Wang, H. Zhu, Z. Li, Y. Jia, X. Gui, N. Guo, X. Li, C. Ma, D. Wu, *Nano Lett.,* **9** (2009) 4338.

[32] V. S. Taur, R. A. Joshi, A. V. Ghule, R. Sharma, *Renewable Energy,* **38** (2012) 219.

[33] A.P. Young, C.M. Schwartz, *J. Phys. Chem. Solids*, **30** (1969) 249.

[34] J. Katayama, K. Ito, M. Matsuoka, J. Tamaki, *J. Appl. Electrochem.*, **34** (2004) 687.

[35] T. Gershon, K .P. Musselman, A. Marin, R. H. Friend, J. L. MacManus-Driscoll, *Sol. Energ. Mater. Sol. Cells*, **96** (2012) 148.

[36] M. A. Green, M. J. Keevers, *Prog. Photovoltaics,* **3** (1995) 189.

[37] S. S. Seong, A. Mittiga, E. Salza, A. Masci, S. Passerini, *Electrochim. Acta,* **53** (2008) 2226.

[38] L. Olsen, R. Bohara, M. Urie, *Appl. Phys. Lett.*, **34** (1979) 47.

[39] C. D. Gu, C. Cheng, H. Y. Huang, T. L. Wong, N. Wang, T. Y Zhang, *Cryst. Growth Des.*, **9** (2009) 3278.

[40] S. H. Ko, D. Lee, H. W. Kang, K. H. Nam, J. Y. Yeo, S. J. Hong, C. P. Grigoropoulos, H. J. Sung, *Nano Lett.*, **11** (2011) 666.

[41] R. L. Hoffman, B. J. Norris, J. F. Wager, Appl. Phys. Lett., **82** (2003) 733.

[42] J. J. Loferski, *J. Appl. Phys.*, **27** (1956) 777.

[43] J. B. Cui, U. J. J. Gibson, *Phys. Chem. C,* **114** (2010) 6408.

[44] T. Minami, Yuki Nishi, T. Miyata, *Appl. Phys. Express,* **8** (2015) 022301.

[45] T. Minami, Y. Nishi, T. Miyata, S. Abe, *ECS. Trans.*, **50** (2013) 59.

[46] Y. Nishi, T. Miyata, T. Minami, *Thin Solid Films,* **72** (2013) 528.

[47] Y. S. Lee, D. Chua, R. E Brandt, S. C. Siah, J. P. Mailoa, S. W. Lee, R. G. Gordon, T. Buonassisi, *Adv. Mater.*, **26** (2014) 4704.

[48] T. Minami, Y. Nishi, T. Miyata, J. Nomoto, *Appl. Phys. Express*, **4** (2011) 062301.

[49] S. W. Lee, Y. S. Lee, J. Heo, S. C. Siah, D. Chua, R. E Brandt, S. B. Kim, J. P. Mailoa, T. Buonassisi, R. G. Gordon, *Adv. Energy Mater.*, **4** (2014) 1301916.

[50] Y. S. Lee, J. Heo, S. C. Siah, J. P. Mailoa, R. E Brandt, S. B. Kim, R. G. Gordon, T. Buonassisi, *Energy Environ. Sci.*, **6** (2013) 2112.

[51] A. Mittiga, E. Salza, F. Sarto, M. Tucci, R. Vasanthi, *Appl. Phys. Lett.*, **88** (2006) 163502.

[52] T. Minami, H. Tanaka, T. Shimakawa, T. Miyata H. Sato, *J. Appl. Phys.*, **43** (2004) L917.

[53] A.T Marin, D. Munoz-Rojas, D. C. Iza, T. Gershon, K. P. Musselman, J. L. MacManus-Driscoll, *Adv. Functional Mater.*, **23** (2013) 3413.

[54] K. P. Musselman, A. Wisnet, D.C. Iza, H. C. Hesse, C. Scheu, J. L. MacManus-Driscoll, L. Schmidt-Mende, *Adv. Mater.*, **22** (2010) E254.

[55] T. Jiang, T. Xie, Y. Zhang, L. Chen, L. Peng, H. Li, D. Wang, *Phys. Chem. Chem. Phys.*, **12** (2010) 15476.

[56] G. K. Paul, R. Ghosh, S. K. Bera, S. Bandyopadhyay, T. Sakurai, K. Akimoto, *Chem. Phys. Lett.*, **463** (2008) 117.

[57] S. Jeong, E. S. Aydil, *J. Cryst. Growth*, **311** (2009) 4188

[58] B. O'Regan, M. Grätzel, *Nature*, **353** (1991) 737.

[59] S. Sakthivel, M. Janczarek, H. Kisch, *J. Phys. Chem. B*, **108** (2004) 19384.

[60] R. Abe, H. Takami, N. Murakami, B. Ohtani, *J. Am. Chem. Soc.*, **130** (2008) 7780.

[61] N. Serpone, E. Borgarello, M. Grätzel, *J. Chem. Soc., Chem. Commun.*, (1984) 342.

[62] M. Long, W. M. Cai, J. Cai, B. X. Zhou, X. Y. Chai, Y. H. Wu, *J. Phys. Chem. B*, **110** (2006) 20211.

[63] T. Arai, M. Yanagida, Y. Konishi, Y. Iwasaki, H. Sugihara, K. Sayama, *J. Phys. Chem. C*, **111** (2007) 7574.

[64] Q. B. Ma, Z. Z. Ye, H. P. He, S. H. Hu, J. R. Wang, L. P. Zhu, Y. Z. Zhang, B.H. Zhao, *J. Cryst. Growth*, **64** (2007) 304.

[65] L. C. Olsen, R. C. Bohara, M. W. Urie, *Appl. Phys. Lett.*, **34** (1979) 47.

[66] Z. Duan, A. Du Paequier, Y. Lu, Y. Xu, E. Garfunkel, *Sol. Energy Mater. Sol. Cells*, **96** (2012) 292.

[67] D. C. Olson, S. E. Shaheen, M. S. William, J. M. Maikel, F. A. M. V. Hest, R. T. Collins, D. S. Ginley, *Adv. Funct. Mater.*, **17** (2007) 264.

[68] K. P. Musselman , A. Marin , L. Schmidt-Mende , J. L. MacManus-Driscoll, *Adv. Funct. Mater.*, **22** (2012) 2202.

[69]Y. Liu , H. K. Turley , J. R. Tumbleston , E. T. Samulski , R. Lopez , *Appl. Phys. Lett.*, **98** (2011) 162105.

[70] T. Shinagawa, M. Onoda, B. M Fariza, J. Sasano, M. Izaki, *J. Mater. Chem. A*, **01** (2013) 9182.

[71] P. Moller, *NASF Surf. Tech.*, **78** (2014) 10.

[72] S. Yagi, *"Potential-PH Diagrams for Oxidation-State Control of Nanoparticles Synthesized via Chemical Reduction." Thermodynamics- Physical Chemistry of Aqueous Systems*, INTECH Open Access Publisher, 2011, p. 231.

[73] K. Wippermann, J. W. Schultze, R Kessel, J Penninger. *Corros. Sci.*, **32** (1991) 205.

[74] M. Izaki, T. Omi, *J. Electrochem. Soc.*, **143** (1996) L53.

[75] L. Wang, M. Tao, *Electrochem. Solid State Lett.*, **10** (2007) H248.

Chapter 2

Transparent p-Cu_2O/n-ZnO and p-Cu_2O/n-AZO heterojunctions fabricated by electrochemical deposition

Chapter 2: Transparent p-Cu_2O/n-ZnO and p-Cu_2O/n-AZO heterojunctions fabricated by electrochemical deposition

2.1 Introduction

Due to the instability of the p-type ZnO and the difficulty of doping n-type Cu_2O nanostructures, the photovoltaic devices are commonly based on p-Cu_2O/n-ZnO heterojunctions. Actually, this device was prepared by many deposition methods such as pulsed laser deposition (PLD), ion beam sputtering and electrochemical deposition (ECD) [1]. The recorded conversion efficiency was greatly dependent on the deposition method. Where, a conversion efficiency of 2 % has been obtained by ion beam sputtering [2], 1.3 % by electrochemical deposition (ECD) [3], and 1.2 % by pulsed laser deposition (PLD) [4]. Compared to the theoretical values, this efficiency is still low. Improving the conversion efficiency requires the amelioration of ZnO and Cu_2O properties, as well as the ZnO/Cu_2O interface quality. In this context, instead of using a non-doped ZnO thin film, doping ZnO film with group III elements such as gallium (Ga) or aluminum (Al), to obtain high n-carrier concentration, will add flexibility in device fabrication [5]. Minami et al. [6] have reported that a high efficiency of 1.5 % was obtained for Al-doped ZnO (AZO)/Cu_2O structure fabricated by depositing a polycrystalline n-type AZO thin film by PLD method on thermally oxidized polycrystalline p-type Cu_2O sheets. Though a high efficiency was obtained, the high cost of those methods remains major inconvenience, which has drawn attention to the electrochemical deposition as a reliable low-cost method.

In this chapter, p-Cu_2O/n-ZnO and p-Cu_2O/n-AZO heterojunctions were prepared by a simple electrochemical deposition. The morphological, structural, optical and electrical properties of the two heterojunctions were studied in details and the effect of AZO layer on the performance was demonstrated.

2.2 Electrodeposition of ZnO/Cu_2O and AZO/Cu_2O heterojunctions

The two heterojunctions were deposited by electrochemical deposition in a potentiostatic mode, using a computer-controlled Potentiostat/Galvanostat (Voltalab 40) as a potential source relied on a three-electrode cell. The fluorine-doped tin oxide substrate (FTO, 10–20 Ω/cm^2 sheet resistance) is used as a working electrode, a platinum wire as counter electrode and saturated calomel electrode (SCE, + 0.241 V vs. SHE) as a reference electrode. All the potentials reported

with reference to the SCE scale. Prior to the ECD, the FTO substrates were degreased ultrasonically in acetone and ethanol for 10 minutes to remove the organic contamination on the surface then well rinsed with distilled water.

A two steps electrodeposition process is used to form the Cu_2O/ZnO and Cu_2O/AZO heterojunctions. Firstly, we deposited ZnO (or AZO) layer on FTO substrate followed by the deposition of Cu_2O layer on ZnO, as shown in figure 2.1.

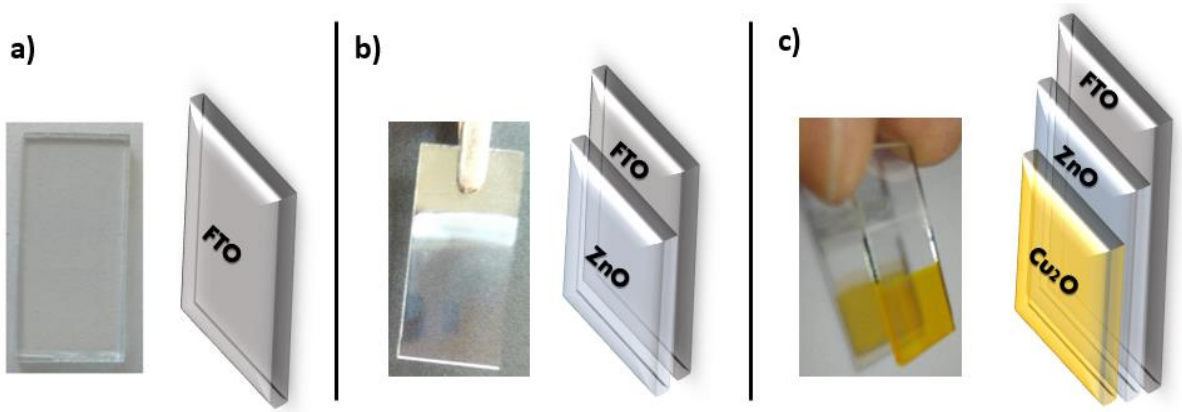

Fig. 2.1. *Schematic diagrams describes the deposition steps of Cu_2O/ZnO transparent heterojunction on FTO substrate.*

A ZnO (or AZO) layer of 200 nm thickness is deposited on FTO substrate at fixed temperature and potential, as described in table 2.1. Then, rinsed with distilled water and air-dried. The Cu_2O layer is deposited on ZnO layer from copper sulfate solution with citric acid as chelating agent and NaOH to adjust the pH to 11 (Table 2.1).The obtained heterojunction was rinsed with distilled water and air-dried. These conditions are the optimal ones for the formation of ZnO, AZO, and Cu_2O layers, they were chosen on the basis of previous studies in our group [7-9].

Using the chronocoulometry method we kept the thickness of ZnO (or AZO) and Cu_2O layers constant at 200 nm and 300 nm, respectively. This method presents the variation of charge quantity (Q) vs. time. As the electrodeposition is a Faradaic charge-transfer reaction, ZnO and Cu_2O layers thickness (d) is estimated from the charge quantity following Faraday's law [10]:

$$d = \frac{QM}{nFA\rho} \qquad (2.1)$$

where M is the molecular weight of the deposited semiconductor, n is the number of electrons exchanged, A is the working electrode area, ρ is the specific density and F is the Faraday

constant. It should be noted that 100 % Faradaic efficiency was assumed in eq. (2.1), which means that every measured electron is from the electrochemical reaction.

Table 2.1. *The electrochemical deposition parameters of ZnO, AZO and Cu_2O layers.*

Layer thickness	**Bath composition**	**pH**	**Temperature** (°C)	**Potential** (V/SCE)
200 nm ZnO	1M KNO_3 0.08M $Zn(NO_3)_2$	6.5	70	-1.3
200 nm AZO	1M KNO_3 0.1M $Zn(NO_3)_2$ 0.005M $Al(NO_3)_3$	6.0	70	-1.7
300 nm Cu_2O	0.05 M $CuSO_4$ 0.05M $C_6H_8O_7$ 4 M NaOH	11	60	-0.5

The conduction type and the carrier concentration were identified by Mott–Schottky (M-S) measurements in 1 M KNO_3 solution and employed frequency of 0.2 kHz for ZnO and AZO layers and in 0.5 M Na_2SO_4 solution with a frequency of 20 kHz for Cu_2O layer. The films morphology was characterized using a field emission scanning electron microscope (FE-SEM) and confirmed by atomic force microscopy (AFM, MFP-3D Asylum Research). The roughness (root-mean-square height deviation) of the samples was obtained directly from the software of the AFM (PicoScan 5.3 from molecular imaging). The crystallographic structure was identified using X-ray diffraction (XRD) on a Rigaku Smartlab® X-ray diffractometer with a $CuK\alpha_1$ radiation (45 kV, 200 mA, λ=0.154056 nm) in the range of 25°-80° of 2θ range. Photoluminescence (PL) spectra were performed at room temperature using the 355 nm line employing a ~~4~~-Nd–YAG laser from Kimmon® Electric model IK3101 R-D. The laser pulse frequency and power were of 20 kHz and 100 mW (15.6 $W.cm^{-2}$), respectively. The optical properties of the heterostructure were carried out with a UV–Vis-NIR spectrophotometer (Shimadzu UV-2401PC) in the UV-visible region. The spectras were corrected to FTO glass substrates contribution. The current-voltage measurement (I-V) were recorded using a picoammeter (Keithley 617) at room temperature. To ensure an ohmic contact on the surface Cu_2O layer, we have deposited gold pads by DC reactive sputtering the ohmicity of these contacts was verified by I–V measurement.

2.3 Results and discussion

2.3.1 Electrochemical characterization

In order to understand the electrical properties of the electrodeposited Cu_2O/ZnO and Cu_2O/AZO heterojunctions, we performed electrochemical impedance. Effectively, the conduction type, the flat band (E_{fb}), and the estimated donor/acceptor densities of ZnO, AZO, and Cu_2O layers were determined by studying the semiconductor/electrolyte interface using Mott–Schottky (M–S) measurements. Where, the depletion layer capacitance C^{-2}vs. E was measured at a fixed frequency and presented as an M–S plot following the equation [11, 12]:

$$\frac{1}{c^2} = \frac{2}{eN_D \varepsilon \varepsilon_0}\left(E - E_{fb} - \frac{kT}{e}\right) \text{ For n-type semiconductor} \quad (2.2)$$

$$\frac{1}{c^2} = \frac{2}{-eN_A \varepsilon \varepsilon_0}\left(E - E_{fb} - \frac{kT}{e}\right) \text{ For p-type semiconductor} \quad (2.3)$$

where C is the space charge capacitance, e is the electron charge, N_A and N_D are the acceptor and donor concentration of p-type and n-type semiconductors, respectively. ε_o is the vacuum permittivity, ε is the dielectric constant of 8.5 for ZnO and AZO [13] and 7.6 for Cu_2O [14], k is the Boltzmann constant, T is the absolute temperature, E is the applied potential and E_{fb} is the flat-band potential. Figure 2.2 presents the M-S plots of 200 nm ZnO, 200 nm AZO and 300 nm Cu_2O layers deposited on FTO glass substrate.

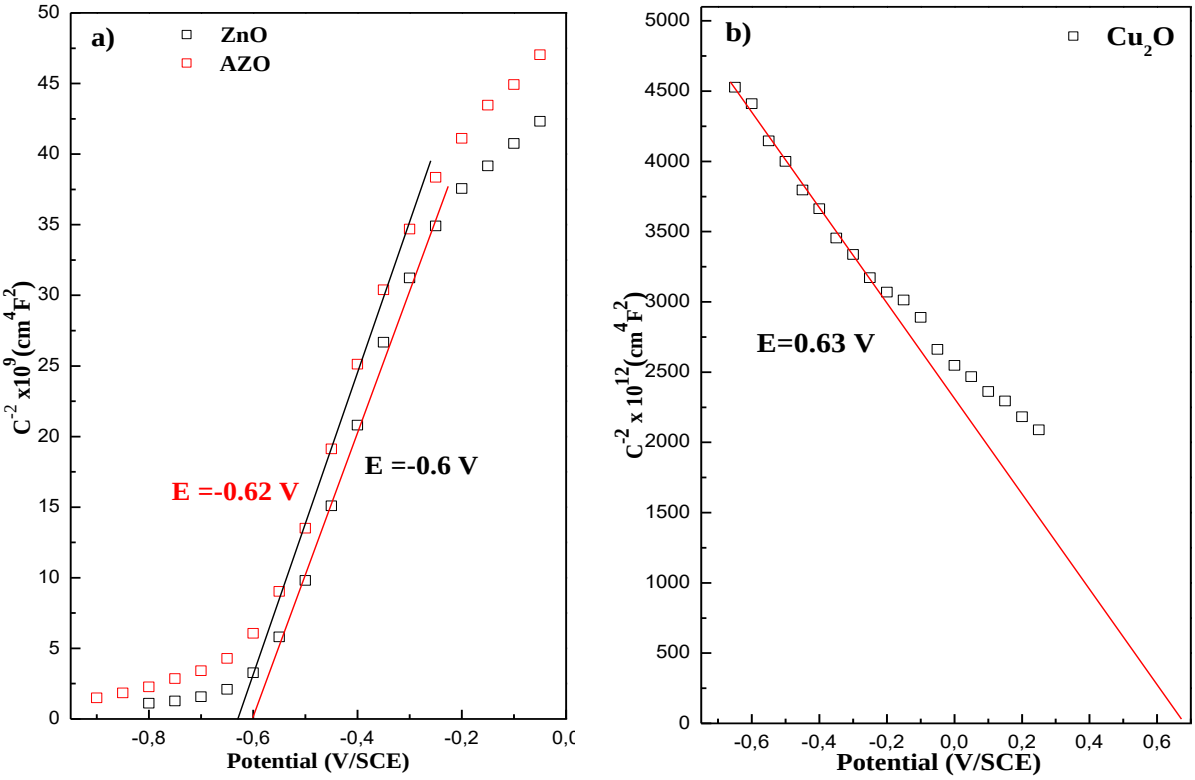

Fig. 2.2. *Mott–Schottky plots of the electrodeposited:* ***a)*** *200 nm ZnO and 200 nm AZO layers.* ***b)*** *300 nm Cu_2O layer.*

According to Mott–Schottky equation, a linear relationship of $(1/C_{CS}^2)$ vs. E should be observed. As can be seen from M-S plots in figure 2.2, straight lines were obtained with a positive slope for ZnO and AZO layers and a negative slope for Cu_2O layer. This confirms n and p-type semiconductor characteristics of these layers, respectively. It is well established that the acceptor and donor densities can be calculated from the M-S plot slope $(2/(N_D \varepsilon\varepsilon_0 e))$, also the intercept at $(1/C_{CS}^2)=0$ equal to $E_{fb}+(kT/e)$. The donor concentration of 200 nm n-ZnO layer was 9.50×10^{19} cm^{-3}, while the 200 nm AZO layer show higher donor concentration of 1.04×10^{20} cm^{-3}, due to the dopant effect of aluminum that increases dramatically ZnO layer conductivity. Those values are within the typical range reported in the literature [15]. On the other hand, the acceptor concentration of Cu_2O was 5.8×10^{15} cm^{-3} which is in accord with the values obtained for Cu_2O formed by electrochemical deposition [16].

The flat band potentials (E_{fb}) noted from M-S plots were -0.6, -0.62 and 0.63 V for ZnO, AZO and Cu_2O layers, respectively. The flat band potential (E_{fb}) can be converted to Fermi level energy (E_f) using the following equations [17].

$$E_{fb}\ (in\ V\ vs.\ NHE) = -\ E_f\ (in\ eV\ vs.\ vacuum) + V_H\ (in\ V) - 4.5 \quad (2.4)$$

$$V_H\ (in\ V) = 0.059\ (pH_{PZZP} - pH) \quad (2.5)$$

where E_{fb} is -0.35, -0.37 and 0.87 V/NHE for ZnO, AZO and Cu_2O, respectively; V_H is the potential drop across the Helmholtz layer and pH_{PZZP} is the point of zero zeta potential. When using pH_{PZZP} of Cu_2O (8.5) and ZnO (8.8) from the literature [18], the estimated Fermi level energies for n-ZnO, n-AZO, and p-Cu_2O were -4.0, -3.9 and -5.22 eV vs. the vacuum, respectively. The actual Fermi levels of ZnO, AZO, Cu_2O layers may differ slightly from the values estimated from the Mott–Schottky plots.

2.3.2 Structural characterization

To confirm the purity and the structural characteristic of the deposited heterojunctions, X-ray diffraction analysis was used. Figure 2.3 shows the XRD patterns of Cu_2O/ZnO and Cu_2O/AZO heterojunctions deposited on FTO glass substrate, with a reference profiles of the Cu_2O cubic structure (JCPDS card n_ 00-034-1354) and ZnO wurtzite structure (JCPDS card n_ 00-036-1451) given as a bar graph.

All the peaks in the patterns correspond to the hexagonal wurtzite and cubic type structures of the ZnO and Cu_2O crystallites, respectively. No phases corresponding to others compounds

were detected by XRD in the detection limit of our technique. In fact, for the two heterojunctions, all the peaks correspond to the reflections from (101) orientation of ZnO wurtzite (JCPDS card n° 00-036-1451) and to (111), (200), (220) and (311) planes of Cu_2O cubic phase (JCPDS card n° 00-034-1354).

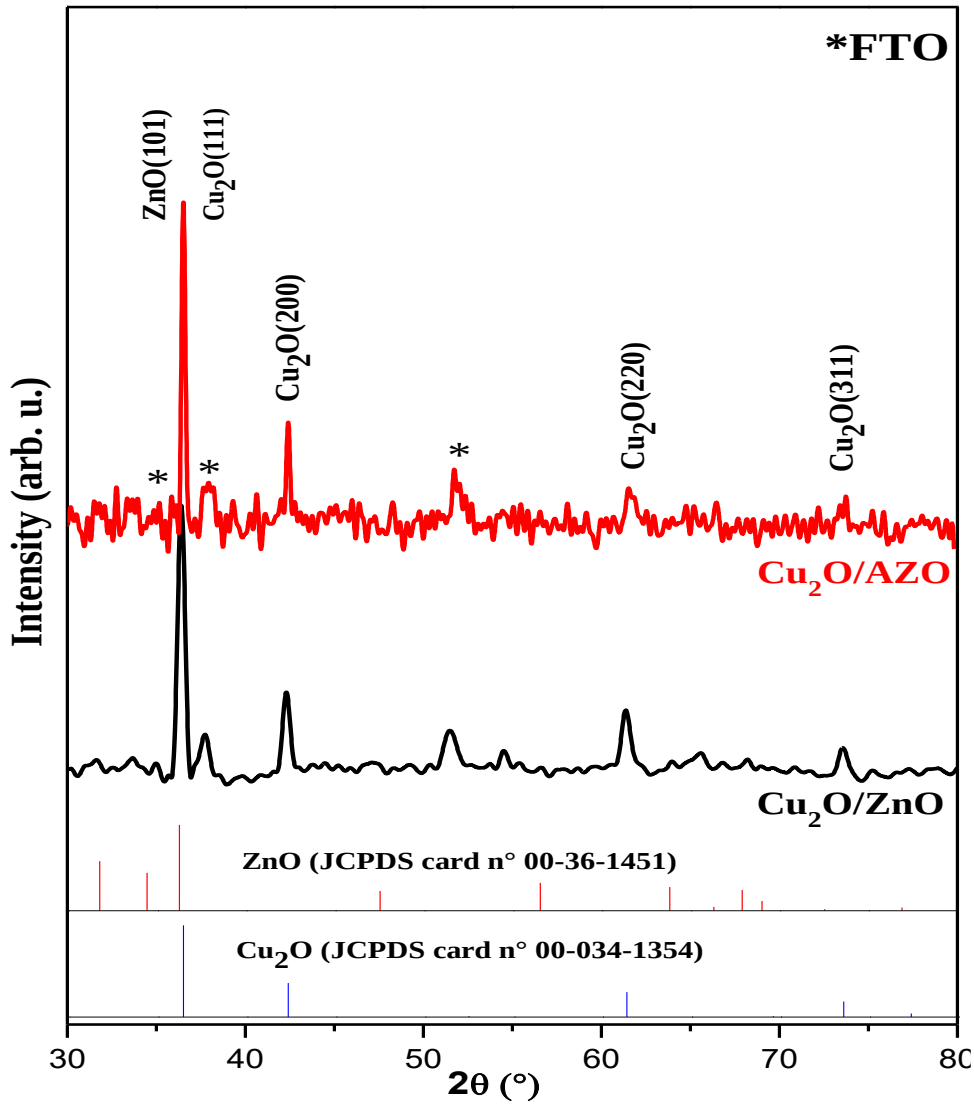

Fig. 2.3. *X-ray diffraction patterns of Cu_2O/ZnO and Cu_2O/AZO heterojunctions. Asterisks mark the XRD peaks of the FTO substrate. The reference profile of cubic Cu_2O (JCPDS card n_00-034-1354) and wurtzite ZnO (JCPDS card n_ 00-036-1451) are given as a bar graph.*

However, the peaks position was slightly shifted to higher values for Cu_2O/AZO heterojunction, indicating the incorporation of Al atoms in ZnO lattice [8]. Furthermore, the sharp and narrow peaks indicate that the nanostructures are highly crystallized, notably, the intensive peak of Cu_2O (111) and ZnO (101). Moreover, the small width at half maximum of the preferential orientations indicates a good crystallization and a large crystallite size.

The average crystallites size can be estimated from the full width at half maximum (FWHM) values of the diffraction peaks. Effectively, an average size of the crystallites in the

perpendicular direction to the plane of the films could be obtained using the Scherrer equation [19]:

$$D = \frac{k\,\lambda}{\beta \cos\theta} \tag{2.6}$$

where D is the mean crystallites size, β is the full-width at half maximum of the diffraction peak, θ is the Bragg angle, K is the shape factor and usually takes a value of 0.94, and λ is the wavelength of the incident X-ray (1.54056 Å). Considering the overlapping of the ZnO (101) diffraction peak with the Cu_2O (111) diffraction peak, we take the Cu_2O (200) diffraction peak to calculate the average crystallites size of Cu_2O [20] using the Scherrer formula. The crystallites sizes estimated from the XRD spectra of Cu_2O/ZnO heterojunction were 35.2 and 36.6 nm for ZnO and Cu_2O, respectively. While the crystallites sizes estimated from the XRD spectra of Cu_2O/AZO heterojunction were 67.7 nm and 72.2 nm for AZO and Cu_2O, respectively. Comparing the results, Cu_2O/AZO heterojunction show a higher crystallites sizes. According to Zhang et al. [21], different crystallite sizes contain different dislocation defects, which have a great effect on the charge transport mechanism in the heterojunction.

2.3.3 Morphological characterization

The samples morphology was studied by field emission scanning electron microscopy (FE-SEM) and atomic force microscopy (AFM) techniques. The plane-view and cross-section FE-SEM images, at 45° inclination, of Cu_2O/ZnO and Cu_2O/AZO heterojunctions are shown in figure 2.4.a-b, respectively. From the observation of the plane-view of the two heterojunctions shown in fig. 2.4, a well-defined a cubic Cu_2O grains (Fig. 2.4a) can be clearly seen over the entire surface of ZnO layer. The cubic grains diameter, estimated by Visiometre software, was approximately between 600 and 900 nm. On the other hand, the whole surface of AZO layer (Fig. 2.4b) was covered by pyramidal shaped Cu_2O grins, with a diameter between 400 and 600 nm, overlapping on top of each other to form a dense film of Cu_2O.

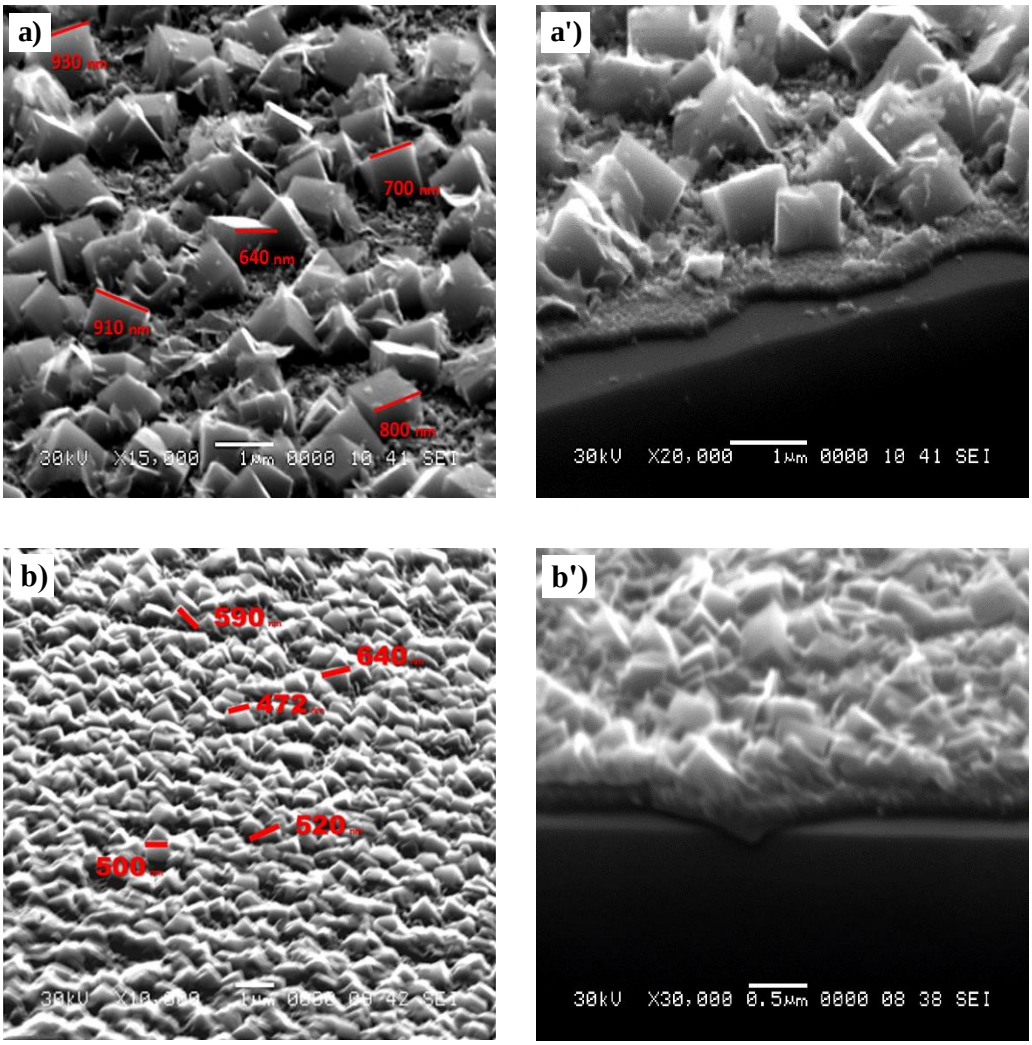

Fig. 2.4. *Typical top view FE-SEM images of* ***a)*** *Cu_2O/ZnO heterojunction and* ***b)*** *Cu_2O/AZO heterojunction.* ***a')-b')*** *the cross-section FE-SEM images of the respective heterojunctions.*

The cross-section image of Cu_2O/ZnO in figure 2.4a' shows a good coverage of the FTO substrate with ZnO layer. This latter presented high quality and homogeneity with a uniform thickness. The Cu_2O cubic grains grew all over the ZnO surface, no pores or defects could be observed. Likewise, the cross-section image of Cu_2O/AZO in figure 2.4b' shows dense film of Cu_2O totally covering a uniform layer of AZO.

Figure 2.5 displays the 3D and 2D AFM images of Cu_2O layer, Cu_2O/ZnO, and Cu_2O/AZO heterojunctions deposited on FTO recorded in the tapping mode. The pure Cu_2O layer shows a rough surface of cubic and pyramidal grains (Fig. 2.5a) with a size between 100 and 400 nm. While Cu_2O layer deposited on ZnO (Fig. 2.5b) shows homogenous pyramidal grains of size between 400 and 900 nm, confirming the results observed by FE-SEM measurements. It is clear that Cu_2O islands coalesced with each other to form a homogenous film, the root mean square (RMS) was 21.3 nm which is slightly lower than the RMS of pure

Cu_2O/FTO (23.3 nm) layer. On the other hand, Cu_2O layer deposited on AZO film (Fig. 2.5c) show mixture of small and large pyramidal shaped grains of Cu_2O, which form inhomogeneous rough surface.

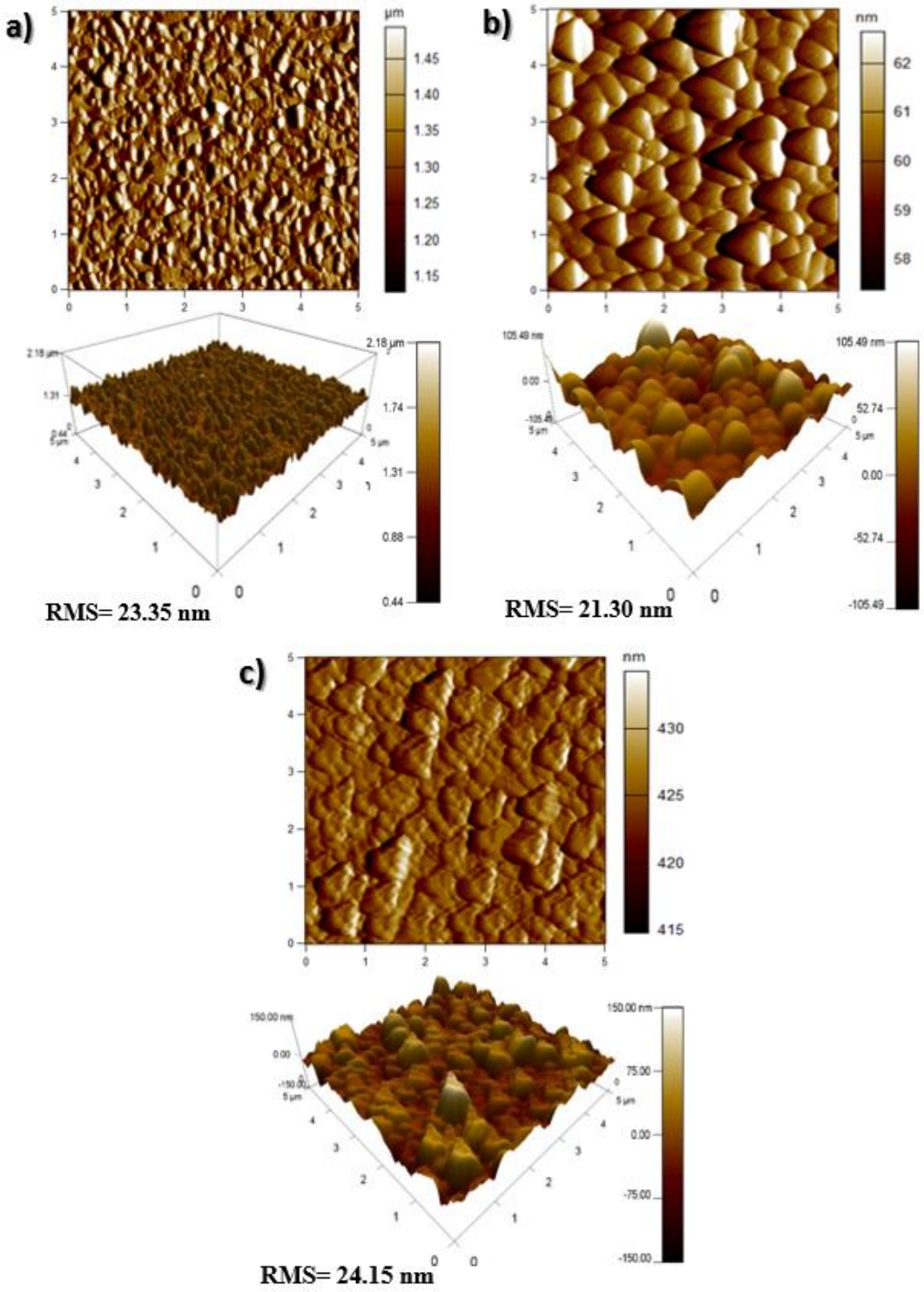

Fig. 2.5. *Tapping mode 2D and 3D AFM images (5×5 µm^2) of:* ***a)*** *Pure 300 nm Cu_2O layer,* ***b)*** *Cu_2O/ZnO heterojunction and* ***c)*** *Cu_2O/AZO heterojunction.*

2.3.4 Optical characterization

3.4.1 Photoluminescence analysais

The ZnO and Cu_2O have a high exciton binding energy of 60 and 150 meV at room temperature [22, 23], which makes them ideal materials for electro-optical devices. In order to obtain information about the excitons generation, recombination and transportation, also to illustrate the band-to-band, sub-band energy transitions and the interfacial energy band structure of Cu_2O/ZnO heterojunction, an analysis photoluminescence (PL) is employed. Figure 2.6a shows the room temperature PL spectra of Cu_2O/ZnO heterojunction.

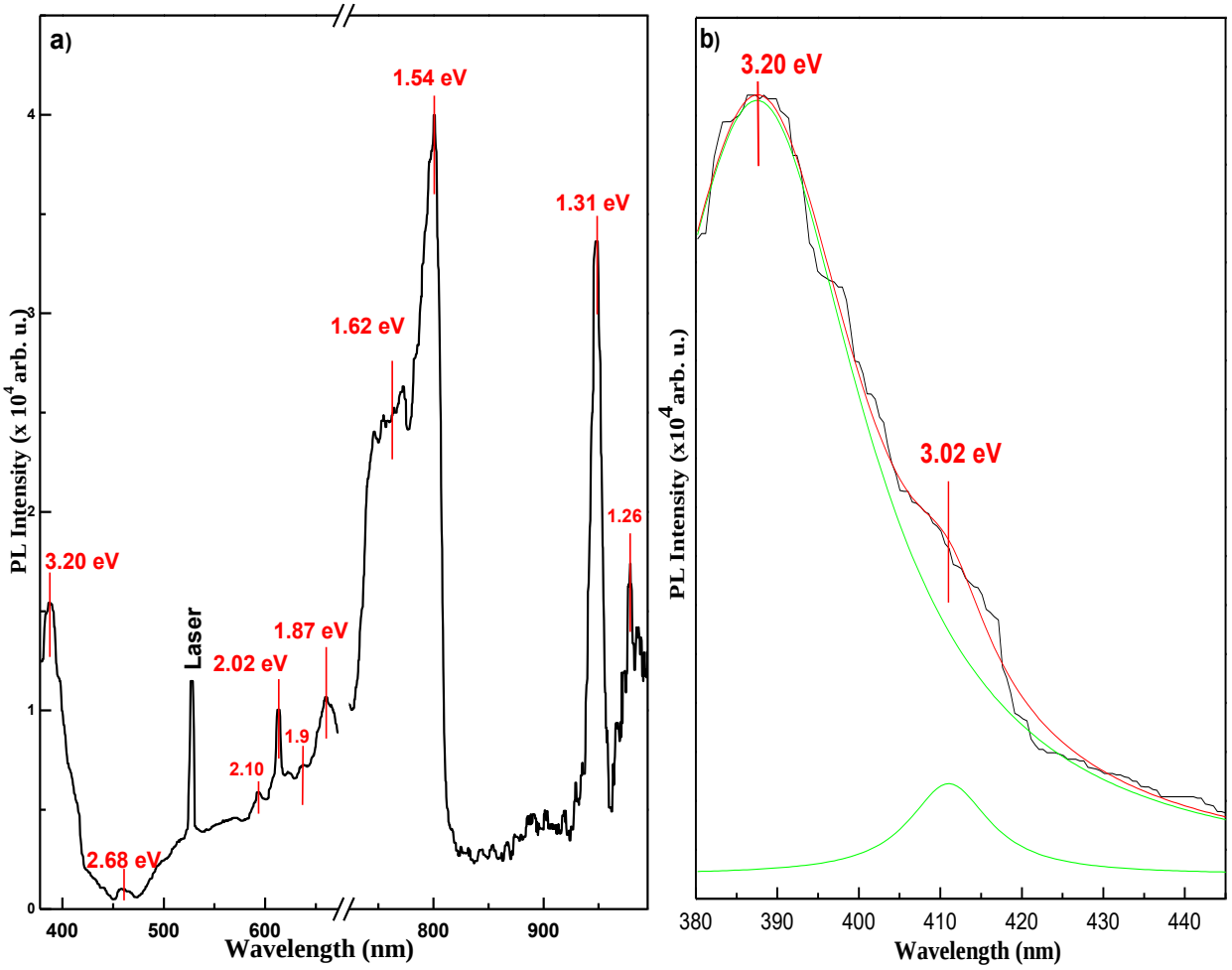

Fig. 2.6. *Photoluminescence emission spectra of:* ***a)*** *Cu_2O/ZnO heterojunction and* ***b)*** *Fitting the first peak of PL spectra (380 nm-440 nm).*

In our investigation, we used the energy levels diagram of ZnO reported by Fan et al. [24] as reference to identify all the emissions of ZnO in our sample. This diagram was constructed based on the energy levels of the intrinsic defects in ZnO calculated by the full potential linear muffin-tin orbital method. The PL spectra in the figure.2.6a reveals a strong and sharp ultraviolet (UV) emission centered at 387 nm (3.20 eV), which coincide with the ZnO near-

band-edge (NBE) electron transition between the valence band and the conduction band. The fitting of this peak is shown in figure 2.6.b, where the black line is the original data, the green lines are the Lorentzian multiple peak fitting curves and the red line, which fitted the original signal well, is the sum of the green lines.

From the fitting curve, a weak peak was noted at 410 nm (3.02 eV) which is attributed to the interstitial zinc (Zn_i) level or to the zinc vacancy (V_{Zn}) level. As the Zn_i defects have very low formation energy [25], we attribute this emission to the transition from the Zn_i to the valence band. Another strong peak was observed at 762 nm (1.62 eV), this match well the energy interval from the conduction band bottom to the oxygen vacancy (V_O) donor level of 1.62 eV. These results confirm that the n-type conductivity of ZnO is attributed to the zinc interstitials and oxygen vacancies native defects. Where the V_O forms a very deep donor level, while, the Zn_i creates a shallow donor level in the forbidden band of ZnO. On the other hand, the Cu_2O has two main groups of PL signals; from 450 to 650 nm range the free excitons, and bound exciton region and from 630 to 1200 nm extend the region of relaxed excitons at oxygen and copper vacancies [26]. Thus, the two emissions noted at 460 nm (2.68 eV) and 593 nm (2.10 eV) are originated from the free excitons. The emission at 610 nm (2.02 eV) corresponds to the direct exciton recombination (X_0-line) without phonons participation [27]. The emission at 802 nm (1.54 eV) corresponds to the recombination of bound excitons at oxygen vacancy to the single charged oxygen vacancy (V_O^+) [28].

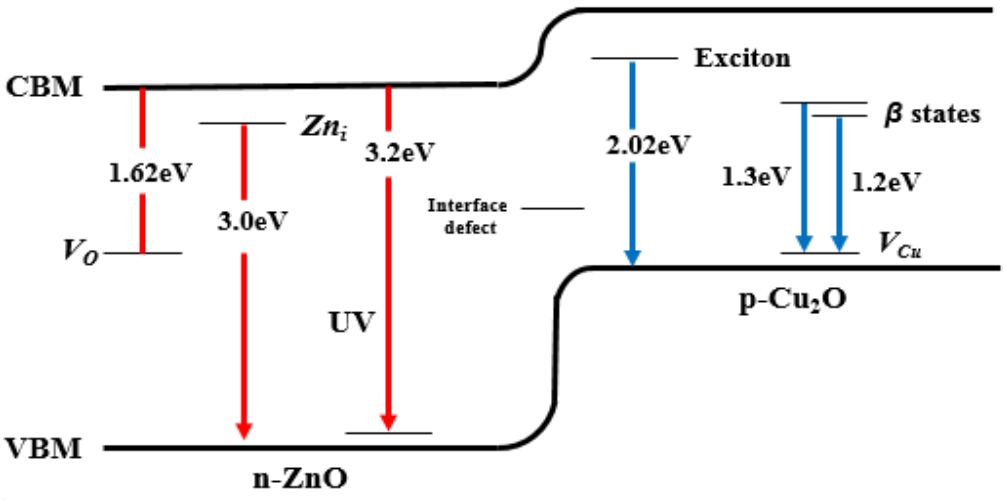

Fig. 2.7. *Schematic energy band diagram of the electrodeposited Cu_2O/ZnO heterojunction.*

The two peaks noted at 945 nm (1.31 eV) and 979 nm (1.26 eV) are attributed to the recombination of bound excitons at copper vacancies (V_{Cu}, β-state) to the copper vacancies level (V_{Cu}) known as β-luminescence series [27, 29]. In our sample, the band at 945 nm related to the copper vacancies (V_{Cu}) was the dominant emission indicating that the p-type conductivity of Cu_2O is attributed to copper vacancies.

The peak at 635 nm (1.95 eV) is due to the large lattice mismatch between Cu_2O and ZnO that create an interfacial defect, which induces new energy level in Cu_2O/ZnO interface. The Cu_2O/ZnO junction shows a new wavelength luminescence due to the formation of the nano-heterojunctions. Based on the PL spectra, we constructed a schematic diagram of the energy levels of defects in Cu_2O/ZnO heterojunction as given in figure 2.7.

3.4.2 UV-Vis analysis

The light absorption–transmission ability is an important factor in evaluating the optical performance of the conductive oxide films. In this section, we investigated the absorbance propriety of Cu_2O/ZnO and Cu_2O/AZO heterojunctions, then compared it with the pure ZnO and AZO layer absorbance before the deposition of Cu_2O. Fig. 2.8a presents the UV-vis absorbance spectra recorded in reference to FTO substrate for all the samples.

As can be seen from figure 2.7a, the ZnO and AZO layers show strong absorbance peak in the UV region with no significant absorbance in the visible region. Comparing the edges of the absorbance peaks, it is clear that ZnO absorbance peak started from higher wavelength (365 nm) than that of AZO layer (350 nm). This blue shift can be explained by the large band gap of AZO layer compared to ZnO. Turning to the absorbance of the Cu_2O/ZnO and Cu_2O/AZO heterojunctions (Fig.2.8a), the deposition of Cu_2O on ZnO (or AZO) induce a red-shift of the absorbance peaks, from UV to the visible region. This shift is due to the combination of Cu_2O narrow band gap with the large band gap of ZnO and AZO, which offer to the heterojunctions better benefit of the sunlight as the energy of the solar light has a maximum in the visible region. It is important to note that Cu_2O/ZnO heterojunction shows larger and higher absorbance peak in the visible region compared to Cu_2O/AZO heterojunction.

Figure 2.8b shows the optical transmittance spectra of Cu_2O/ZnO and Cu_2O/AZO heterojunctions. A transmittance of 50 and 70 % were noted for Cu_2O/ZnO and Cu_2O/AZO, respectively. The two samples present a high transmittance in the visible region. Thus, the

incident light higher than 450 nm can penetrate throughout the whole heterojunction, while the transmittance of incident irradiation lower than 450 nm is almost zero.

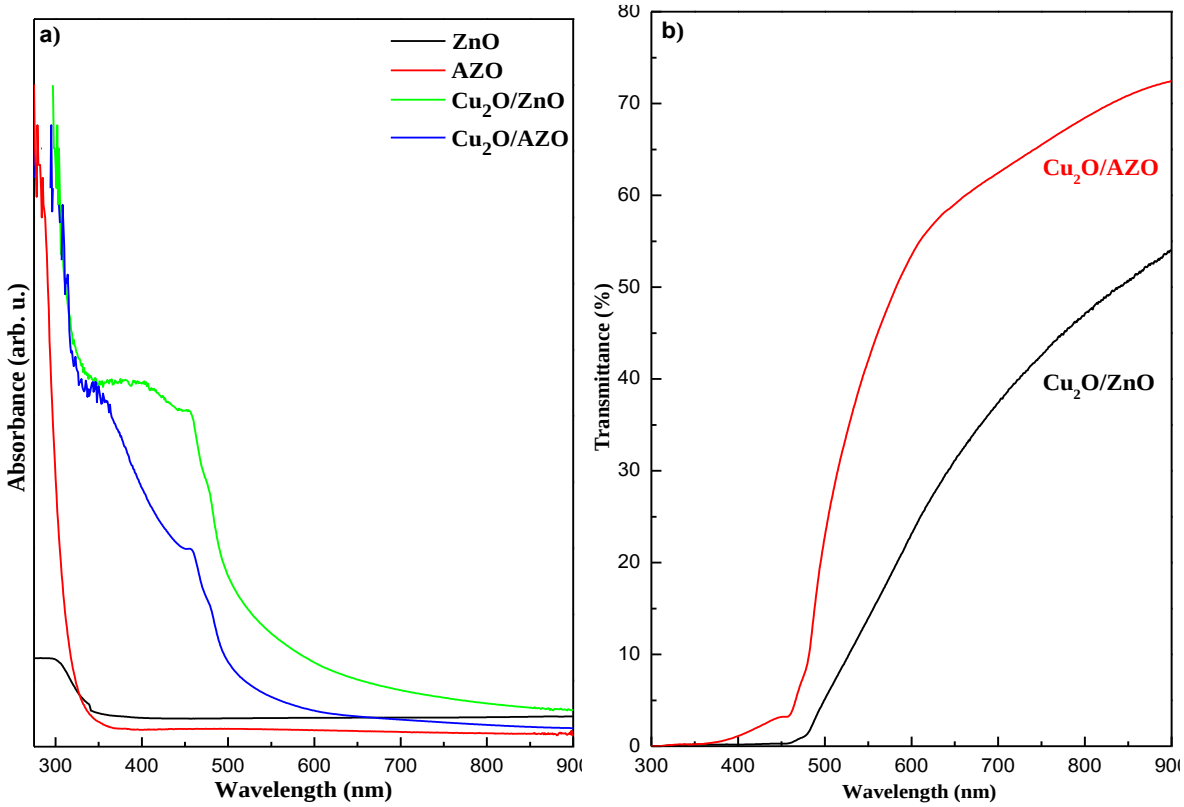

Fig. 2.8. a) *UV–Vis absorbance spectras of pure AZO layer, ZnO layer, Cu_2O/ZnO and Cu_2O/AZO heterojunctions.* ***b)*** *UV-vis transmittance spectras of Cu_2O/ZnO and Cu_2O/AZO heterojunctions.*

This indicates that small amount of photons can reach the interface between n- ZnO (or n-AZO) and p-Cu_2O at 450 nm and shorter wavelength if the light irradiates from n-ZnO (or n-AZO) side of the heterojunction.

The optical band gap energies of the Cu_2O and ZnO thin films were determined through the plot of the so-called Tauc relation [30]:

$$(\alpha h\nu) = A(h\nu - E_g)^n \qquad (2.7)$$

where α is the absorption coefficient and hν is the photon energy, A is a constant, Eg is the band gap of the material, n is a number that depends on the nature of the transition. It was found that n = 1/2 is the best fit for our results and is a characteristic of the direct band gap materials. Accordingly, the optical band gap Eg is obtained from the intercept of the straight-line portion of the curves at α=0 in the Tauc plot [31]. Figure 2.9 shows the plot of $(\alpha h\nu)^2$ versus the photon

energy (hν) from which the Cu_2O/ZnO and Cu_2O/AZO optical band gap energies were determined.

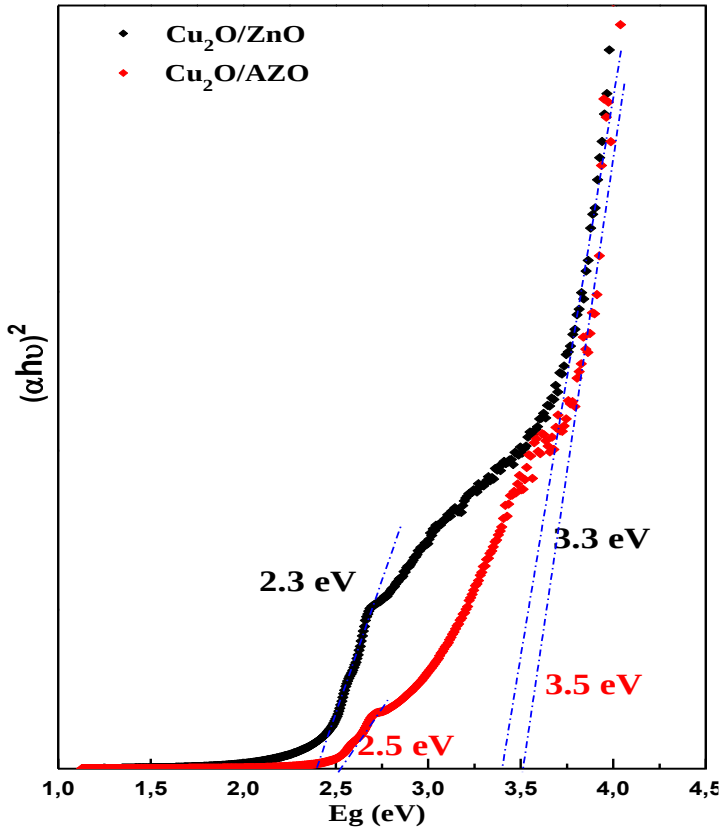

Fig. 2.9. *Tauc's plots of Cu_2O/ZnO and Cu_2O/AZO heterojunctions.*

The band gap values estimated for Cu_2O/ZnO heterojunction are 3.3 and 2.3 eV for ZnO and Cu_2O, respectively. While the second heterojunction shows two band gap values of 3.5 and 2.5 eV for AZO and Cu_2O, respectively. As figure 2.9 shows, there is a blue shift of the Cu_2O band gap values in the two heterojunctions, which is associated with the increase in carrier concentration corresponding to a shift of the Fermi level within the conduction band [32], compared to the bulk Cu_2O (2.17 eV). This increase may be attributed to quantum confinement effects [33].

2.3.5 Electrical characterization

To investigate the performance of the two heterojunctions we used I-V characterization. Au pads were deposited on Cu_2O film to form Au/Cu_2O/ZnO/FTO and Au/Cu_2O/AZO/FTO heterojunction diodes. Before the measurements, we confirmed that both FTO and Au/Cu_2O electrodes show ohmic behavior. The current-voltage curves recorded in the dark for Au/Cu_2O/ZnO/FTO and Au/Cu_2O/AZO/FTO heterojunctions are presented in figure 2.10.

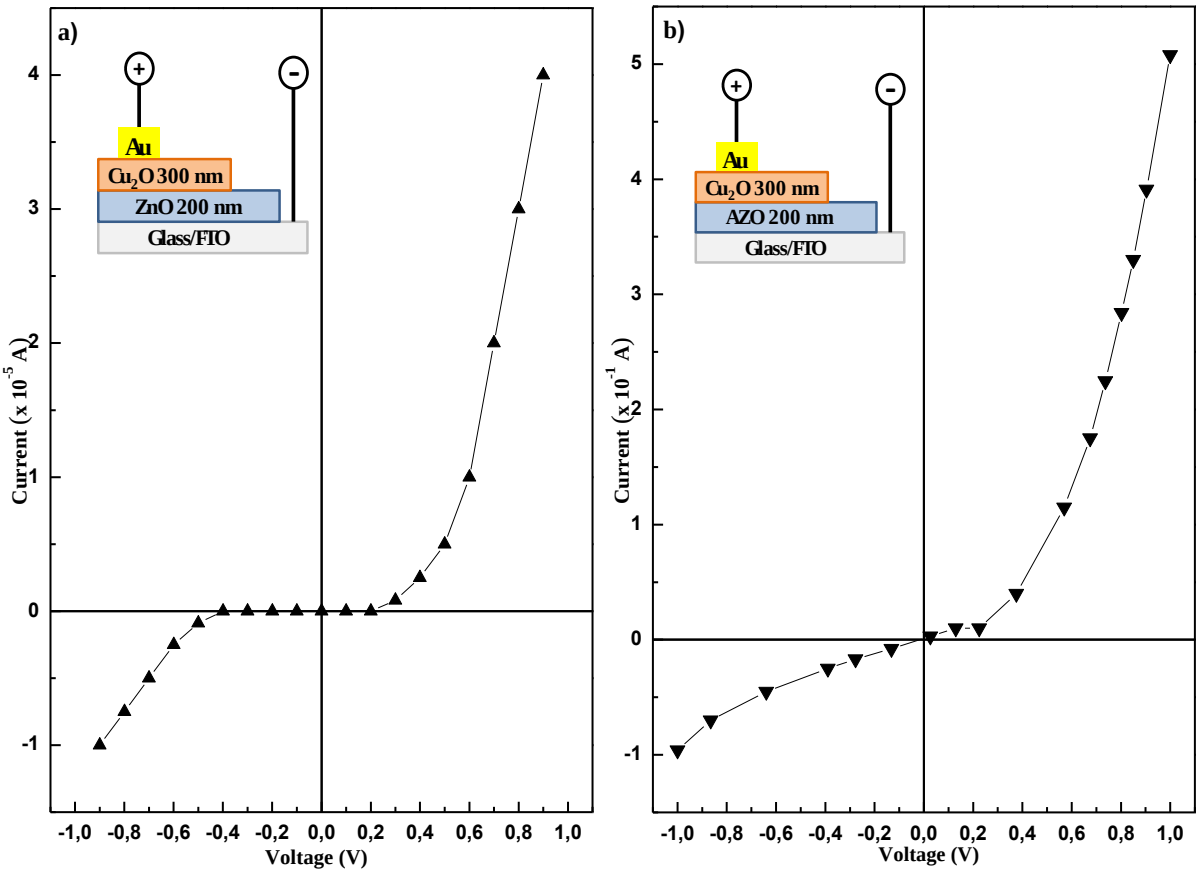

Fig. 2.10. *Current –voltage characteristics of:* ***a)*** *Au/p-Cu_2O/n-ZnO/FTO and* ***b)*** *Au/p-Cu_2O/n-AZO/FTO heterojunctions in dark. The upper inset image shows the device structure.*

The p-Cu_2O/n-ZnO presents significant rectification behavior (Fig. 2.10a). Moreover, the rectifying characteristics were reproducible and stable, indicating that a p–n junction is successfully formed in p-Cu_2O/n-ZnO. In the absence of defect states, the built-in potential of heterojunctions is equal to the difference in the work function between two semiconductors. Therefore, it is predicted to be ~ 1.0 eV for the ideal case. The turn on voltage estimated from the dark I-V curves for Cu_2O/ZnO heterojunction was 0.5 eV, which is comparable with other studies [34] and can be attributed largely to the presence of defect states. In the reverse bias we noted a slight leakage current, for example, at a reverse bias of -0.5V, the leakage-current was -5.0×10^{-6}A. On the other hand, the p-Cu_2O/n-AZO does not show fairly rectifying behavior (Fig. 2.10b). As the bias voltage increase, the reverse current is as large as the forward current, a high leakage current of 5×10^{-2} A was noted, which is due to the carrier leakage and the trap-assisted tunneling [34] attributed to the interface defect states between p-Cu_2O and the n-AZO layer.

A comparison of the two I-V curves reveals that p-Cu_2O/n-ZnO show better performance than that of p-Cu_2O/n-AZO. Surprisingly, p-Cu_2O/n-AZO show a poor performance despite the good conductivity of Al-doped ZnO compared to the non-doped ZnO. Thus, it can be suggested that

the alignment of the energy bands in p-Cu_2O/n-ZnO heterojunction is better, i.e. the band offset in p-Cu_2O/n-ZnO heterojunction is lower than that in p-Cu_2O/n-AZO heterojunction, as the band offsets are critical to many properties such as quantum confinement [35]. To confirm this hypothesis we construct the band diagram of the two heterojunctions.

To construct the band diagram, the model proposed by Anderson [36] will be used here. As described in the following equation:

$$\Delta E_c = \chi_2 - \chi_1 \tag{2.8}$$

$$\Delta E_v = Eg_2 - Eg_1 + \Delta E_c \tag{2.9}$$

where ΔE_c is the conduction band offset, ΔE_v is the valence band offset, χ is the electron affinities and Eg is the band gap energy. In our calculation, the electron affinities (χ) were assumed to be 4.6, 4.2 and 3.2 eV for AZO, ZnO, [37] and Cu_2O [38] semiconductors, respectively. The Fermi level energies estimated from Mott–Schottky analyses were - 4.0, -3.9 and -5.2 eV for ZnO, AZO and Cu_2O, respectively. Also, the measured band gap energies (Eg) of p-Cu_2O/n-ZnO were 3.3 eV for ZnO and 2.3 eV for Cu_2O, while the band gap energies obtained from p-Cu_2O/n-AZO were 3.5 and 2.5 eV for AZO and Cu_2O, respectively. The energy-band diagrams of the two heterojunctions are shown in figure 2.11.

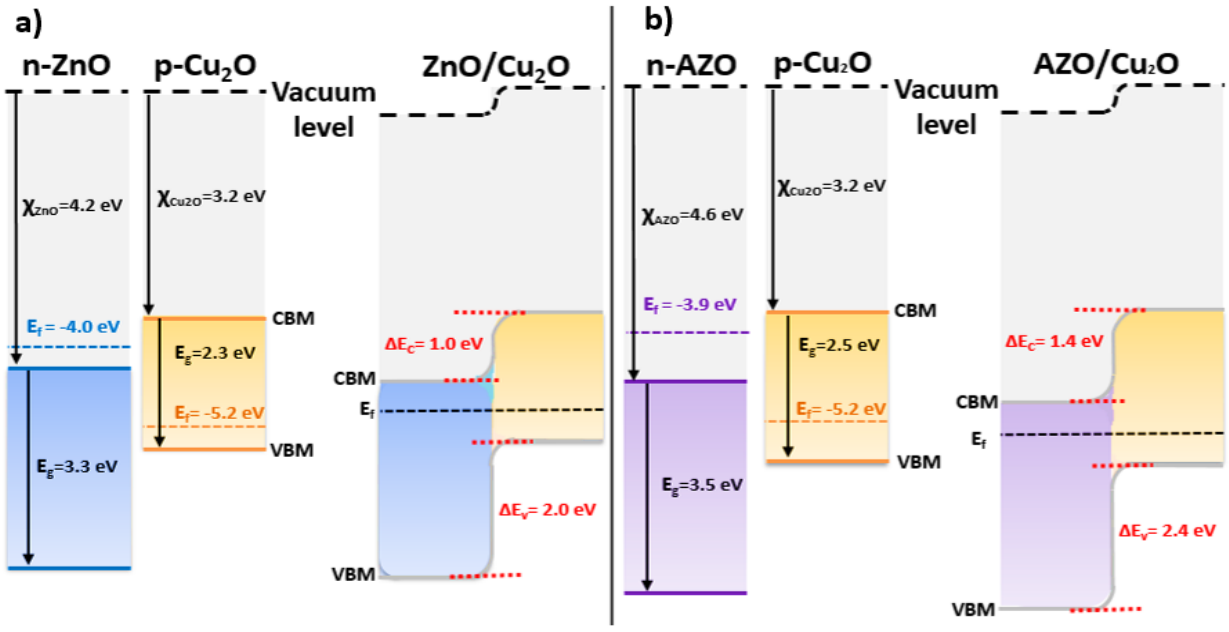

Fig. 2.11. *Band diagrams of:* ***a)*** *Isolated states of n-ZnO, p-Cu_2O and p-Cu_2O/n-ZnO heterojunction under equilibrium condition,* ***b)*** *Isolated states of n-AZO, p-Cu_2O and p-Cu_2O/n-AZO heterojunction under equilibrium condition.*

As the two materials p-type Cu_2O and n-type ZnO are brought into contact (Figure 2.11a), a constant Fermi-level formed at equilibrium. This is caused by the transfer of electrons in the n-ZnO layer to the p-Cu_2O layer. At the same time, in the opposite direction, the holes in the Cu_2O layer are transferred until the equilibrium. The calculated conduction band offset (ΔE_c) was 1.0 eV, and the valence band offset (ΔE_v) was 2.0 eV. The large valence band offset and the small conduction band offset should results in an easy way for electron injection from the n-type ZnO to the p-type Cu_2O and blocks the holes injection from the p-to-n side under the forward applied voltage. On the other hand, the band diagram of p-Cu_2O/n-AZO heterojunction in figure 2.10b revealed a conduction band offset (ΔE_c) of 1.4 eV, and a valence band offset (ΔE_v) of 2.4 eV. The large ΔE_c hinder the injection of electrons from the n-type side to the p-type side. Which explain the poor performance of p-Cu_2O/n-AZO heterojunction.

The performance of Cu_2O/ZnO heterojunction was investigated under the illumination (100 mW/cm^2) using I-V measurement. Figure 2.12 reveals the current-voltage curve of the Au/Cu_2O/ZnO/FTO heterojunction with and without light illumination.

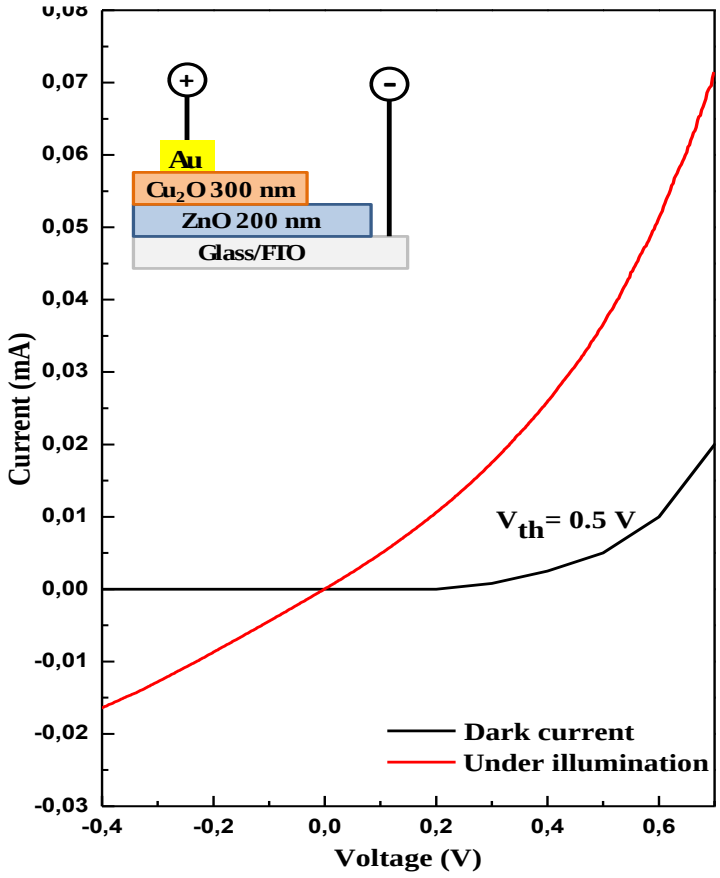

Fig. 2.12. *Current –voltage characteristics of Au/p-Cu_2O/n-ZnO/FTO heterojunction in dark and under illumination. The upper inset shows the structure of the device.*

During the measurement, we applied the light from Cu_2O layer side. It is clear that the response of the heterojunction significantly changed under illumination, at the forward bias the current significantly increases. The photoresponse (I_{ph}) of the junction was calculated by the following equation [39]:

$$I_{ph} = \frac{I - I_d}{I_d} \tag{2.10}$$

where I is the current noted under the light and I_d is the current noted in the dark.

For an applied potential of +0.7 V, a high photoresponse of 268 % was obtained. Lei *et al.* [39] have reported a higher photoresponse of 530 % for ZnO/Cu_2O heterojunction formed by depositing ZnO nanowires (NRs) on top of Cu_2O layer. This huge difference may be explained by the high thickness of ZnO (NRs) and Cu_2O used in their study (~ 2.0 and 0.5 µm, respectively) [39], compared to the thickness of ZnO and Cu_2O layers in our study (200 nm). At a reverse bias of -0.4 V, a leakage-current of 0.66 µA was noted in the dark and it increases 26 times under light illumination to 17.2 µA (Fig. 2.12). This is attributed to the presence of defects in the Cu_2O/ZnO interface.

2.4 Conclusion

In this chapter, the Cu_2O/ZnO and Cu_2O/AZO heterojunctions were successfully prepared by simple two steps electrochemical deposition, under the optimal conditions. The structural characterization confirms high crystallinity of Cu_2O/ZnO and Cu_2O/AZO heterojunctions following cubic (111) and wurtzite (101) structures, respectively. The cross-section FE-SEM images confirm the formation of large cubic Cu_2O grains on continuous flat ZnO layer (for Cu_2O/ZnO) and dense film of overlapping pyramidal Cu_2O grains on AZO layer (for Cu_2O/AZO). From photoluminescence measurement, the zinc interstitial donor level (Zn_i) and the copper vacancies acceptor level (V_{Cu}) were identified as a source of n-type ZnO and p-type Cu_2O conductivity. The current-voltage (I–V) measurements confirmed the junction formation in both p-Cu_2O/n-ZnO and p-Cu_2O/n-AZO. The rectifying behavior of p-Cu_2O/n-ZnO heterojunction was better than that of p-Cu_2O/n-AZO may be due to the high mismatch between AZO and Cu_2O. Which creates more recombination sites at the interface of p-Cu_2O/n-AZO heterojunction. Thus, this heterojunction needs more improvement, we proposed the insertion of a buffer layer between AZO and Cu_2O layers to improve the interface quality. The detailed results are described in the next chapter.

References

[1] Q. Shu, J. Wei, K. Wang, H. Zhu, Z. Li, Y. Jia, X. Gui, N. Guo, X. Li, C. Ma, D. Wu, *Nano Lett.*, **9** (2009) 4338.

[2] A. Mittiga, E. Salza, F. Sarto, M. Tucci, R. Vasanthi, *Appl. Phys. Lett.*, **88** (2006) 163502.

[3] M. Izaki, T. Shinagawa, K.T. Mizuno, Y. Ida, M. Inaba, A. Tasaka, *J. Phys. D: Appl. Phys.*, **40** (2007) 3326.

[4] T. Minami, Y. Nishi, T. Miyata, S. Abe, *ECS Trans.*, **50** (2013) 59.

[5] Q.-B. Ma, Z.-Z. Ye, H.-P. He, S.-H. Hu, J.-R. Wang, L.-P. Zhu, Y.-Z. Zhang, B.-H. Zhao, *J. Cryst. Growth*, **64** (2007) 304.

[6] T. Minami, T. Miyata, K. Ihara, Y. Minamino, S. Tsukada, *Thin Solid Films*, **47** (2006) 494.

[7] O. Baka, A. Azizi, S. Velumani, G. Schmerber, A. Dinia, *J. Mater Sci: Mater. Electron.*, **25** (2014) 1761.

[8] L. Mentar, O. Baka, M.R. Khelladi, A. Azizi, S. Velumani, G. Schmerber, A. Dinia, *J. Mater Sci: Mater. Electron.*, **26** (2015) 1217.

[9] S. Laidoudi, A. Y. Bioud, A. Azizi, G. Schmerber, J. Bartringer, S. Barre, A. Dinia, *Semicond. Sci. Technol.*, **28** (2013) 115005.

[10] M. Kralji, Z. Mandic, L. Dui, *Corrosion Sci.*, **45** (2003) 181.

[11] A. Paracchino, N. Mathews, T. Hisatomi, M. Stefik, S. D. Tilley, M. Grätzel, *Energy Environ. Sci.*, **5** (2012) 8673.

[12] L. C. Wang, M. Tao, *Electrochem. Solid State Lett.*, **10** (2007) H248.

[13] H. Noh, M. Scharrer, M. A. Anderson, R. P. H. Chang, H. Cao, *Phys. Rev.*, **B 77** (2008) 115136.

[14] Z. Zhang, P .Wang, *J. Mater. Chem.*, **22** (2012) 2456.

[15] F. Caballero-Briones, J. M. Artes, I. Diez-Perez, P. Gorostiza, F. Sanz, *J. Phys. Chem. C* **113** (2009) 1028.

[16] N. Tabuchi, H. Matsumura, *Jpn. J. Appl. Phys.*, **41** (2002) 5060.

[17] P. Colleen, M. McShane, K.-S. Choi, *Phys. Chem. Chem. Phys.*, **14** (2012) 6112.

[18] Y. Xu, M. A. A. Schoonen, *Am. Mineral.*, **85** (2000) 543.

[19] B. D. Cullity, *Am. J. Phys.*, **25** (1957) 06.

[20] Y. Chen, H. Yan, B. Yang, Y. Lv, M. Wen, J. Xu, M. Wu, X. Zhu, Z. Fu, *Appl. Phys. A: Mater. Sci. Process.*, **98** (2010) 467.

[21] D. Zhang, Y. Liu, Y. Liu, H. Yang, *Phys. B*, **351** (2004) 178.

[22] Y. Li, G. W. Meng, L. D. Zhang, F. Phillipp, *Appl. Phys. Lett.*, **76** (2000) 2011.

[23] P. Wang, X. Zhao, L. Hairong, L. Lingshan, L. Jing, M. Guofu, J. Chang, *RSC Adv.*, **4** (2014) 37542.

[24] X.M. Fan, J.S. Lian, Z.X. Guo, H.J. Lu, *App. Sur. Sci.*, **239** (2005) 176.

[25] O. Fumiyasu, C. Minseok, T. Atsushi, T. Isao, *Sci. Technol. Adv. Mater.*, **12** (2011) 034302.

[26] T. Ito, T. Masumi, *J. Phys. Soc. Jpn.*, **66** (1997) 2185.

[27] H. Solache-Carranco, G. Juarez-Dıaz , A. Esparza-Garcıa, M. Briseno-Garcıa, M. Galvan-Arellano , J. Martınez-Juarez, G. Romero-Paredes, R. Pena-Sierra. *J. Lumin.*, **129** (2009) 1483.

[28] S.V. Gastev, A.A. Kaplyanskii, N.S. Sokolov, *Solid State Commun.*, **42** (1982) 389.

[29] N. Harukawa, S. Murakami, S. Tamon, S. Ijuin, A. Ohmori, K. Abe, T. Shigenari, *J. Lumin.*, **87–89** (2000) 1231.

[30] S. Hussain, C. Cao, G. Nabi, W. S. Khan, Z. Usman, T. Mahmood, *Electrochimica Acta*, **56** (2011) 8342.

[31] J. Tauc, *"Optical Properties of Solids"*, Course 22, in: F. Abeles (Ed.), North Holland Pub, Amsterdam, 1970.

[32] E. Burstein, *Phys. Rev.*, **93** (1954) 632.

[33] F. Janene, H. Dhaouadi, N. Etteyeb, F. Touati, *Ionics*, **21** (2015) 477.

[34] L. Peiwei, Z. Weifeng, L. Limei , P. Fuchuan, H. Zhigao, L. Fachun, *Physica B*, **406** (2011) 1253.

[34] C.L. Kuo, R.C. Wang, J.L. Huang, C.P. Liu, C.K. Wang, S.P. Chang, W.H. Chu, C.H. Wang, C.H. Tu, *Nanotechnology*, **20** (2009) 365603.

[35] M. Zemzemi, S. Alaya, *Superlattices Microstruct.*, **64** (2013) 311.

[36] A. G. Milnes, D. L. Feucht, *"Heterojunctions and Metal–Semiconductor Junctions"*, Academic, New York, 1972.

[37] W. Siripala, A. Ivanovskaya, T. F. Jaramillo, S. H. Baeck, E. W. McFarland, *Sol. Energ. Mater. Sol. Cells*, **77** (2003) 229.

[38] H. Kobayashi, H. Mori, T. Ishida, Y. Nakato, *J. Appl. Phys.*, **77** (1995) 1301.

[39] P. Lin, X. Yan, X. Chen , Z. Zhang, H.Yuan1, P. Li, Y. Zhao, Y. Zhang, *Nano Res.*,(2014) 01.

Chapter 3

Improving p-Cu_2O/n-Al:ZnO (AZO) heterojunction by the insertion of ZnO buffer layer

Chapter 3: Improving p-Cu_2O/n-Al:ZnO (AZO) heterojunction by the insertion of ZnO buffer layer

3.1 Introduction

The Cu_2O/AZO heterojunction deposited by two steps electrodeposition shows a low performance, due to the high band offset and the high lattice mismatch between Cu_2O and AZO as discussed in chapter 2. The band alignment between the absorber layer (Cu_2O) and the transparent conducting oxide (Al-doped ZnO; AZO) is of critical importance. Therefore, introducing a buffer layer between the absorber and the TCO will be necessary to improve the performance.

A thin layer of non-doped ZnO with band gap and lattice constant between Cu_2O and AZO layer will be a good choice as a buffer layer in Cu_2O/AZO heterojunction. Nishi et al. [1] have reported that conversion efficiency of 4.08 % was obtained in a Cu_2O/non-doped ZnO/AZO heterojunction solar cell with an n-type ZnO buffer layer deposited by pulsed laser deposition (PLD). Very recently, Sujuan et al. [2] have reported that the crystal orientation and the morphology of the Cu_2O layer play a key role in the photovoltaic conversion efficiency of p-Cu_2O/n-ZnO heterojunction solar cell. Moreover, the characteristic of Cu_2O film grown by electrodeposition is strongly dependent on the substrate [3]. It's well known that the most important deposition parameter in electrodeposition is the electrical conductivity of the substrate, which influences significantly the structural, electrical, and optical properties of the electrodeposited Cu_2O [4]. Hence, n-ZnO buffer layer properties will control Cu_2O quality and consequently determine p-Cu_2O/n-ZnO heterojunction efficiency. Indeed, to the best of to our knowledge, the fabrication of Cu_2O/ZnO/AZO into FTO by electrochemical deposition has not yet been reported.

In this chapter, p-Cu_2O/n-ZnO/n-AZO tri-heterojunction was fabricated by three steps electrodeposition on a transparent substrate (FTO). A thin layer of ZnO with different thicknesses (from 50 to 200 nm) was used as a buffer layer to reduce the high mismatch between Cu_2O layer and AZO layer. The effect of n-ZnO buffer layer thickness on the performance of the Cu_2O/ZnO/AZO heterojunction was investigated in details.

3.2 Electrodeposition of Cu_2O/ZnO/AZO heterojunctions

The electrochemical deposition was carried out using a computer-controlled Potentiostat/Galvanostat (Voltalab 40) as a potential source. Three-electrode cells equipped with a saturated calomel electrode (SCE, +0.241 V vs. SHE) as a reference electrode, a platinum wire as a counter electrode and fluorine-doped tin oxide (FTO, 10–20 Ω/cm^2 sheet resistance) as a working electrode. Prior to the electrodeposition, the substrates were ultrasonically cleaned with acetone, ethanol, and distilled water for 10 min, respectively.

The p-Cu_2O/n-ZnO/n-AZO heterojunctions, with different thicknesses of ZnO, were deposited by three steps electrochemical deposition. Firstly, AZO layer was deposited on FTO at a potential of -1.7 V and 60 °C. Then ZnO layer was deposited on AZO layer at a fixed potential of -1.3 V. After the deposition of AZO or ZnO layers, the samples were rinsed with distilled water and methanol 50 %, to remove the un-reacted products from the surface, then dried with air. Finally, a Cu_2O layer was deposited on ZnO/AZO at a potential of -0.5 V. The obtained sample was rinsed with distilled water then dried in air. Figure 3.1 presents photographs of the ZnO/AZO and Cu_2O/ZnO/AZO heterojunction.

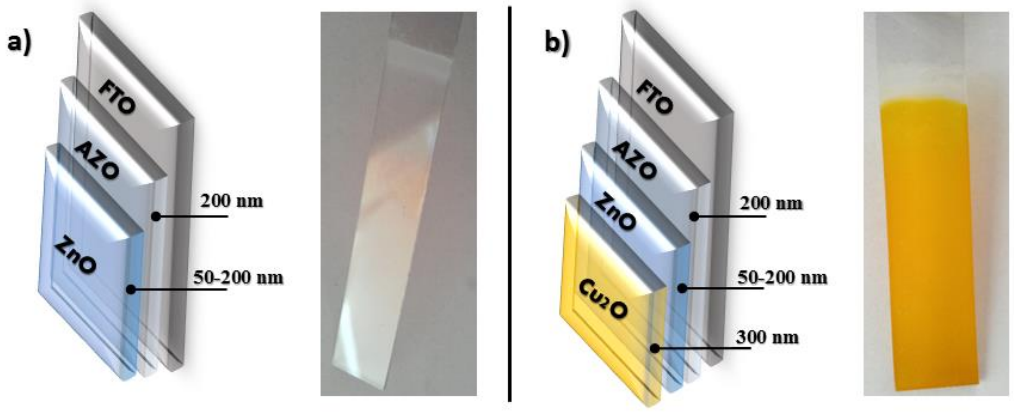

Fig. 3.1. *Schematic diagram and photographs of:* ***a)*** *ZnO/AZO structure and* ***b)*** *Cu_2O/ZnO/AZO heterojunctions.*

The chronocoulometry method was used to control the thickness of the deposited layers, following Faraday's law (as ascribed in section 2.2). The thickness of AZO and Cu_2O layers was kept fixed at 200 and 300 nm, respectively. While ZnO thickness was varied from 50 to 200 nm. The electrodeposition parameters are summarized in table 3.1. Those conditions are the same ones used for the deposition of Cu_2O/AZO in chapter 2.

Table 3.1. *The parameters used in ZnO, AZO and Cu_2O electrochemical deposition.*

Layer thickness	Bath composition	pH	Temperature (°C)	Potential (V/SCE)
ZnO (50-200 nm)	1M KNO_3 0.08 M $Zn(NO_3)_2$	6.5	70	-1.7
AZO (200 nm)	1M KNO_3 0.1M $Zn(NO_3)_2$ 0.005 M $Al(NO_3)_3$	6.0	70	-1.3
Cu_2O (300 nm)	0.05 M $CuSO_4$ 0.05 M $C_6H_8O_7$ 4 M NaOH	11	60	-0.5

For the electrochemical, structural, morphological, optical and electrical characterization, we used the same techniques and employed the same parameters reported in chapter 2. In exception of the electrochemical impedance spectroscopy (EIS) measurements employed here to study the conductivity of ZnO layers with different thickness (50, 100, 150 and 200 nm). It was performed using an alternative current voltage of 10 mV and an applied potential of 1.0 V with a frequency range from 10^5 to 5.10^{-2} Hz.

3.3 Results and discussion

3.3.1 Electrochemical characterization

One of the most important parameters in the electrodeposition is the electrical conductivity of the substrate, Baek *et al.* [4] have reported that the conductivity of the working electrode determines the electrical and crystallographic properties of the Cu_2O layers. In our work, a ZnO/AZO with different thickness of ZnO layer was used as a substrate for the deposition of Cu_2O layer. Therefore, the n-ZnO buffer layer properties will control Cu_2O quality and consequently determine the p-Cu_2O/n-ZnO heterojunction efficiency. Before the characterization of Cu_2O/ZnO/AZO heterojunction properties, we studied the electrical properties of AZO, ZnO, and Cu_2O layers separately by electrochemical characterization.

Mott-Schottky measurements were performed to determine the flat band potential and the acceptor/donor concentration of n-AZO, n-ZnO, and p-Cu_2O layers. Figure 3.2a-c displays the Mott–Schottky plots obtained for the Al-doped ZnO (AZO), pure ZnO with different thickness and Cu_2O layer.

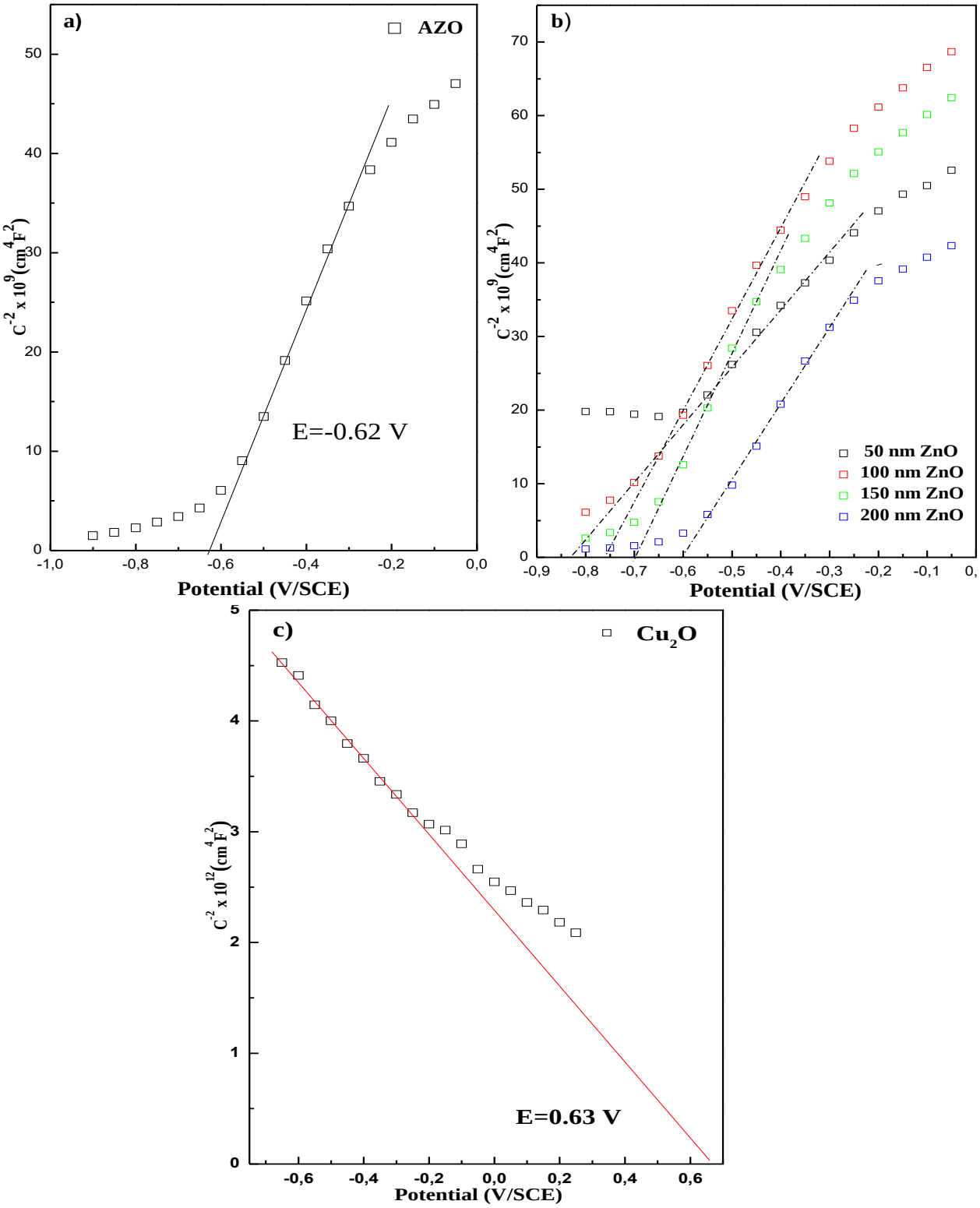

Fig. 3.2. *Mott–Schottky plots of:* ***a)*** *200 nm AZO layer,* ***b)*** *ZnO layer with different ZnO layer thicknesses and* ***c)*** *300 nm Cu_2O layer.*

At the interface of a semiconductor layer and electrolyte, the potential dependence of space charge layer capacitance is described by Mott-Schottky equation [5, 6]:

$$\frac{1}{c^2} = \frac{2}{eN_D \varepsilon \varepsilon_0}\left(E - E_{fb} - \frac{kT}{e}\right)$$ For n-type semiconductor (3.1)

$$\frac{1}{c^2} = \frac{2}{-eN_A \varepsilon \varepsilon_0}\left(E - E_{fb} - \frac{kT}{e}\right)$$ For p-type semiconductor (3.2)

where C is the space charge capacitance, *e* is the electron charge, N_A and N_D are the acceptor and donor concentration of p-type and n-type semiconductors, respectively. ε_0 is the vacuum permittivity, ε is the dielectric constant, 8.5 for AZO and ZnO [7] and 7.6 for Cu_2O [8], *k* is the Boltzmann constant, T is the absolute temperature, E is the applied potential, and E_{fb} is the flat band potential. As shown in Figs. 3.2 a-b, the Mott-Schottky equation is valid within a wide potential range, of about 0.6 V, which indicates a well-defined electronic surface state of the AZO and ZnO films. Wider linear potential range, that surpasses 1.0 V, can be achieved only from highly organized solids (single crystals). Also, the presence of multiple linear regions in M-S plots of AZO and ZnO layers indicate the existence of multiple donor levels [9].

As well, the positive slope of the M-S plot confirms n-type semiconductor characteristic of these films. However, the negative slope of M-S plot obtained from the Cu_2O layer (Fig. 3.2c) confirms the p-type semiconductor characteristics. According to latter Mott–Schottky equation, a plot of $1/C^2$ vs. E should present a straight line. The slope of this plot ($\frac{2}{\varepsilon \varepsilon_0 eN_D}$) allows the calculation of the donor and acceptor concentration. Moreover, the flat band potential can be extrapolated from $1/C^2=0$. The concentration of donor/acceptor and flat band potential (E_{fb}) obtained from the M-S plots are summarized in table 3.2.

Table 3.2. *The flat band potential, the carrier concentration and the depletion layer width of all layers in the Cu_2O/ZnO/AZO heterojunction.*

Layer thickness	Flat band potential E_{fb} (V/SCE)	Carrier concentration $N_{D,A}$ (cm^{-3})	Depletion layer width W (nm)
AZO (200 nm)	-0.62	1.04×10^{20}	2.303
ZnO (50 nm)	-0.85	3.41×10^{19}	4.768
ZnO (100 nm)	-0.75	7.84×10^{19}	2.767
ZnO (150 nm)	-0.70	8.85×10^{19}	2.677
ZnO (200 nm)	-0.60	9.50×10^{19}	2.335
Cu_2O (300 nm)	+0.63	5.85×10^{15}	32.4

As can be seen from these data, the donor concentration of n-AZO was 1.04×10^{20} cm^{-3}, this value is comparable to the typical value observed in the literature [10]. While the un-doped ZnO layer shows lower carrier concentration in the order of 10^{19}. We also noted that ZnO donor concentration increase significantly from 3.41×10^{19} to 9.5×10^{19} cm^{-3} with increasing ZnO thickness. The most likely cause of this is the rise in crystal defects with increasing ZnO thickness. Accordingly, the flat band potential of ZnO layers increase from -0.85 to -0.6 V with increasing ZnO thickness from 50 to 200 nm. This shift could be attributed to the increase of donor concentration in n-type ZnO films with increasing the thickness [11]. Turning to Cu_2O layers, the acceptor concentration was 5.8×10^{15} cm^{-3} which is within the typical value of 10^{15} to10^{18} cm^{-3} reported for Cu_2O [12,13].

Since the acceptor/ donor concentrations of the deposited AZO, ZnO, Cu_2O layers are known, the depletion layer width can be calculated from the following equation [14]:

$$W = \left(\frac{2\varepsilon\varepsilon_0}{eN_D}\right)^{\frac{1}{2}}\left(V - V_{fb} - \frac{K\,T}{e}\right)^{\frac{1}{2}} \qquad (3.3)$$

As can be seen from table 3.2, the carrier concentration affect greatly the depletion layer width. For ZnO layers with different thickness, the thinnest depletion region was found for 200 nm of ZnO indicating a higher mobility of the charge carriers [15].

Electrochemical impedance spectroscopy (EIS) is a useful analysis for the qualitative study of ZnO films conductivity. The Nyquist diagrams of the impedance spectra for ZnO layers with different thickness obtained in 1M KNO_3 solution at a frequency ranging from 10^5 to 5.10^{-2} Hz are presented in figure 3.3.

As can be seen, the EIS spectra of all the samples show a single semi-circle at high frequencies. It is well known that in Nyquist plot the semicircle at high frequencies is the characteristic of the charge transfer process. The charge transfer resistance (R_{ct}) is equal to the diameter of the semicircle. Smaller is the diameter lower is the charge transfer resistance [16]. By fitting the Nyquist plots we obtained the charge transfer resistance (R_{ct}) values for ZnO layers with different thickness. As can be seen from figure 3.3, the arch decrease with increasing ZnO thickness, accordingly, the charge transfer resistance R_{ct} decreases gradually from 1.036 to 0.323 kΩ with increasing ZnO thickness from 50 to 200 nm; indicating the increase of ZnO conductivity with increasing the thickness. Thus, the 200 nm ZnO layer shows the highest conductivity. This result can be explained by the high donor concentration calculated from Mott

Schottcky plots and the high charge mobility obtained for 200 nm ZnO layer compared to the other samples. The electrochemical characterizations suggest that Cu_2O/ZnO/AZO heterojunction with ZnO layer of 200 nm thickness will have a good electrical proprieties compared to the other samples.

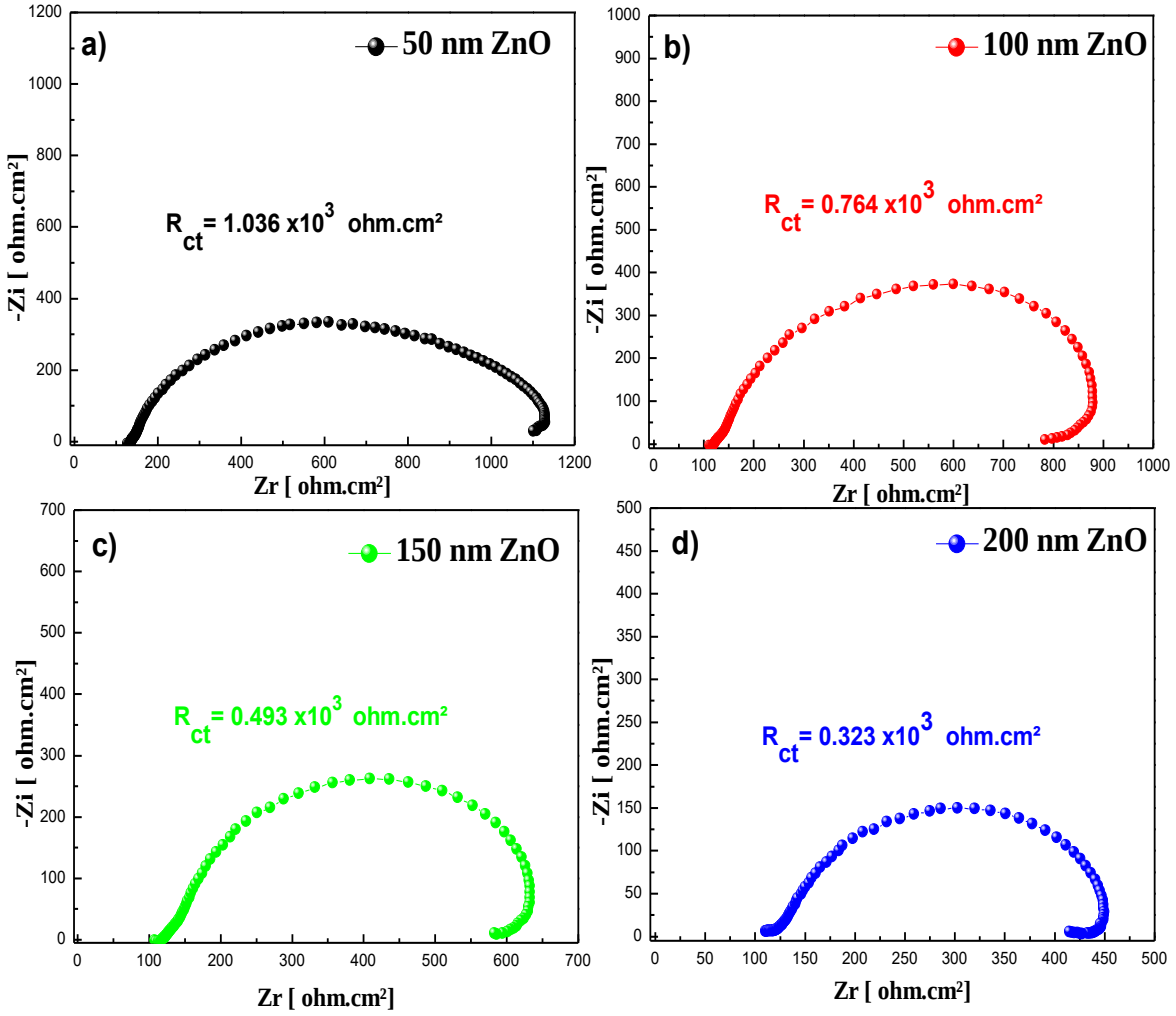

Fig. 3.3. *Nyquist diagrams of ZnO films with different thickness:* ***a)*** *50,* ***b)*** *100,* ***c)*** *150 and* ***d)*** *200 nm, carried out in 1.0M* KNO_3.

3.3.2 Structural characterization

The phases of the obtained Cu_2O/ZnO/AZO heterojunctions were confirmed with XRD measurements. Figure 3.4 presents the XRD patterns of Cu_2O/ZnO/AZO heterojunctions with different thickness of ZnO. Besides the diffraction peak of the FTO substrate (marked by asterisks), all other diffraction peaks can be ascribed to cubic Cu_2O structure (JCPDS card n° 00-034-1354) and ZnO wurtzite structure (JCPDS card n° 00-036-1451) and prove their pure phases. The noted peaks at 29.46, 42.27, 61.33, and 73.59 were indexed to (110), (200), (220) and (311) orientations of Cu_2O, respectively. The overlapped peaks at 36.31° correspond to

both ZnO (101) and Cu_2O (111) orientations. Moreover, the (111) direction of Cu_2O and (101) of ZnO are very intense, indicating that the obtained heterojunctions are preferentially oriented along (111) and (101) directions, respectively. The sharp and narrow peaks show that the heterostructures are highly crystallized in particular for samples with 50 and 200 nm ZnO buffer layer. This indicates that the electrodeposition method could also be useful for the preparation of crystalline Cu_2O/ZnO nanostructures. It is important to note that the presence of different diffraction peaks from basic planes of Cu_2O layers indicates that the dense films were composed of Cu_2O crystallites with random orientation.

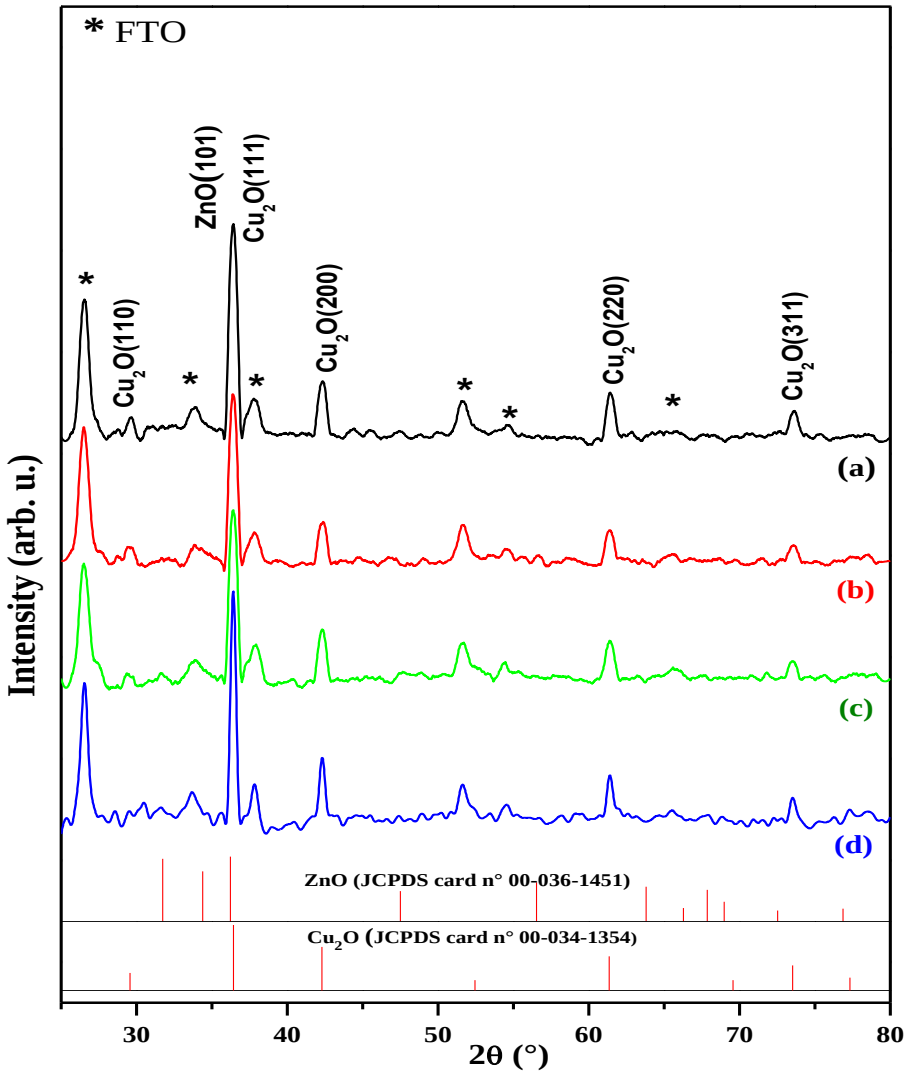

Fig. 3.4. *XRD patterns of Cu_2O/ZnO/AZO samples with different ZnO buffer layer thicknesses:* ***a)*** *50,* ***b)*** *100,* ***c)*** *150 and* ***d)*** *200 nm. The reference profile for the Cu_2O cubic structure (JCPDS card n° 00-034-1354) and ZnO wurtzite structure (JCPDS card n° 00-036-1451) are given as a bar graph.*

The average coherence lengths (D) of the crystals have been estimated from the main (111) Bragg peak of cubic Cu_2O structure, using the Scherrer formula [17]:

$$D = \frac{0.94\lambda}{\beta \cos \theta} \quad (3.4)$$

where D is the average crystallite size (nm), λ=1.54056 Å is the wavelength of the incident radiation, β is the full width at half maximum [FWHM] (rad), and θ is the Bragg angle (rad). The FWHMs have been determined by fitting Gaussian profile peaks to the experimental data. As the crystals are not exactly of spherical symmetry, the values have to be considered as approximations. The values of the average crystallites size of Cu_2O layers deposited on 50, 100, 150 and 200 nm of ZnO buffer layer are 32, 23, 24 and 32 nm, respectively. It is well known that the different crystallites size contains different dislocation defects, which have a great effect on the electronic property of the heterojunction [18].

3.3.3 Morphological analysis

The surface morphology was determined by field emission scanning electron microscopy (FE-SEM) and atomic force microscopy (AFM) techniques. Figure 3.5.a-d is top view FE-SEM images of Cu_2O grown on ZnO/AZO structures with a different ZnO buffer layer thicknesses. The grains size was estimated by Visiometre software. The FE-SEM images reveal a continuous film of Cu_2O for all the samples. It is clear that increasing the thickness of ZnO layers affects greatly the size and the morphology of Cu_2O. Also, the cubic structures were damaged with increasing the thickness of ZnO, for example, the Cu_2O layers deposited onto 50 nm of ZnO buffer layer shows a mixture of cubic structure and four-sided pyramid grains. The estimated grains size range from 307 to 550 nm (Fig. 3.5a), the edges and the corners were clearly observed at higher magnification (Fig. 3.5a′). While onto 100 nm of ZnO buffer layer (Fig. 3.5b), larger cubic crystals of Cu_2O were formed, with a grain size between 400 and 630 nm, at higher magnification we can see the formation of granular particles (Fig. 3.5b′). On ZnO layer of 150 nm thickness (Fig. 3.5c), the sharpness of Cu_2O grains decreased and many poorly defined needles and aggregates were covering its surface (Fig. 3.5c). On the higher thickness of ZnO layer (Fig. 3.5d), the cubic structure had almost completely disappeared and the majority of the surface was covered by large needles and aggregates.

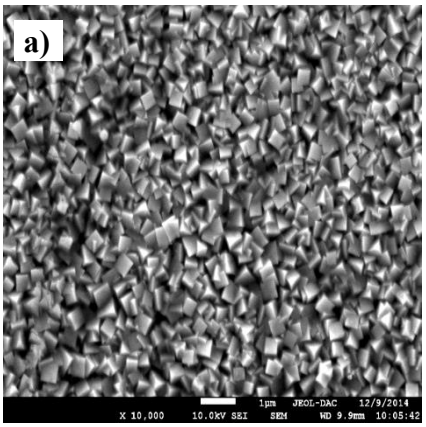
a)
X 10,000 10.0kV SEI SEM WD 9.9mm 10:05:42

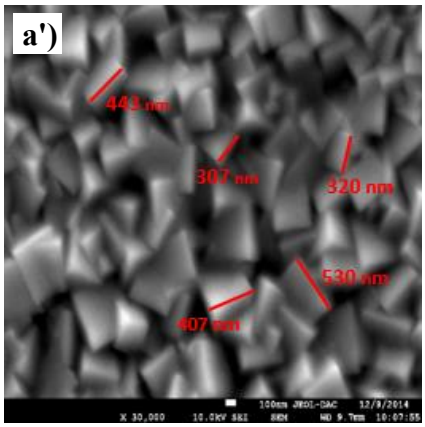
a')
443 nm
307 nm
320 nm
530 nm
407 nm

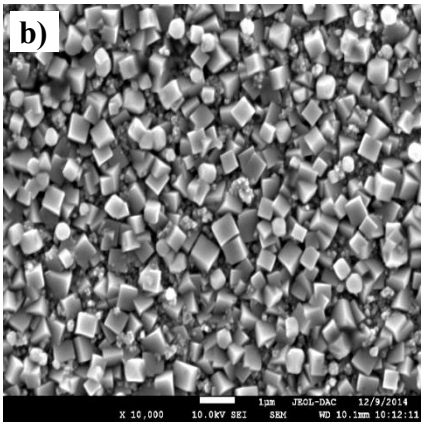
b)
X 10,000 10.0kV SEI SEM WD 10.1mm 10:12:11

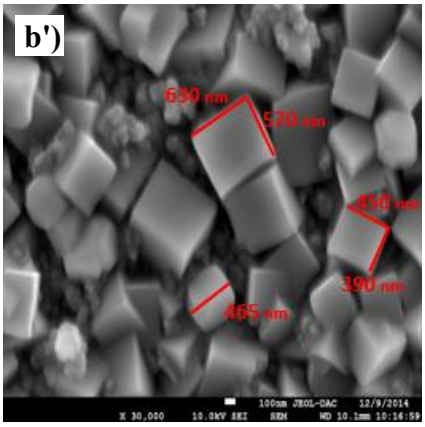
b')
630 nm
520 nm
450 nm
390 nm
495 nm

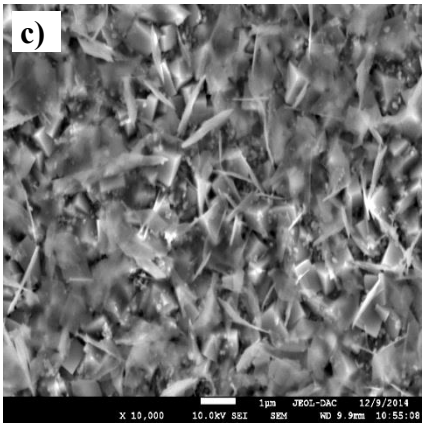
c)
X 10,000 10.0kV SEI SEM WD 9.9mm 10:55:08

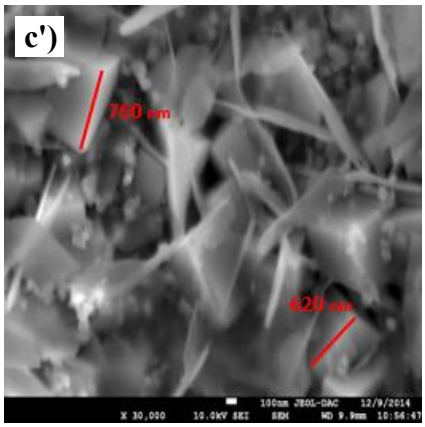
c')
700 nm
620 nm

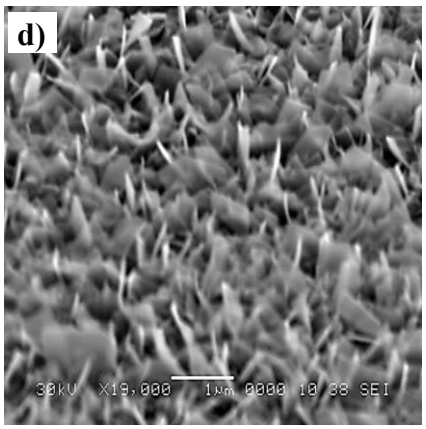
d)
30kV X19,000 1μm 0000 10 38 SEI

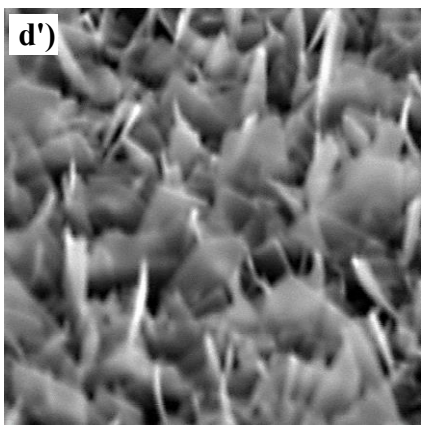
d')

Fig. 3.5. *FE-SEM images of Cu_2O films deposited on ZnO/AZO with different ZnO thicknesses values:* ***a)*** *50,* ***b)*** *100,* ***c)*** *150,* ***d)*** *200 nm.* ***a′) - d′)*** *show the higher magnification images of the same samples.*

Figure 3.6 displays the 3D and 2D AFM images of a Cu_2O layer deposited onto ZnO/AZO with different thicknesses of ZnO buffer layer. It can be seen from the images that Cu_2O morphology changed greatly with increasing ZnO layer thickness. As the ZnO thickness increase, the surface morphology transformed from a pyramidal shape with clear edges (Fig. 3.6a-b) to granular form (Fig. 3.6c-d). Which is in accordance with the deterioration of Cu_2O morphology with the increase of ZnO thickness observed by FE-SEM measurements. The Root mean square (RMS) roughness obtained from the AFM data indicate that the surface roughness is strongly dependent on the ZnO/AZO structures (used as a substrate for Cu_2O deposition). The average surface roughness of Cu_2O layer deposited on a ZnO/AZO structure with 50 and 100 nm of ZnO buffer layer are 92 and 72 nm, respectively. This is significantly higher than the roughness of Cu_2O deposited on a 150 or 200 nm of ZnO (40 and 17 nm, respectively).

It is possible that the decrease of the roughness with increasing ZnO thickness is due to a sterical hindrance, where crystals with the fastest growth rate gradually develop in all dimensions at the expense of the slower growing ones [19]. Consequently, this broadening is expected to result in a marked increase in both the grain size and the surface roughness.

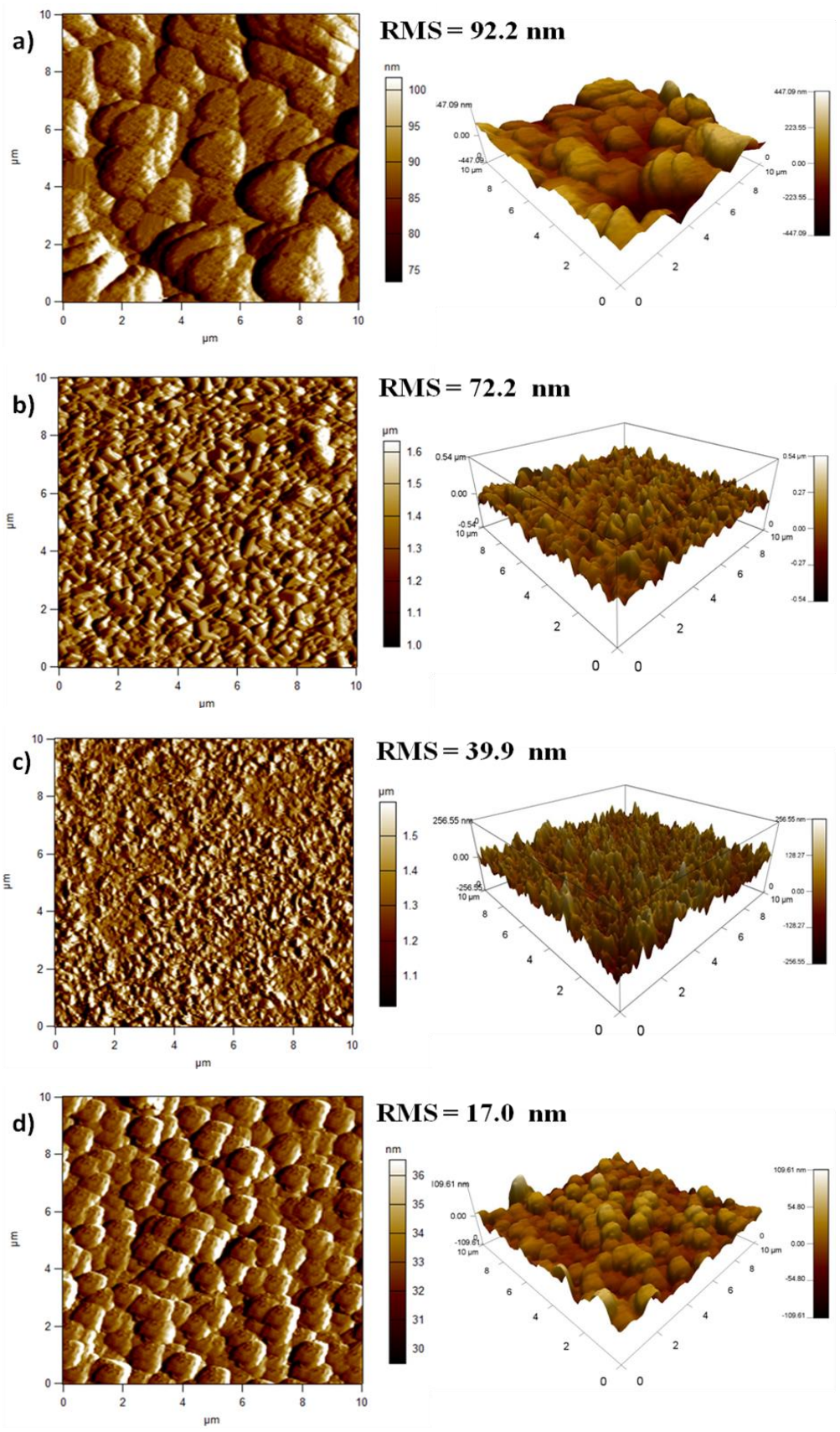

Fig. 3.6. *Tapping mode 3D and 2D AFM images of Cu_2O/ZnO/AZO heterojunctions with different ZnO buffer layer thicknesses:* ***a)*** *50,* ***b)*** *100,* ***c)*** *150 and* ***d)*** *200 nm.*

3.3.4 Optical characterization

3.4.1 Photoluminescence analysais

The energy bands and the crystalline quality of our samples were examined by an analysis photoluminescence (PL). Before performing the PL analysis of Cu_2O/ZnO/AZO heterojunctions, it is necessary to present the PL analysis of ZnO/AZO structure (used as substrate). Figure 3.7 presents the room temperature PL spectra of AZO layer and ZnO/AZO structure with 50 and 200 nm ZnO thickness, respectively. It is apparent from PL spectra that all the samples show a typical luminescence behavior with two emissions, a narrow UV peak centering at 401 nm (3.08 eV) and a broad green emission peak centering around 523 nm (2.36 eV). The first peak (at 3.08 eV) indicates the near band emission (NBE) of ZnO [20], while the second peak (at 2.36 eV) is deep level emission (DLE), probably relative to the intrinsic defects in ZnO [21-24], such as, zinc vacancy (V_{Zn}), oxygen vacancy (V_O), interstitial zinc (Zn_i), interstitial oxygen (O_i), and anti-site oxygen (O_{Zn}).

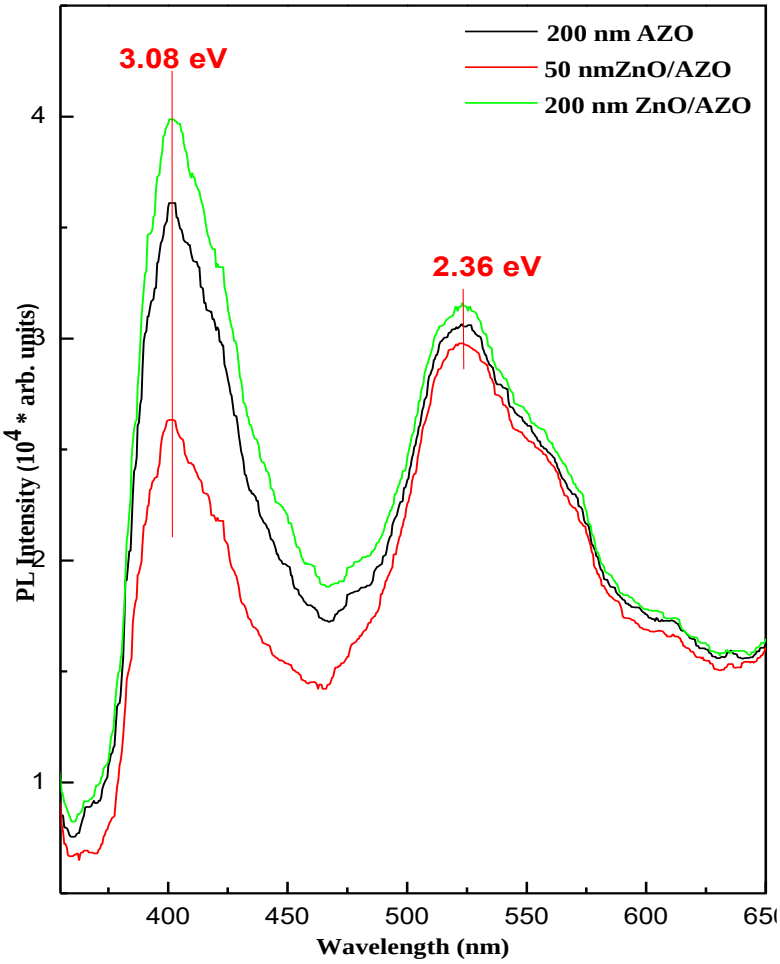

Fig. 3.7. *Room-temperature photoluminescence (PL) spectra of AZO, 50 nm ZnO/AZO and 200 nm ZnO/AZO structures.*

Several studies have suggested that the green emission centering at 2.38 eV should correspond to the electron transition from the bottom of the conduction band to the anti-site defects O_{Zn} level [21, 25]. Thus, in our samples, the green emission centering at 2.36 eV is related to the anti-site oxygen defects level. It is well known that the intensity ratio of the ultraviolet emission at 401 nm to the visible emission at 523 nm depends significantly on the ZnO quality [26]. Therefore, the quality of our samples may be classified on the basis of this ratio. The 200 nm ZnO/AZO presents a high ratio of 1.3 compared to AZO/FTO and 50 nm ZnO/AZO (1.2 and 0.87, respectively). This confirms the high quality and the good crystallinity of 200 nm ZnO/AZO structure.

Turning now to photoluminescence property of Cu_2O/ZnO/AZO heterojunction, figure 3.8 exhibits the PL spectra of Cu_2O layer deposited on ZnO/AZO structures with different thicknesses of ZnO buffer layer, 50, 100, 150 and 200 nm, respectively.

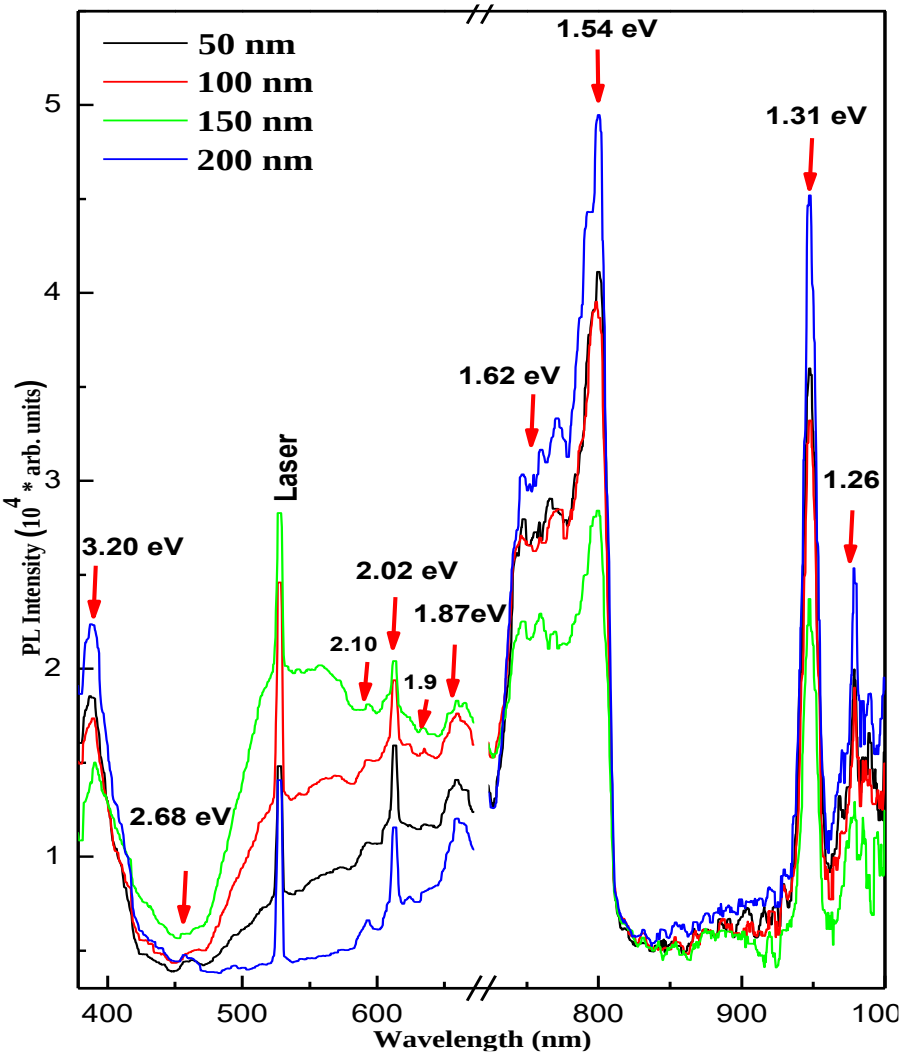

Fig. 3.8. *Room-temperature photoluminescence (PL) spectra of Cu_2O/ZnO/AZO heterojunctions samples with different ZnO buffer layer thicknesses.*

All the samples show the same allure, a strong and sharp ultraviolet (UV) emission centered at 388 nm (3.19 eV) correspond to the ZnO near-band-edge (NBE) electron transition between the valence band and the conduction band [25]. The strong peak observed at 760 nm (1.63 eV) is attributed to the transition from the conduction band bottom to the oxygen vacancy (V_O) donor level. It is important to mark the disappearance of the green emission peak, which means the reduction of the ZnO film defects in Cu_2O/ZnO/AZO heterojunctions. This may result from the passivation of the surface defect states after capping ZnO buffer layer with Cu_2O layer [27]. The rest of the peaks corresponds to Cu_2O emissions. Where the two emissions at 462 nm (2.68 eV) and 592 nm (2.09 eV) are generated from the free excitons [28]. The emission at 613 nm (2.02 eV) corresponds to the direct exciton recombination without phonons participation [29]. The emission at 800 nm (1.55 eV) is produced from the recombination of the bound excitons at oxygen vacancy to the single charged oxygen vacancy (V_O^+) [30]. The two peaks noted at 947 nm (1.30 eV) and 978 nm (1.26 eV) are attributed to the recombination of bound excitons to the copper vacancies level (V_{Cu}) known as β-luminescence series [29, 31]. The band at 947 nm related to copper vacancies (V_{Cu}) was the dominant emission indicating that the p-type conductivity of Cu_2O is attributed to copper vacancies. The formation of the nano-heterojunction at the interface of Cu_2O/ ZnO buffer layer with different thickness induces a new energy level, which is the source of the peak centering at 635 nm (1.95 eV) [32]. It is clear that the Cu_2O/200 nm ZnO/AZO heterojunction reveals narrow peaks with the highest intensity indicating the good crystallinity of this sample.

3.4.2 UV-Vis analysis

The light absorption–transmission is an essential property that defines the heterojunction optical performance. In this section, we studied the absorbance and transmittance of the ZnO/AZO structure (substrate), then compared it with Cu_2O/ZnO/AZO heterojunctions with different thickness of ZnO. The transmittance and absorbance spectra of AZO, ZnO/AZO, and Cu_2O/ZnO/AZO heterojunctions with different thicknesses of ZnO buffer layer, recorded in a wavelength range from 200 to 900 nm, are shown in Fig. 3.9. From the figure 3.9a, we can see that the 200 nm AZO layer show a transmittance of 75 %, the deposition of 50 nm ZnO layer on AZO layer caused an increase in the transmittance to 82 %. It is well established that the high optical transmission in the visible range is important for ZnO/AZO structures as solar cell windows. It is important to note that increasing ZnO thickness from 50 to 200 nm didn't affect

the transmission of ZnO/AZO structure, thus, any change in Cu_2O/ZnO/AZO transmission will depend on Cu_2O layer performance.

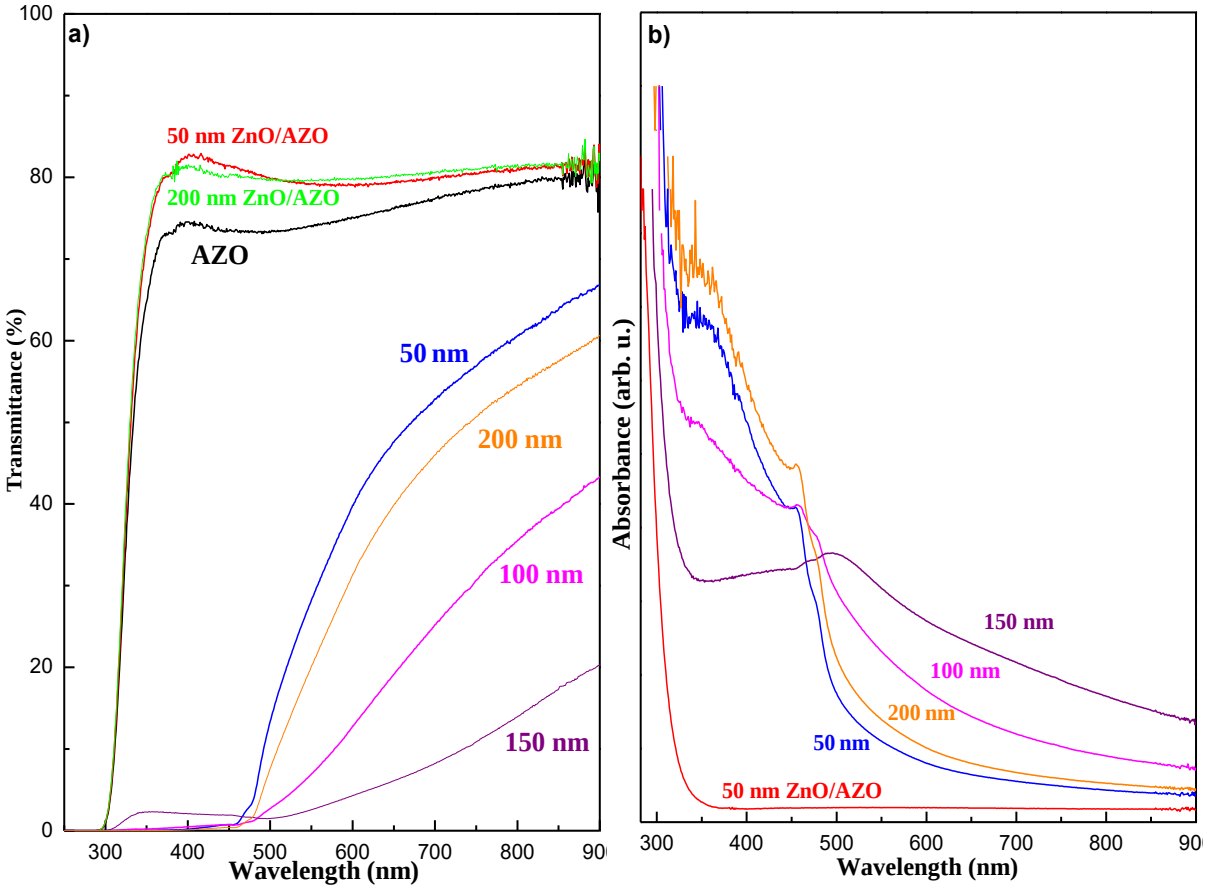

Fig. 3.9. a) *UV-vis transmittance spectras of 200 nm AZO layer, ZnO/AZO and Cu_2O/ZnO/AZO heterojunctions with different thicknesses of ZnO buffer layer.* ***b)*** *UV–vis absorbance spectras of the respective samples.*

A lower transmittance was observed for Cu_2O/ZnO/AZO heterojunctions as Cu_2O layer have yellow-orange color, high transmittances of 65 and 60 % were obtained for Cu_2O/ZnO/AZO heterojunctions with 50 and 200 nm of ZnO buffer layer. Turning to the absorbance spectra shown in figure 3.9b, the ZnO/AZO with 50 nm ZnO presents a strong absorption in the ultraviolet range (< 350 nm). The same absorption edge was obtained from AZO and 200 nm ZnO/AZO samples (Fig. 3.9a); which is in contrast with the absorption red-shift observed by Shi *et al.* [33] with increasing ZnO buffer layer thickness from 50 to 200 nm. This difference can be due to the high thickness of AZO used in their study (600 nm) [33] compared to AZO thickness in our study (200 nm). The deposition of Cu_2O on the ZnO/AZO caused a red shift of the absorption to the visible region as illustrated in figure 3.9.b. This could be attributed to the combinational effect of the narrow bandgap of Cu_2O (approximately 2.17 eV) and a wide band gap of ZnO (approximately 3.37 eV) [34]. This property ensured to the

photovoltaic device a more benefit of the sunlight as the visible region contains the maximum of the solar energy.

In order to find the effect of ZnO thickness on the absorption edge, the optical band gap energies of our samples were determined through the plot of Tauc relation [35]:

$$(\alpha h\nu)^2 = A(h\nu - Eg) \qquad (3.5)$$

where α is the absorption coefficient, hν is the photon energy, A is a constant and Eg is the band gap of the material. Accordingly, the optical band gap can be obtained by extrapolating the corresponding straight lines downwards to the photon energy axis in the Tauc plot [36]. Figure 3.10 shows the Tauc's plots from which the optical band gap energies were determined for AZO, ZnO/AZO bilayer and Cu_2O/ZnO/AZO heterojunction.

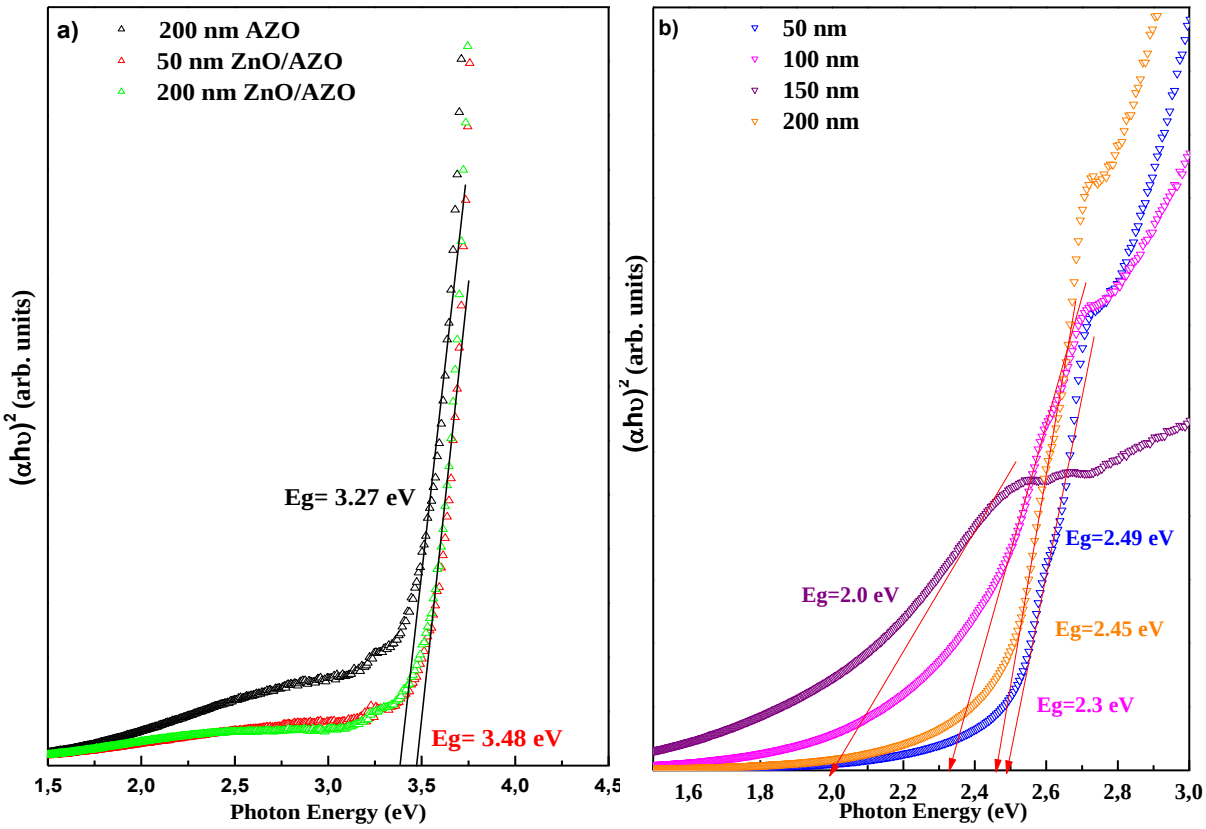

Fig. 3.10. *Tauc's plot of:* ***a)*** *200 nm AZO layer and ZnO/AZO structure and* ***b)*** *Cu_2O/ZnO/AZO heterojunctions with different ZnO buffer layer thicknesses.*

As illustrated in figure 3.10a, the estimated energy band gap of 200 nm AZO layer was 3.27 eV, the deposition of ZnO layer on AZO/FTO induce an increase in the band gap to 3.48 eV, this assumed to be the Moss-Burstein shift [33]. Figure 3.10b illustrates the Tauc plots of Cu_2O/ZnO/AZO heterojunction with different thicknesses. The estimated band gap of Cu_2O

layer was between 2.0 and 2.45 eV. These values are intermediate, lower than that of ZnO and larger than that of Cu_2O. It is clear that the energy band gap decreases from 2.4 to 2.0 eV then increases to 2.45 eV with increasing ZnO thickness from 50 to 150 and to 200 nm, respectively. This variation may be explained by the crystallinity deterioration with increasing ZnO thickness.

3.3.5 Electrical characterization

The charge transport mechanism and the performance of the obtained heterojunctions were investigated using the current-voltage electrical characterization. This method based on the quantification of the currents crossing a junction under the effect of an external electric field. Figure 3.11 shows the current current-voltage characteristics of p-Cu_2O/n-ZnO/n-AZO heterojunctions in the dark at room temperature with different ZnO buffer layers thickness. It is well established that all the heterostructures provide nonlinear behavior confirming the successful fabrication of the p-n heterojunction. However, the I–V curves of p-Cu_2O/n-ZnO/n-AZO heterojunctions with n-ZnO buffer layer thickness of 100 and 150 nm does not show properly rectifying behaviour. A good electrical rectification is clearly observed for ZnO buffer layer of 50 and 200 nm, though the p-Cu_2O/ n-ZnO (50 nm)/n-AZO presents wide reverse current. As can be seen from the curve p-Cu_2O/ n-ZnO (200 nm)/n-AZO show high forward current of 53 µA under 0.6 V. While at - 0.6 V applied bias small reverse leakage current of -2.8 µA was noted. Thus, p-Cu_2O/ n-ZnO (200 nm)/n-AZO presents the highest performance, which can be explained by the high crystallinity of this sample confirmed by XRD and PL measurements.

Concerning the performance of Cu_2O/ZnO and Cu_2O/AZO heterojunctions discussed in chapter 2, it is clear that Cu_2O/ ZnO (200 nm)/AZO heterojunction reveal a better performance and a low leakage current of 2.8 $\times 10^{-6}$A at - 0.6V compared to 5.9×10^{-6} and 6.0×10^{-2} A for Cu_2O/ZnO and Cu_2O/AZO heterojunctions, respectively. Thus, the insertion of ZnO buffer layer between p-Cu_2O and n-AZO reduced the band offsets and improve the band alignment which increases the Cu_2O/ZnO (200 nm)/AZO heterojunction performance.

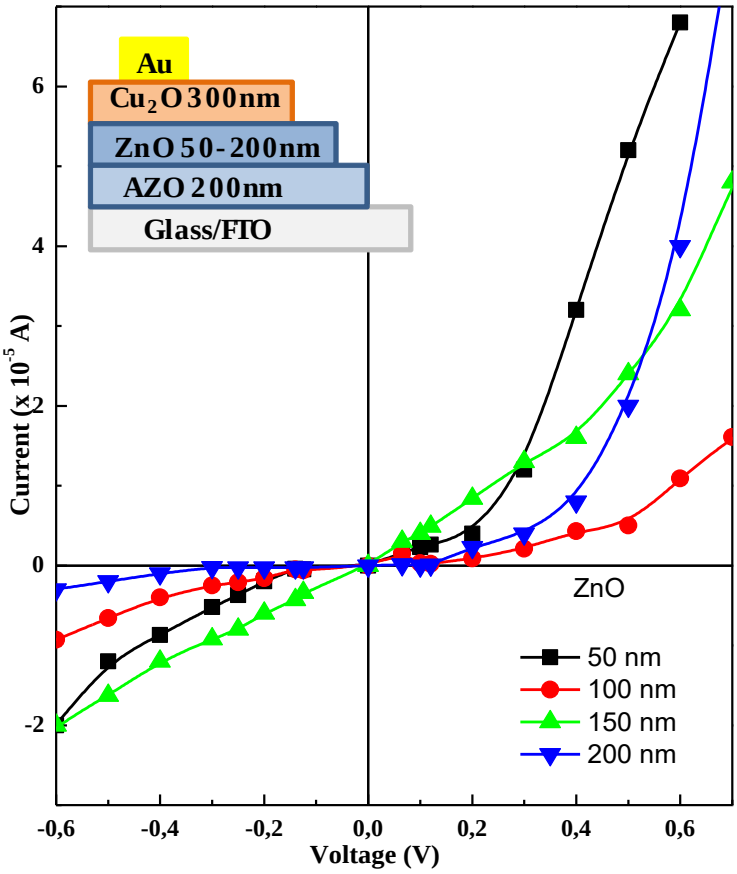

Fig. 3.11. *Current–voltage characteristics of p-Cu_2O/n-ZnO/n-AZO heterojunctions in the dark with different ZnO buffer layer thicknesses: a) 50 nm, b) 100 nm, c) 150 nm and d) 200 nm.*

To understand the effect of ZnO buffer layer on the performance of Cu_2O/ZnO (200 nm)/AZO heterojunction, we constructed the band diagram according to Anderson model [37]. Where the conduction band offset (ΔE_c) and the valence band offset (ΔE_v) of the heterojunction are represented by the following equation:

$$\Delta E_c = \chi_2 - \chi_1 \tag{3.6}$$

$$\Delta E_v = Eg_2 - Eg_1 + \Delta E_c \tag{3.7}$$

It is well known that ZnO, AZO and Cu_2O electron affinity (χ) are 4.2, 4.6 and 3.2 eV respectively [38, 39]. Also, the measured band gaps (Eg) were 3.47, 3.25 and 2.36 eV for AZO, ZnO, and Cu_2O, respectively. The energy-band diagram of the p-Cu_2O/200nm ZnO/n-AZO heterojunction is shown in figure 3.12.

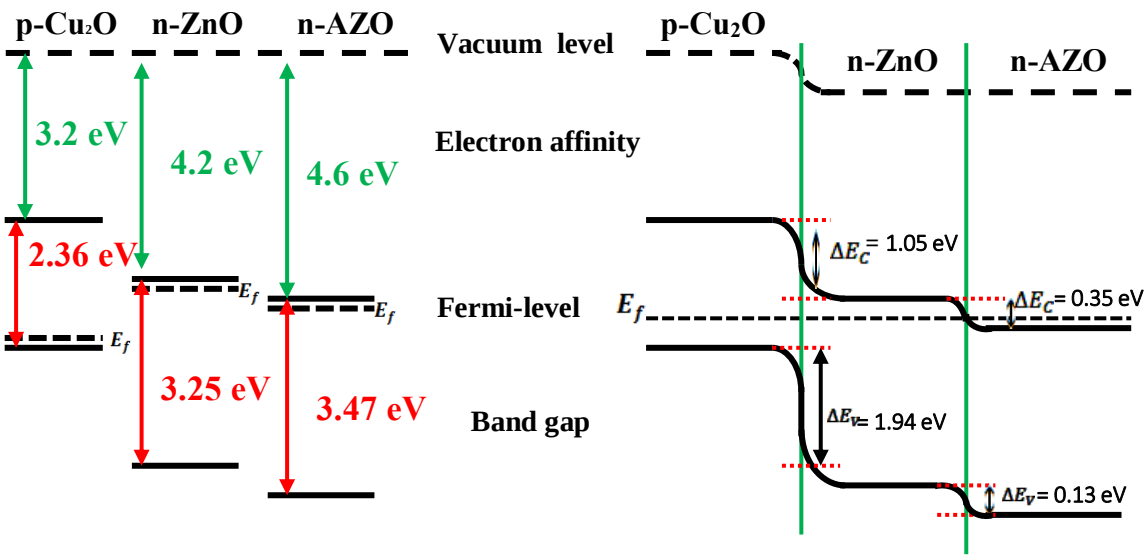

Fig. 3.12. *Band energy diagram of the isolated states of n-AZO, n-ZnO, p-Cu_2O and the p-Cu_2O/n-ZnO/n-AZO heterojunction under equilibrium condition.*

As can be seen from the energy band diagram, as the three semiconductors p-type Cu_2O, n-type ZnO, and n- AZO are in contact, a p–n junction at their interface will be formed and the electrons in the n-AZO layer are transferred to the p-Cu_2O layer through the n-ZnO buffer layer. At the same time, the holes in the Cu_2O layer are transferred in the opposite direction until a constant Fermi-level formed at equilibrium. The calculated conduction band offset (ΔE_c) of the Cu_2O/ZnO heterojunction was 1.05 eV, and the valence band offset (ΔE_v) was 1.94 eV. Those values are much lower than that of Cu_2O/AZO (ΔE_c of 1.4 eV, and ΔE_v of 2.4 eV). Therefore, the ZnO buffer layer makes the energy band between n-AZO and p-Cu_2O smoother which facilitate the electrons passage. The large valence band offset should result in a thin tunneling barrier across the p–n junction [40].

3.4 Conclusion

In this Chapter, Cu_2O/ZnO/AZO tri-layers heterojunction was synthesized by simple potentiostatic electrodeposition under the optimal conditions. In this structure, we inserted ZnO thin film with different thicknesses as a buffer layer between n-AZO and p-Cu_2O films to improve the band alignment in Cu_2O/AZO heterojunction interface. The electrochemical characterization by M-S and EIS analysis confirmed that ZnO conductivity increases with increasing ZnO thickness from 50 to 200 nm. In addition, we found that the Cu_2O properties were mainly affected by ZnO thickness. Thus, a high crystallinity was confirmed to Cu_2O/ZnO/AZO heterojunction with 200 nm of ZnO buffer layer by XRD analysis. Also, strong

absorption in the visible region with large band gap energy of 2.4 eV was noted from UV-Vis spectra, which ensures a better consumption of sunlight to the photovoltaic devices. The I–V characteristics of p-Cu_2O/n-ZnO/n-AZO heterojunctions with 200 nm ZnO buffer layer show well defined rectifying behavior. Moreover, the performance of this letter was better than that of Cu_2O/ZnO and Cu_2O/AZO heterojunction. Which confirm the improvement of the band alignment Cu_2O/AZO by the insertion of the 200 nm ZnO buffer layer.

References

[1] Y. Nishi, T. Miyata, T. Minami, *J. Vac. Sci. Technol. A*, **30** (2012) 04D103.

[2] S. Chen, L. Lin, J. Liu, P. Lv, X. Wu, W. Zheng, F. Lai, Y. Qu, *J. Alloys & Compds.*, **644** (2015) 378.

[3] D. Lincot, *Thin Solid Films*, **487** (2005) 40.

[4] S. K. Baek, J. H. Shin, S. W. Cho, H. K. Cho, *J. Vac. Sci. Technol. B*, **33** (2015) 02B104.

[5] A. Paracchino, N. Mathews, T. Hisatomi, M. Stefik, S. D. Tilley, M. Grätzel, *Energy Environ. Sci.*, **5** (2012) 8673.

[6] A. W Bott, "*Electrochemistry of Semiconductors*" *Curr. Sep.*, **17** (1998) 87.

[7] H. Noh, M. Scharrer, M. A. Anderson, R. P. H. Chang, H. Cao, *Phys. Rev. B: Condens. Matter Mater. Phys.*, **77** (2008) 115136.

[8] Z. Zhang, P .Wang, *J. Matter. Chem.*, **22** (2012) 2456.

[9] M. Colleen, McShane, K-S. Choi, *Phys. Chem. Chem. Phys.*, **14** (2012) 6112.

[10] A. C. Aragonès, A. Palacios-Padrós, F. Caballero-Briones, F. Sanz, *Electrochim. Acta*, **109** (2013) 117.

[11] Y. Yang, J. Han, X. Ning, W. Cao, W. Xu, L. Guo, *ACS Appl. Mater. Interfaces*, **6** (2014) 22534.

[12] F. Caballero-Briones, J. M. Artes, I. Diez-Perez, P. Gorostiza, F. Sanz, *J. Phys. Chem. C* **113** (2009) 1028.

[13] N. Tabuchi, H. Matsumura, *Jpn. J. Appl. Phys.*, **41** (2002) 5060.

[14] R. Beranek, *Adv. Phys. Chem.*, **2011** (2011) 20.

[15] S. Khan, M. J. M. Zapata, M. B. Pereira, R. V. Gonçalves, L. Strizik, J. Dupont, M. J. L. Santos, S. R. Teixeira, *J. Phys. Chem. Chem. Phys.* **17** (2015) 23952.

[16] N. Sobti, A. Bensouici, F. Coloma C. Untiedt, S. Achour. *J Nanopart. Res.* **16** (2014) 2577.

[17] B. D. Cullity, "*Elements of X-ray Diffraction*", 2nd edition (1978)

[18] D. Zhang, Y. Liu, Y. Liu, H. Yang, *Phys. B: Condens. Matter.*, **351** (2004) 178.

[19] T. Dimopoulos, A. Peic´, P. Mullner, M. Neuschitzer, R. Resel, S. Abermann, M. Postl, E. J. W. List, S. Yakunin, W. Heiss, *J. Renewable Sustainable Energy*, **5** (2013) 011205.

[20] F. K. Shan, G. X. Liu, W. J. Lee, G. H. Lee, I. S. Kim, B. C. Shin, Y. C. Kim, *J. Crystal Growth,* **277** (2005) 284.

[21] B. Lin, Z. Fu, Y. Jia, *Appl. Phys. Lett.,* **79** (2001) 943.

[22] E.G. Bylander, *J. Appl. Phys.*, **49** (1978) 1188.

[23] K. Vanheusden, C.H. Seager, W.L. Warren, D.R. Tallant, J.A. Voiget, *Appl. Phys. Lett.,* **68** (1996) 403.

[24] M. Liu, A.H. Kitai, P. Mascher, *J. Lumin.,* **54** (1992) 35.

[25] X. M. Fan, J.S. Lian, Z.X. Guo, H.J. Lu, *App. Sur. Sci.,* **239** (2005) 176.

[26] B. M. Fariza, J. Sasano, T. Shinagawa, S. Watase, M. Izaki, *Thin Solid Films,* **520** (2012) 2261.

[27] Y. Cui, C. Wang , G. Liu, H. Yang, S. Wu, T. Wang, *Mater. Lett.* **65** (2011) 2284.

[28] T. Ito, T. Masumi, *J. Phys. Soc. Jpn.,* **66** (1997) 2185.

[29] H. Solache-Carranco, G. Juarez-Dıaz , A. Esparza-Garcıa, M. Briseno-Garcıa, M. Galvan-Arellano , J. Martınez-Juarez, G. Romero-Paredes, R. Pena-Sierra. *J. Lumin.,* **129** (2009) 1483.

[30] S.V. Gastev, A.A. Kaplyanskii, N.S. Sokolov, *Solid State Commun.*, **42** (1982) 389.

[31] N. Harukawa, S. Murakami, S. Tamon, S. Ijuin, A. Ohmori,K. Abe and T. Shigenari, *J. Lumin.* **87–89** (2000) 1231.

[32] Y. Wang, S. Li, H. Shi, K. Yu, *Nanoscale*, **4** (2012) 7817.

[33] J. H. Shi, S. M. Huang, J. B. Chu, H. B. Zhu, Z. A. Wang, X. D. Li, D. W. Zhang, Z. Sun, W. J. Cheng, F. Q. Huang, X. J. Yin, *J. Mater. Sci.: Mater. Electron.,* **21** (2010) 1005.

[34] X. Jiang, Q. Lin, M. Zhang, G. He, Z. Sun, *Nanoscale Research Lett.,* **10** (2015) 30.

[35] S. Hussain, C. Cao, G. Nabi, W. S. Khan, Z. Usman, T. Mahmood, *Electrochim. Acta,* **56** (2011) 8342.

[36] J. Tauc, Optical Properties of Solids, Course 22, in: F. Abeles (Ed.), North Holland Pub, Amsterdam, 1970.

[37] A. G. Milnes and D. L. Feucht, "*Heterojunctions and Metal-Semiconductor Junctions*", *Academic*, New York, 1972d.

[38] W. Siripala, A. Ivanovskaya, T. F. Jaramillo, S. H. Baeck, E.W. McFarland, *Sol. Energ. Mater. Sol. Cells*, **77** (2003) 229.

[39] H. Kobayashi, H. Mori, T. Ishida, Y. Nakato, J. Appl. Phys. **77** (1995) 1301.

[40] T.J. Hsueh, C.-L. Hsu, S.-J. Chang, P.-W. Guo, J.-H. Hsieh, I-Cherng Chen, *Scr. Mater.*, **57** (2007) 53.

Chapter 4

Improving p-Cu_2O/n-ZnO heterojunction optical absorption by engineering Cu_2O layer properties

Chapter 4: Improving p-Cu_2O/n-ZnO heterojunction optical absorption by engineering Cu_2O layer properties

4.1 Introduction

Improving the conversion efficiency of Cu_2O/ZnO solar cells requires the amelioration of ZnO and Cu_2O properties, as well as the ZnO/Cu_2O interface quality. In the previous chapters, we focused on improving Cu_2O/ZnO heterojunction properties by engineering the window layer (using Al-doped ZnO and ZnO buffer layer). Hence, in this chapter, we are aiming to enhance the absorber layer (Cu_2O).

The copper oxide has been the subject of several studies and many methods have been used to prepare Cu_2O. As example, metallic copper oxidation [1], chemical vapor deposition [2], chemical bath deposition [3], sol-gel [4] and electrochemical deposition [5]. Among them, the electrodeposition allows an easy control of Cu_2O properties by monitoring the deposition parameters, such as the applied potential, temperature and the pH of the deposition bath. In particular, the solution pH has great influences on the properties of Cu_2O films. Several studies [6, 7] have reported that the carrier concentration of Cu_2O depends strongly on the values of the electrolyte pH. The carrier concentration of Cu_2O is one of the crucial factors that can determine the overall performance of Cu_2O/ZnO solar cells. In an early report [8], Cu_2O films were deposited on ZnO nanowires from an alkaline bath of different pH values. It was found that Cu_2O prepared in strongly alkaline solution (pH~11) has higher carrier concentrations, which improve the performance of Cu_2O/ZnO heterojunction.

In this chapter, in order to improve the carrier concentration, Cu_2O films were deposited from strongly alkaline solutions of two different pH values and the pH effect on Cu_2O properties was carefully examined. In addition, we used these films as an absorber layer in Cu_2O/ZnO heterojunction with different thickness. The effect of Cu_2O properties and thickness on the performance of Cu_2O/ZnO heterojunction was demonstrated.

4.2 Electrodeposition of Cu_2O/ZnO heterojunctions

All the samples were deposited by electrochemical deposition in a potentiostatic mode, using a computer-controlled Potentiostat/Galvanostat (Voltalab 40) as a potential source relied to three-electrode cell. The fluorine-doped tin oxide substrate (FTO, 10–20 Ω/cm^2 sheet resistance) is used as a working electrode, a platinum wire as a counter electrode and saturated

calomel electrode (SCE, + 0.241 V vs. SHE) as a reference electrode. All potentials reported with reference to the SCE scale. Prior to the ECD, the FTO substrates were degreased ultrasonically in acetone and ethanol for 10 minutes to remove the organic contamination on the surface then well rinsed with distilled water.

All the Cu_2O/ZnO heterojunctions are constructed by two steps electrodeposition process on FTO substrate. Firstly, we deposited ZnO layer on FTO coated glass substrate followed by the deposition of Cu_2O layer on ZnO, as shown in figure 4.1.

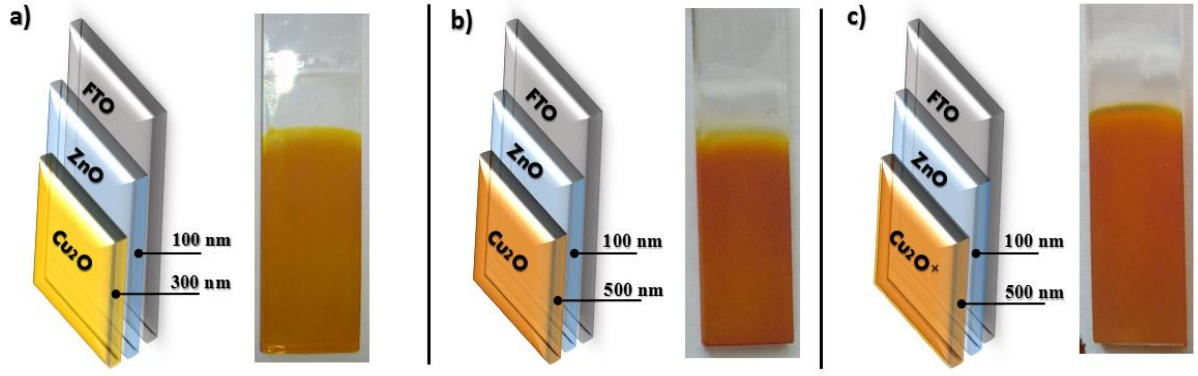

Fig. 4.1. *Schematic diagram and photographs of* ***a)*** *300 nm Cu_2O/ZnO,* ***b)*** *500 nm Cu_2O/ZnO and* ***c)*** *500 nm Cu_2O^+/ZnO/AZO heterojunctions.*

The ZnO layer (100 nm) is deposited from nitrate bath under the same deposition parameter (Tab.1.1) for all samples. However, the Cu_2O layers were deposited under different ECD conditions including pH, temperature, and applied potentials as summarized in table 4.1. To avoid the notation confusion, the Cu_2O deposited at high pH will be noted as '' Cu_2O^+ '' while that deposited at low pH will be noted as **''**Cu_2O**''**. The thickness of the deposited layers was controlled using the chronocoulometry method.

Table 4.1. *The electrochemical deposition parameters of ZnO, Cu_2O and Cu_2O^+ layers.*

Layer thickness	Bath composition	pH	Temperature (°C)	Potential (V/SCE)
100 nm ZnO	1M KNO_3 0.08M $Zn(NO_3)_2$	6.5	70	-1.7
300-500 nm Cu_2O	0.05 M $CuSO_4$ 0.05M $C_6H_8O_7$ 4 M NaOH	11	60	-0.5
500 nm Cu_2O^+	0.05 M $CuSO_4$ 0.06 M $C_6H_8O_7$ 4 M NaOH	12	70	-0.65

For the electrochemical, structural, morphological, optical and electrical characterizations, we used the same techniques and employed the same parameters reported in the previous chapters. In exception of the photocurrent measurements used, in this chapter, to study the photo-activity of Cu_2O layers. It was recorded in 0.5 M Na_2SO_4 solution at an applied potential of - 0.5 V/SCE with a Xenon lamp (500 w) as a light source.

4.3 Results and discussion

4.3.1 Effect of the pH on the properties of Cu_2O layer

3.1.1 Electrochemical characterization

As a starting point, we investigated the effect of the bath pH on the electrical properties of 300 nm Cu_2O layer. Mott-Schottky measurements were performed to determine the flat band potential and the acceptor concentration of Cu_2O layers. The depletion layer capacitance (C^{-2}) was measured as a function of the applied potential (E), at a fixed frequency of 20 kHz, and presented as M–S plot following the equation below [9]:

$$\frac{1}{c^2} = \frac{2}{-eN_A \varepsilon \varepsilon_0}\left(E - E_{fb} - \frac{kT}{e}\right) \quad (4.1)$$

where C is the space charge capacitance, e is the electron charge, N_A is the acceptor concentration of p-type semiconductor, ε_o is the vacuum permittivity, ε is the dielectric constant of Cu_2O (7.6) [10], *k* is the Boltzmann constant, T is the absolute temperature, E is the applied potential and E_{fb} is the flat-band potential. Figure 4.2 displays the Mott–Schottky plots recorded in 0.5M Na_2SO_4 with Cu_2O layers deposited at different pH set as the working electrode. The two plots show straight lines with negative slopes, which confirm p-type semiconductor characteristics of these layers, respectively.

It is well established that the acceptor concentration (N_A) can be calculated from the M-S plot slope (S) and the E_{fb} can be calculated from the intercept (V_0) at $(1/C_{CS}^2) = 0$ as indicated in the following equations:

$$N_A = \frac{2}{-e \varepsilon \varepsilon_0 S} \quad (4.2)$$

$$E_{fb} = V_0 + \frac{kT}{e} \quad (4.3)$$

The acceptor concentration of 300 nm Cu_2O layer deposited at pH 11 was 5.8×10^{15} cm^{-3}, while the Cu_2O layer deposited at pH 12 have an acceptors concentration of 3.28×10^{17} cm^{-3}, which is several orders of magnitude higher than the carrier concentration of Cu_2O deposited at pH 11. This may be due to the increase of copper vacancies (V_{Cu}) at high pH.

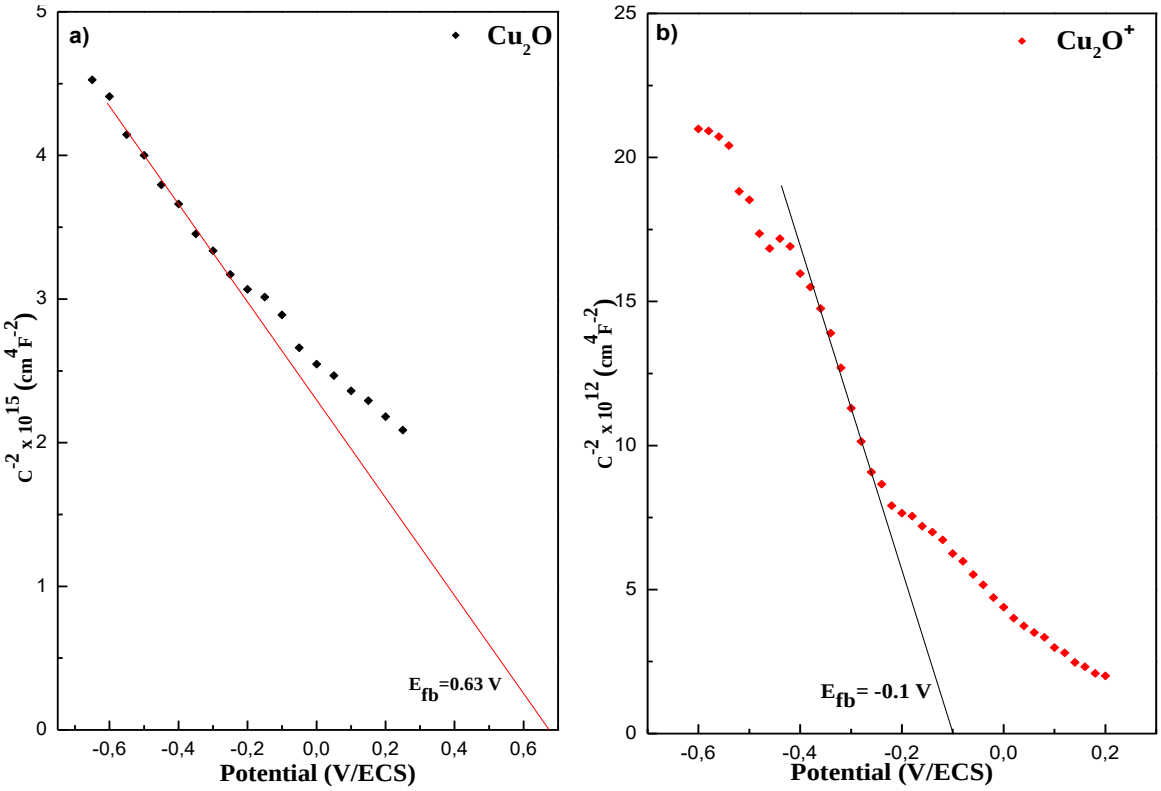

Fig. 4.2. *Mott–Schottky plots of 300 nm Cu_2O deposited at alkaline pH:* ***a)*** *pH 11and* ***b)*** *pH 12.*

Since the p-type conductivity of Cu_2O is ascribed to a native point defect known as the copper vacancies (V_{Cu}) that act as acceptor centers in Cu_2O layer [11]. Increasing the bath pH induce an excess of oxygen to the deposition medium which helps the formation of V_{Cu}; consequently, increase the acceptors concentration. The flat band potentials (E_{fb}) noted from M-S plots were 0.63 and -0.10 V for Cu_2O layers deposited at pH 11 and 12, respectively. It is clear that the flat band potential decrease with the increase of carrier concentration at high pH, this is due to the shift of Fermi level away from the valence band as the carrier concentration increase [12].

The Cu_2O is the absorbent layer in the Cu_2O/ZnO heterojunction, so it plays an important role in the conversion of light into electricity. Beside the acceptor concentration, many other parameters can affect the absorbent layer performance such as the carrier mobility and the light absorption. The photocurrent analysis is a powerful tool that gives information about the semiconductor behavior in dark and under illumination. In order to investigate the photo-generation and the separation of the electron-hole pairs in Cu_2O layers, deposited at different pH, we performed a photocurrent analysis using home-made montage. Figure 4.3 shows the transient photocurrent responses recorded under chopped illumination in 0.5 M Na_2SO_4

solution and an applied potential of - 0.5 V with Cu_2O layers deposited at different alkaline pH set as working electrode.

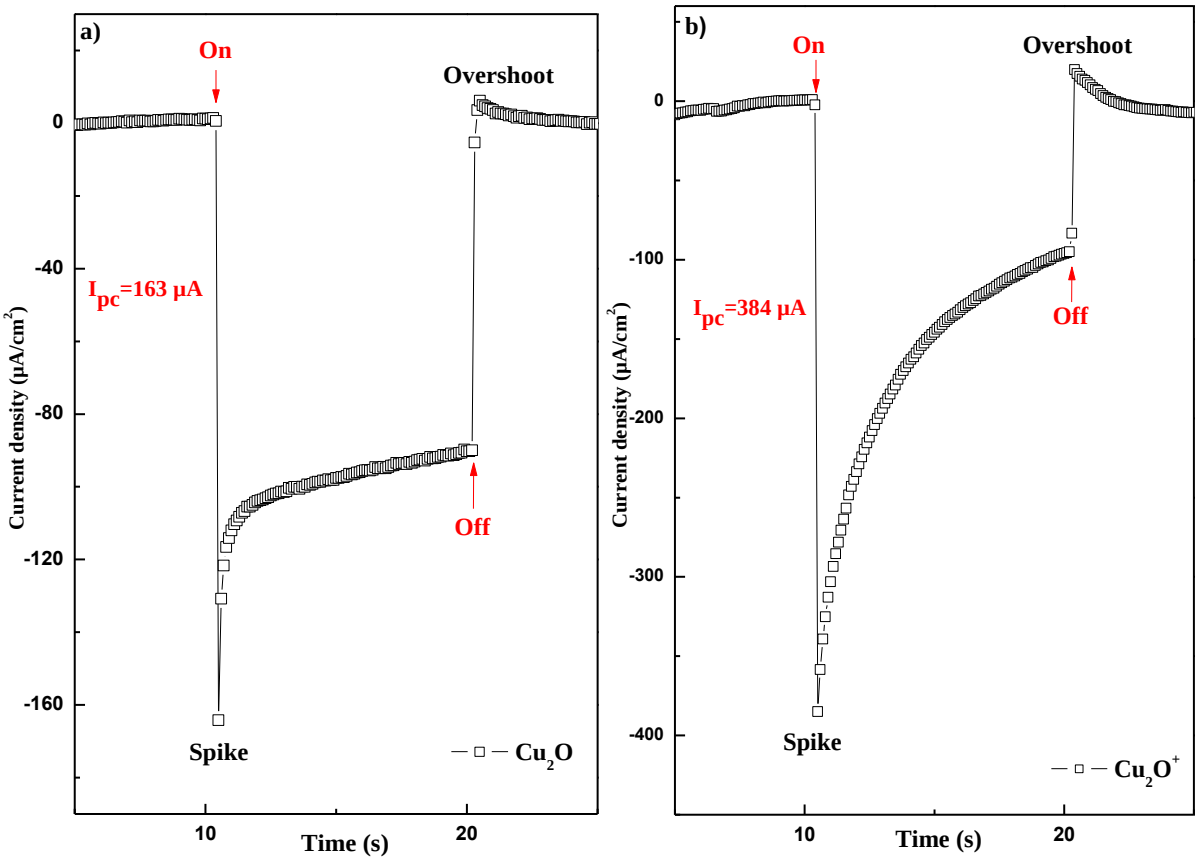

Fig. 4.3. *The transient photocurrent responses of 300 nm Cu_2O layer deposited on FTO substrate at different alkaline pH:* ***a)*** *pH 11 and* ***b)*** *pH 12.*

The two samples present a stable and reproducible photocurrent with time. In the dark, there is no current noted (Fig. 4.3a,b), as the light switched on, the two samples show an abrupt decrease in the current density refers to a high kinetics of electron-hole generation and separation. This cathodic photocurrent (negative current) confirms the p-type characteristic of Cu_2O layers deposited at pH 11 and 12, respectively. Thus, under illumination, the Cu_2O layers generate the electrons as a minor carrier that reach the surface to react with the electrolyte [13]. The reduction of H^+ ions present in the solution by the photogenerated electrons shows a cathodic photocurrent. When the light switched off the current increase sharply up to zero. It is important to note that the Cu_2O layer deposited at pH 12 show a photocurrent (I_{ph}) of 384 µA (fig. 4.3b), which is two times higher than I_{ph} generated by Cu_2O deposited at pH 11 (Fig. 4.3a) indicating a higher generation of electron-hole pairs. This improvement may be due to the high donor concentration on Cu_2O layer deposited at pH 12 as reported in Mott-Schottky measurements.

Comparing the shape of the two responses, the spike and the overshoot are stronger in the response of Cu_2O deposited at pH 12 (Fig. 4.3b) referring to an abundant decay of the photocurrent with time. Which means that a high recombination of the photogenerated electron−hole pairs occurs in this layer [14], i.e. the photogenerated electrons moved to Cu_2O surface and recombined with the holes from the valence band rather than reacted with the electrolyte.

3.1.2 Structural characterization

Figure 4.4 presents the XRD patterns of Cu_2O layers deposited on FTO substrate at different alkaline pH values.

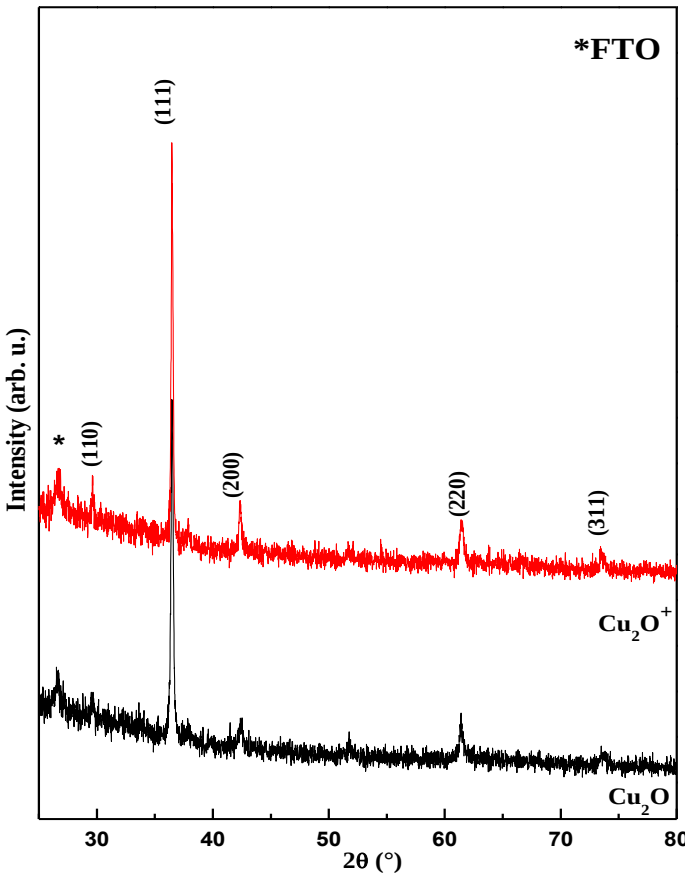

Fig. 4.4. *XRD patterns of Cu_2O layers deposited on FTO substrate at different alkaline pH: pH 11 (Cu_2O) and pH 12 (Cu_2O^+).*

The diffraction peak with an asterisk corresponds to the FTO conductive thin layer coated on glass (substrate). All the diffraction peaks in the two patterns correspond to the cubic Cu_2O structure (JCPDS card n° 00-034-1354). No peaks of impurities such as cupric oxide (CuO) or metallic copper (Cu) are detected. Which confirm the deposition of pure polycrystalline Cu_2O layers for the two values of pH. Moreover, the sharp and narrow peaks indicate that Cu_2O is highly crystallized and preferentially oriented along (111). This orientation is the favorable one

for good epitaxial growth on ZnO layer. Many studies have reported that the bath pH controls the microstructural properties by affecting the deposition rate [15-17]. In this context, Wang et al. [18] investigated the effect of pH on Cu_2O properties by varying the bath pH from 7.0 to 12.0 with a step of 0.2, it was found that (111) is the preferred orientation for bath pH above ~10.2; which is in accordance with our results. It is well known that each plane in the Cu_2O structure have different oxygen density, where, (111) plane have the highest number of oxygen atoms per unit area (N_o) as shown in fig 4.5a. On the other hand, the reduction of Cu^{+2} ions is the source of Cu^+ (constant during the deposition of Cu_2O) and the hydroxyl ions (OH^-) are the source of O^{2-} atoms and they control the growth rate of Cu_2O. Thus, increasing OH^- concentration (increasing the pH) will favor the formation of the crystallographic plane of high N_o, i.e (111) plane. This defines the shape of the obtained crystallite as 3-sided pyramid [18], with {100} crystallographic planes as side faces and the <111> axis perpendicular to the substrate (Figure 4.5b).

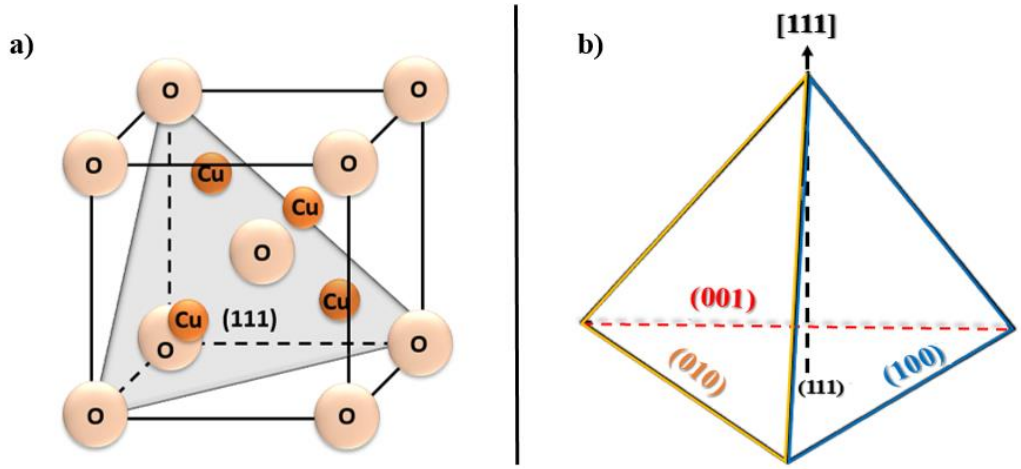

Fig. 4.5. a) *(111) crystallographic plane in a cuprous oxide cell,* ***b)*** *Crystallite shape of differently expected of (111) orientated grain.*

In this section, it has been shown that the deposition bath pH has a great effect on the properties of Cu_2O. The Cu_2O deposited in strongly alkaline solution (pH~12) shows a huge improvement especially the absorption and donor concentration. The section that follows moves on to Cu_2O/ZnO heterojunctions properties. Where ZnO layer of 100 nm deposited on FTO substrate is used as a window layer and Cu_2O deposited at different alkaline pH (pH 11 and pH 12) were used as absorbent layers. We will present the principal findings of the effect of the absorbent layer (Cu_2O) on the performance of Cu_2O/ZnO heterojunction.

4.3.2 Effect of Cu_2O absorber layer properties on Cu_2O/ZnO heterojunction performance

To investigate the effect of Cu_2O absorbent layer on the Cu_2O/ZnO heterojunction properties, we deposited Cu_2O layers in different alkaline bath pH (pH 11 and pH 12) and for different thicknesses (500 and 300 nm) on 100 nm ZnO layer. To simplify the notation, the Cu_2O deposited at pH 12 will be marked as Cu_2O^+, thus, the three samples studied in this section are 300 nm Cu_2O/ZnO, 500 nm Cu_2O/ZnO and 500 nm Cu_2O^+/ZnO heterojunctions deposited on FTO substrate.

3.2.1 Structural characterization

The structure of the electrodeposited Cu_2O/ZnO and Cu_2O^+/ZnO heterojunctions with different thickness of Cu_2O was confirmed using XRD analysis. Figure 4.6 presents the XRD patterns of Cu_2O/ZnO and Cu_2O^+/ZnO heterojunctions with different thickness of Cu_2O.

Besides the diffraction peak of the FTO substrate (marked by asterisks), all other diffraction peaks can be ascribed to cubic Cu_2O structure (JCPDS card n° 00-034-1354) and ZnO wurtzite structure (JCPDS card n° 00-036-1451) and prove their pure phases. The overlapped peaks at 36.31 correspond to both ZnO (101) and Cu_2O (111) orientations. Other peaks noted at 29.46, 42.27, 61.33, 73.59 and 77.3 were indexed to Cu_2O (110), (200), (220), (311) and (222) orientations, respectively. Which indicates that the deposited films are composed of Cu_2O crystallites with random orientation. Moreover, the high intensity of (111) and (101) direction of Cu_2O and ZnO, respectively, indicating that the obtained heterojunctions are preferentially oriented along (111) and (101) directions, respectively. The sharp and narrow peaks show that the heterostructures are highly crystallized in particular for samples with 500 nm Cu_2O^+.

The average crystallite size (D) of the deposited heterojunctions was estimated using the Scherrer formula [19]:

$$D = \frac{0.94\lambda}{\beta \cos \theta} \qquad (4.4)$$

where D is the crystallite size (nm), λ=1.54056 Å is the wavelength of the incident radiation, β is the full width at half maximum [FWHM] (rad), and θ is the Bragg angle (rad). The FWHMs have been determined by fitting Gaussian profile peaks to the experimental data. The crystallites size of Cu_2O layers deposited at pH 11 were 35 and 43 nm for 300 and 500 nm Cu_2O thickness, respectively. While a higher crystallites size of 53 nm was obtained for 500 nm Cu_2O layer

deposited at pH 12. This may be due to the increase of deposition rate at high pH and temperature.

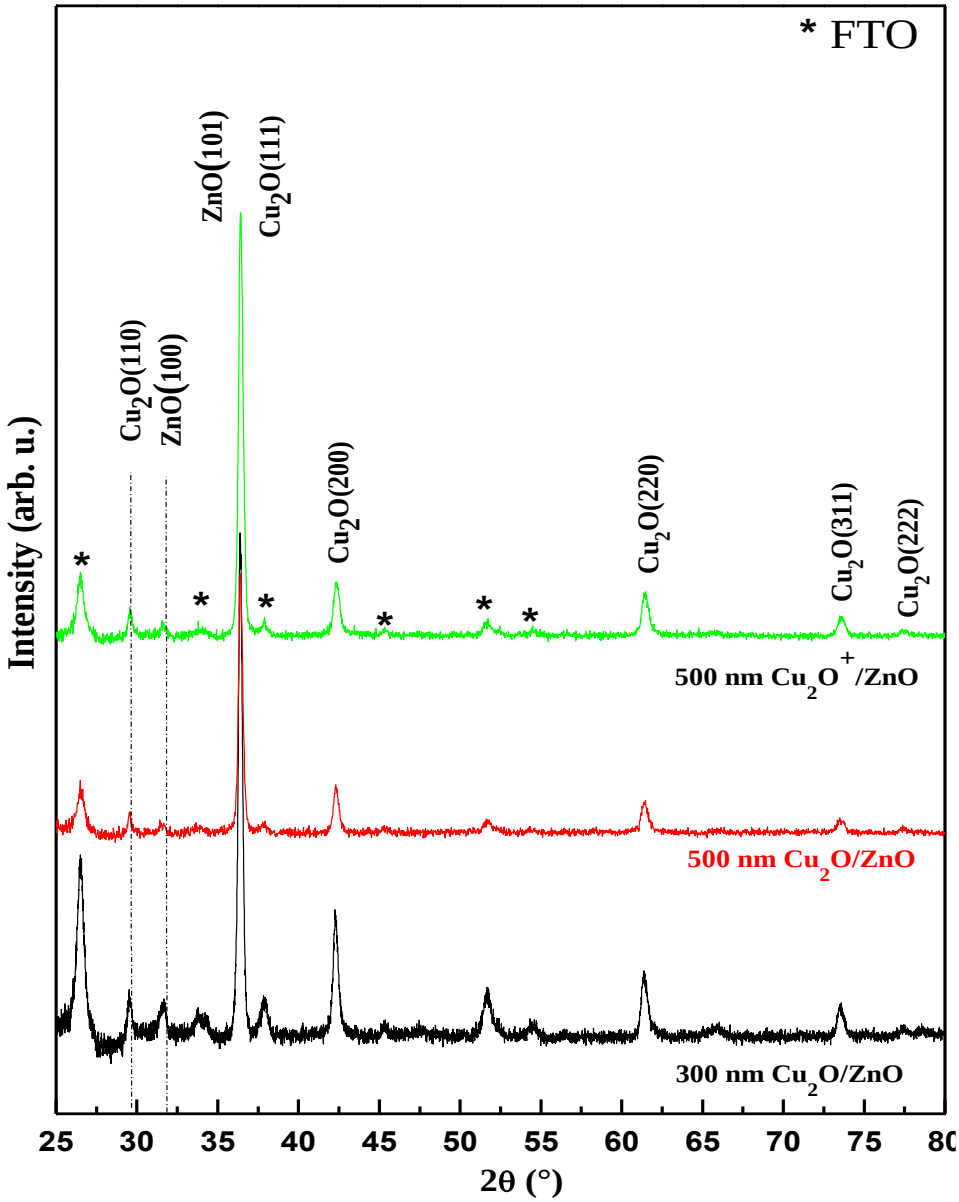

Fig. 4.6. *XRD* patterns *of 300 nm Cu_2O/ZnO, 500 nm Cu_2O/ZnO and 500 nm Cu_2O^+/ZnO heterojunctions.*

3.2.2 Morphological characterization

The morphology of the samples was studied by field emission scanning electron microscopy (FE-SEM). Figure 4.7a-e presents top-view and cross-section SEM images, at 45° inclination, of Cu_2O/ZnO heterojunction with Cu_2O deposited at pH 11 and pH 12 for different thickness. The grains size was estimated using the Visiometre software. For the 300 nm layer of Cu_2O deposited at pH 11, the top view image (Fig.4.7a) reveals a continuous film of Cu_2O pyramidal grains spread all over the top surface of ZnO layer. The estimated size of Cu_2O grains

vary between 100 nm and 286 nm; it is important to note the presence of large pores of different sizes (average size about 30 nm) in the Cu_2O grains as shown in figure 4.7a'. The cross-section image in fig.4.7d reveals a good coverage of the FTO substrate with flat layer ZnO of 98 nm. This latter was covered by 308 nm Cu_2O thick layer. The (111) orientation of Cu_2O layer results in the triangular texturing surface noted from this FE-SEM image.

When the thickness of Cu_2O, deposited at pH 11, was increased to 500 nm (Fig.4.7b), the Cu_2O crystal particles started to form a dense film with well-defined shape and the holes disappeared completely from the film surface (Fig.4.7b'). The cross-section image in Fig.4.7e presents a good coverage of the FTO substrate with 100 nm flat layer of ZnO, on top of this latter, 508 nm of Cu_2O was covering the whole surface. It is worth pointing out that the thickness of Cu_2O and ZnO measured from the cross-section image (Fig.4.7d,e) was about the same as the theoretical values calculated using Faraday equation. This indicates a high Faradaic efficiency of the electrodeposition of Cu_2O and ZnO, i.e. every measured electron is from the electrochemical reaction.

The figure 4.7c shows a top view image of 500 nm Cu_2O layer deposited at pH 12, we noted the formation of poorly defined needles and aggregates with the deterioration of the cubic morphology compared to the Cu_2O layer deposited at pH 11 (Figure 4.7b). However, the fig. 4.7c' reveals an increase in the size of Cu_2O grains to range between 370 and 550 nm. This may be due to the large crystallite size of Cu_2O deposited at pH 12 compared to the other samples, calculated by Scherrer formula (eq.4.4).

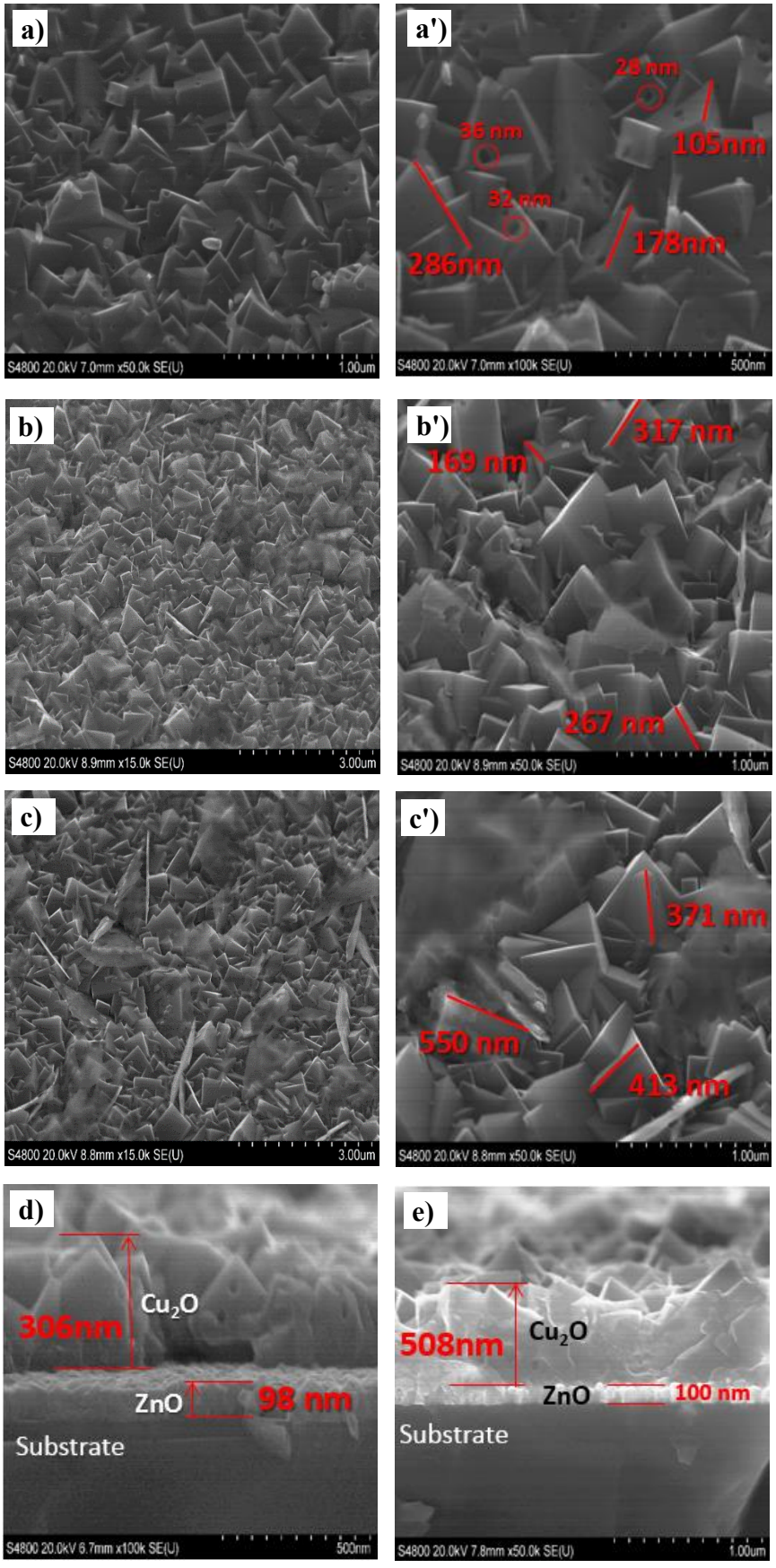

Fig. 4.7. *Typical top view FE-SEM images of Cu_2O/ZnO heterojunctions with:* ***a)*** *300 nm Cu_2O (pH 11)* ***b)*** *500 nm Cu_2O (pH 11) and* ***c)*** *500 nm Cu_2O (pH 12).* ***a')-c')*** *Higher magnification images.* ***d)-e)*** *Cross-section FE-SEM images of the respective heterojunctions (**a** and **c**).*

3.2.3 Optical characterization

In this section, we studied the absorbance and transmittance ability of the Cu_2O/ZnO heterojunctions with Cu_2O layer deposited in two values of solution pH. Before performing the UV-Vis analysis of Cu_2O/ZnO heterojunctions, it is necessary to present that of Cu_2O layer deposited in different solution pH. Figure 3.8 presents the UV-Vis spectra of Cu_2O layer deposited in different solution pH with 300 and 500 nm thickness, respectively.

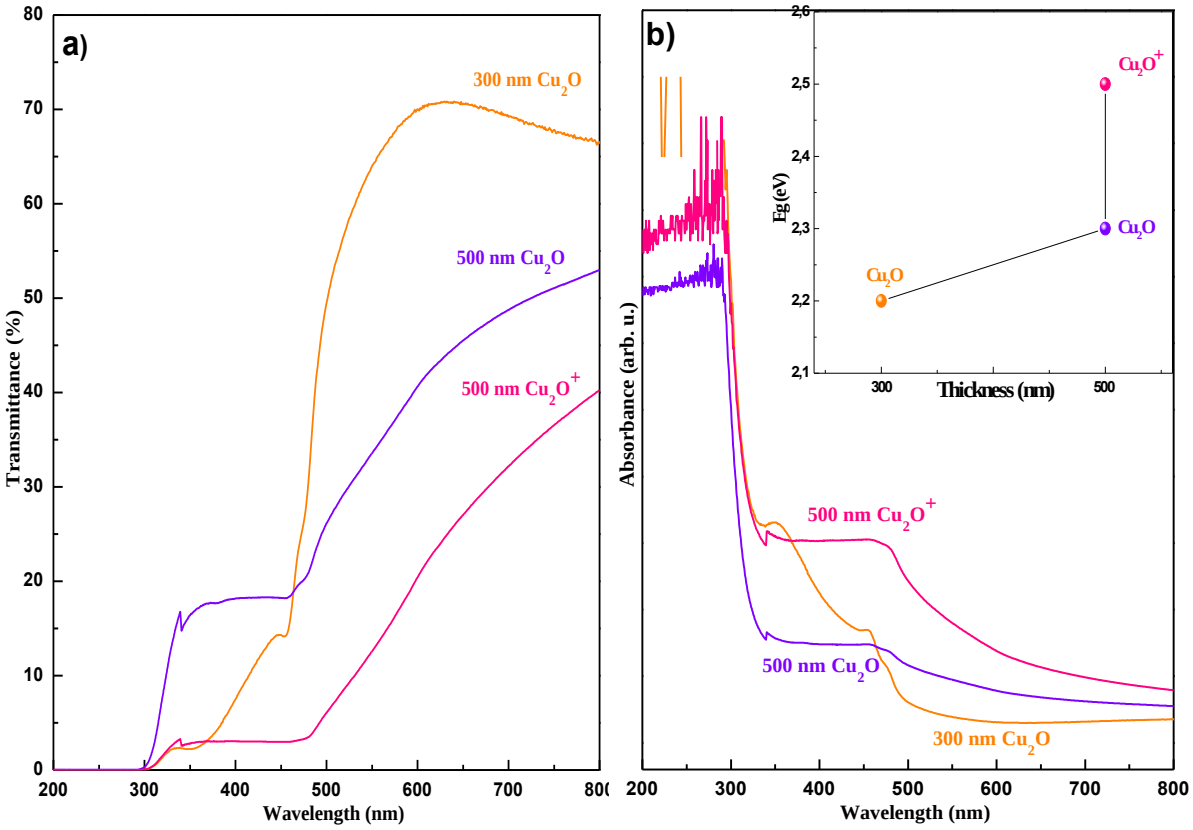

Fig. 4.8. a) *UV-VIS transmittance spectra and* ***b)*** *Absorbance spectras of 300 nm Cu_2O (pH 11), 500 nm Cu_2O (pH 11) and 500 nm Cu_2O^+ (pH 12) layers.*

For the Cu_2O deposited at pH 11, high transmittance values of about 60 and 55 % were noted for 300 and 500 nm thickness, respectively (Fig. 4.8a). This decrease is due to the decline of Cu_2O layer transparency with increasing the thickness. The 500 nm Cu_2O (pH 12) shows a transmittance of 40 %. On the other hand, the absorbance spectra in Fig. 2.8b reveals strong absorbance in the visible region for all the samples. Moreover, increasing the thickness of Cu_2O (pH 11) from 300 to 500 nm induces a red shift of the absorbance to the visible wavelength (from 450 nm to 500 nm). This may be due to the improvement of Cu_2O crystallinity at high thickness. As well, the 500 nm Cu_2O deposited at pH 12 indicates a high absorbance in the visible region (<500 nm). As the maximum of the solar energy is within the visible region, a high absorbance in this region is favorable for the absorber materials such as Cu_2O. The inset

of figure 2.8b shows the values of the band gap energies estimated by extrapolating the linear part in $(\alpha h\nu)^2$ vs. $(h\nu)$ plots. The obtained band gap energies were 2.20 and 2.30 eV for 300 and 500 nm of Cu_2O (pH 11), and 2.5 eV Cu_2O (pH 12).

The following section discusses the optical properties of Cu_2O/ZnO heterojunctions. Fig. 4.9a presents the UV-vis transmittance spectra of Cu_2O/ZnO heterojunction with Cu_2O layer deposited in different pH solution, recorded in reference to FTO substrate. All the samples show a significant transmittance starting 480 nm. A transmittance of 60 and 30 % was noted for Cu_2O/ZnO with 300 and 500 nm Cu_2O (pH 11), respectively, and 40 % for 500 nm Cu_2O (pH 12). There is no significant difference between those values and Cu_2O layers transmittance values (Fig. 4.8a). Turning to the absorbance spectra in fig. 2.9b. All the heterojunctions show a strong absorbance in the visible region, increasing the thickness of Cu_2O from 300 to 500 nm induces a red shift of the absorbance to the visible wavelength (from 450 to 500 nm) indicating the improvement of the absorbance with increasing the thickness.

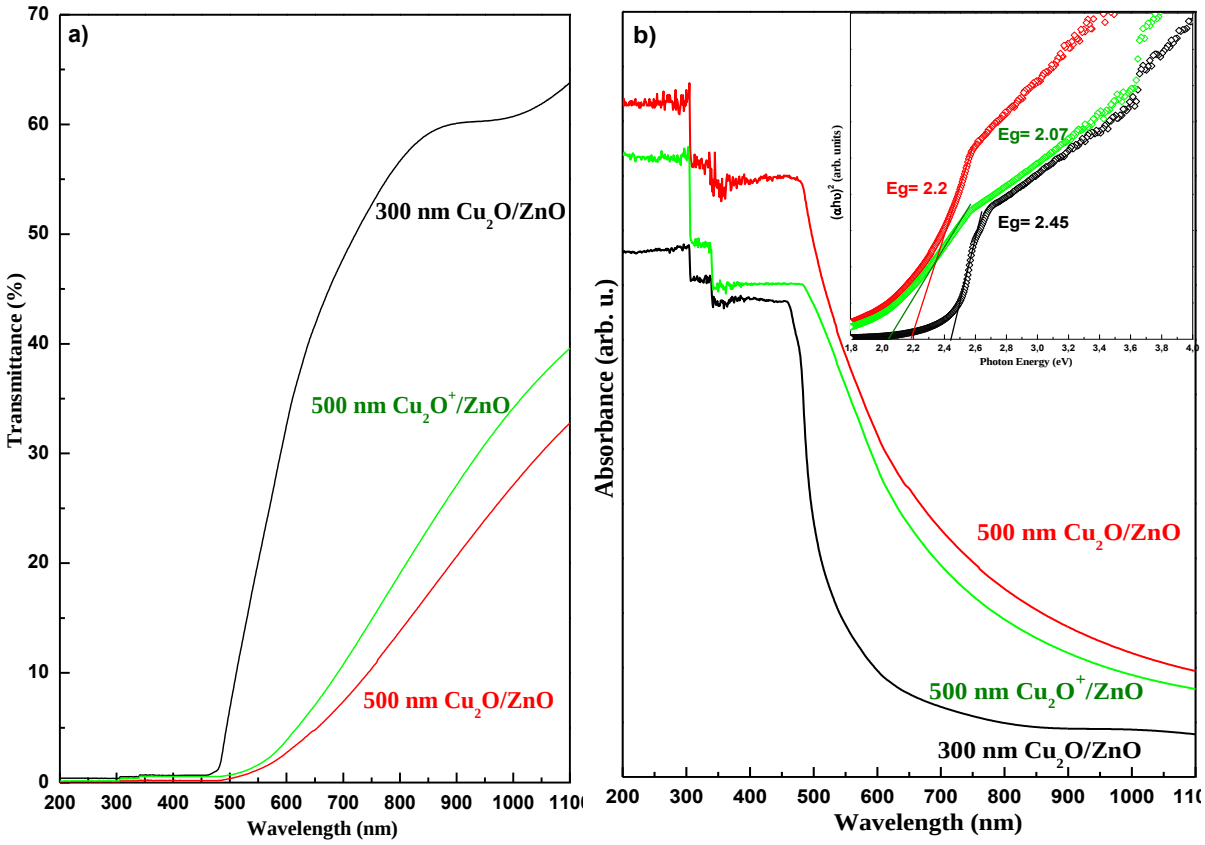

Fig. 4.9. a) *UV-VIS transmittance spectras and* ***b)*** *Absorbance spectras of 300 nm Cu_2O, 500 nm Cu_2O and 500 nm Cu_2O^+ deposited onto ZnO/FTO.*

The inset of figure 2.9b presents the Tauc's plots of Cu_2O/ZnO heterojunctions with Cu_2O deposited in two different solution pH. The values of the band gap energies estimated by

extrapolating the linear part in Tauc's plots. The obtained band gap energies were 2.45 and 2.2 eV for 300 and 500 nm of Cu_2O (pH 11), and 2.07 eV Cu_2O (pH 12).

3.2.4 Electrical characterization

The charge transport mechanism and the performance of the obtained heterojunctions were investigated using the current-voltage electrical characterization. This method based on the quantification of the currents crossing a junction under the effect of an external electric field. Figure 4.10 presents the current current-voltage characteristics, in the dark, of Au/p-Cu_2O/n-ZnO/FTO heterojunctions with Cu_2O deposited in two values of solution pH.

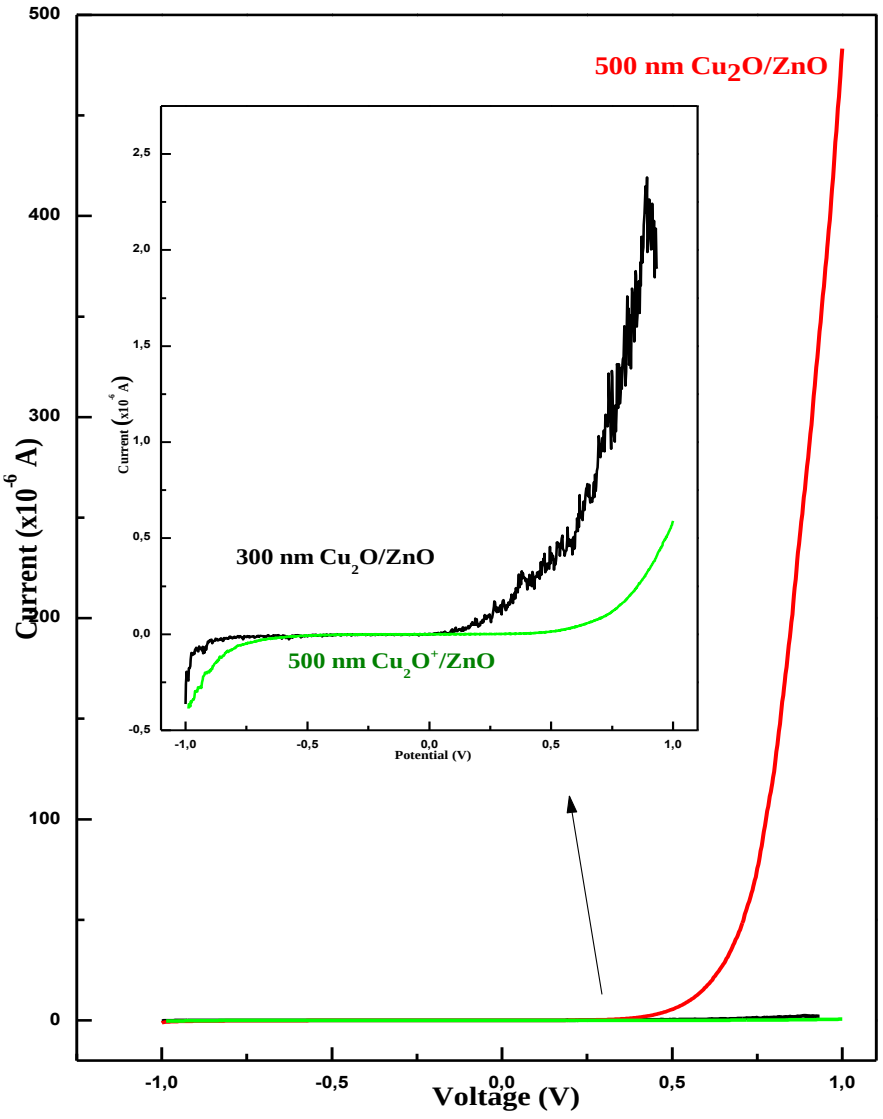

Fig. 4.10. *Current–voltage characteristics, in the dark, for Au/p-Cu_2O/n-ZnO/FTO heterojunctions with 300 nm Cu_2O, 500 nm Cu_2O and 500 nm Cu_2O^+ deposited on ZnO/FTO.*

It is clear that all the samples provide nonlinear behavior confirming the successful formation of the p-n heterojunction. However, 300 nm Cu_2O/ZnO heterojunction shows

unstable response with low turn-on voltage (0.3 V) under the positive bias with high leakage current (-0.4×10^{-6} A) at the reverse bias. This may due to the porous surface of Cu_2O layer (presence of holes on Cu_2O grains) observed in FE-SEM image (Fig. 4.7a'). While 500 nm Cu_2O/ZnO heterojunction provides near perfect response with turn-on voltage about 0.5 V. Moreover, we noted a high forward current of 4.8×10^{-4}A under positive bias of 0.6 V and small leakage current of -1.0×10^{-6}A at reverse bias of - 0.6 V. This improvement may be explained by the amelioration of morphology noted in FE-SEM image (Fig. 4.7b') and the increase of Cu_2O layer carrier concentration [20] with increasing Cu_2O layer thickness. Turning to the Cu_2O deposited at pH 12, a good electrical rectification is clearly observed for 500 nm Cu_2O^+/ZnO heterojunction with the highest turn on voltage of 0.6 V and low leakage current of -0.7×10^{-6} A (at -0.6 V). Therefore, the 500 nm Cu_2O^+/ZnO heterojunction have the highest performance, may be due to the high crystallinity of this sample confirmed by XRD and the high carrier concentration of Cu_2O deposited at pH 12 estimated from Mott-Schottky measurements.

In order to identify the effect of Cu_2O absorber layer on the performance of Cu_2O/ZnO heterojunction, we constructed the energy band diagrams of each sample based on Anderson model [21]. Figure 4.11 presents the energy band diagrams of p-Cu_2O/n-ZnO heterojunctions with different thickness of Cu_2O deposited in different solution pH.

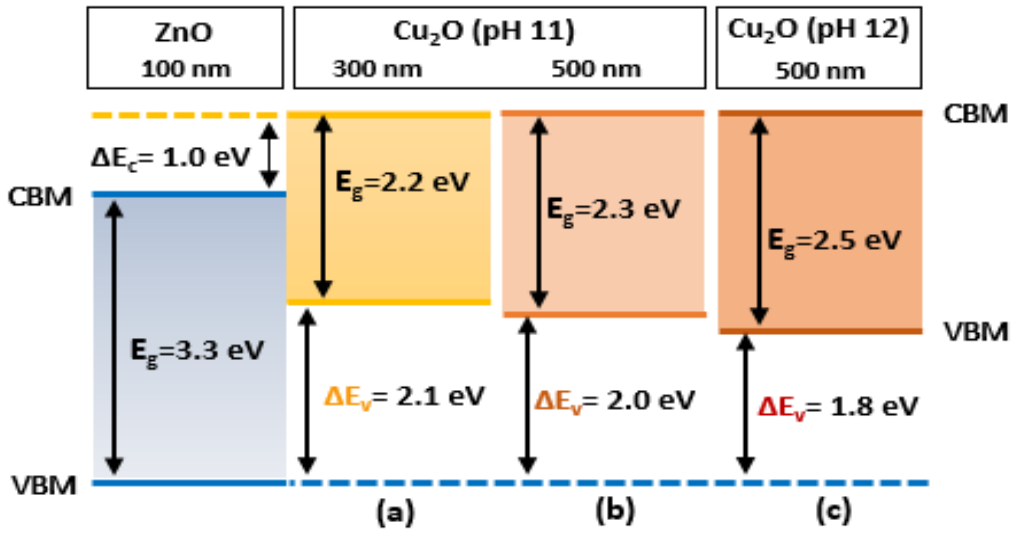

Fig. 4.11. *Band diagrams of p-Cu_2O/n-ZnO heterojunctions with* ***a)*** *300 nm Cu_2O (pH 11),* ***b)*** *500 nm Cu_2O (pH 11) and* ***c)*** *500 nm Cu_2O^+ (pH 12). For the simplicity, all the Cu_2O/ZnO heterojunctions were drown with one ZnO in the left side.*

The conduction band offset (ΔE_c) and the valence band offset (ΔE_v) of the heterojunction are calculated using the following equation [21]:

$$\Delta E_c = \chi_2 - \chi_1 \quad (4.5)$$

$$\Delta E_v = Eg_2 - Eg_1 + \Delta E_c \quad (4.6)$$

The electron affinity (χ) values of ZnO and Cu_2O are 4.2 and 3.2 eV, respectively [22, 23]. The obtained band gap energies (Eg) were 2.2, 2.3 and 2.5 eV for 300 nm Cu_2O (pH 11), 500 nm Cu_2O (pH 12) and 500 nm Cu_2O^+ (pH 12), respectively.

As shown in figure 4.11, the calculated conduction band offset (ΔE_c) was 1.0 eV for all the samples. Whereas, the valence band offset (ΔE_v) was affected by the thickness of Cu_2O layer and the deposition bath pH. For Cu_2O layer deposited in bath pH 11, the ΔE_v decreased from 2.1 to 2.0 eV with increasing Cu_2O thickness from 300 to 500 nm. Lower ΔE_v (1.8 eV) was obtained for 500 nm Cu_2O^+ layer deposited at higher bath pH (pH 12). This facilitates the electrons passage between the p-Cu_2O^+ and the n-ZnO layers, which explains the high performance of Cu_2O^+/ZnO heterojunction compared to the other samples.

4.4 Conclusion

In the first part of this chapter, the Cu_2O absorber layer was deposited in a strongly alkaline solution of two pH values. The effect of the bath pH on the structural, optical and electrical properties of Cu_2O was investigated. Increasing the pH to 12 enhanced the carrier concentration and improved the photo-response of Cu_2O layer. Moreover, a high quality Cu_2O layer of a cubic structure following (111) orientation with large crystallite size was obtained at this pH. In the second part, the Cu_2O layers deposited at pH 11 and 12 with different thickness were used as an absorber layer in Cu_2O/ZnO heterojunction. The effect of Cu_2O layer properties on the structural, morphological, optical and electrical properties of the heterojunction was carefully examined. The structural characterization confirms a high crystallinity of Cu_2O/ZnO heterojunctions following cubic (111) and wurtzite (101) structures, respectively. The cross-section FE-SEM images confirm the formation of a porous film of Cu_2O at pH 11; increasing the Cu_2O thickness to 500 nm shows a textured film of Cu_2O grains deposited on continuous flat ZnO layer for Cu_2O/ZnO. The current-voltage (I–V) curves confirm the formation of a junction in all the samples. However, unstable response with high leakage current noted for 300 nm p-Cu_2O/n-ZnO. The best response was attained for 500 nm p-Cu_2O^+/n-ZnO heterojunction. Overall, depositing the Cu_2O at high pH improve the carrier concentration and the crystallinity of the film, which enhance the performance of p-Cu_2O/n-ZnO heterojunction.

References

[1] W. Zhao, W. Fu, H. Yang, C. Tian, M. Li, Y. Li, L. Zhang, Y. Sui, X. Zhou, H. Chen, G. Zou, *Cryst. Eng. Comm.*, **13** (2011) 2871.

[2] N. Gupta, R. Singh, F. Wu, J. Narayan, C. McMillen, G.F. Alapatt, K.F. Poole, S.J. Hwu, D. Sulejmanovic, M. Young, G. Teeter, H.S. Ullal, *J. Mater. Res.*, **28** (2013) 1740.

[3] S. Bijani, L. Martınez, M. Gabas, E.A. Dalchiele, J.R. Ramos-Barrado, *J. Phys. Chem. C*, **113** (2009) 19482.

[4] A.S. Zoolfakar, A. Rani, A.J. Morfa, S. Balendhran, A.P.O. Mullane, K. Kalantarzadeh, *J. Mater. Chem.*, **22** (2012) 21767.

[5] I. Y. Bouderbala, A. Herbadji, L. Mentar, A. Beniaiche, A. Azizi, *J. Elec. Mater.*,(2017) 1.

[6] W. C. Wang, D. X. Wu, Q. M. Zhang, L. C. Wang, M. Tao, *J. Appl. Phys.*, **107** (2010) 123717.

[7] L. C. Wang, M. Tao, *Electrochem. Solid-State Lett.*, **10** (2007) H248.

[8] T. Jiang, T. Xie, L. Chen, Z. Fun, D. Wang, *Nanoscale*, **5** (2013) 2938.

[9] A. W Bott, *Electrochemistry of Semiconductors. Curr. Sep.*, **17** (1998) 87.

[10] Z. Zhang, P .Wang, *J. Matter. Chem.*, **22** (2012) 2456.

[11] H. Solache-Carranco, G. Juarez-Dıaz , A. Esparza-Garcıa, M. Briseno-Garcıa, M. Galvan-Arellano , J. Martınez-Juarez, G. Romero-Paredes, R. Pena-Sierra. *J. of Lumin.* **129** (2009).

[12] Y. Yang, J. Han, X. Ning, W. Cao, W. Xu, L. Guo, *ACS Appl. Mater. Interfaces*, **6** (2014) 22534.

[13] X. Shi, L. Cai, M. Ma, X. Zheng, J. H. Park, *Chem. Sus. Chem.*, **8** (2015) 3192.

[14] L. Peter, *J. Solid State Electrochem,* **17** (2013) 315.

[15] Y. Zhou, J. A. Switzer, *Scripta. Mater.*, **38** (1998) 1731.

[16] T. D. Golden, M. G. Shumsky, Y. Zhou, R. A. Werf, R. A. Van Leeuwen, J. A. Switzer, *Chem. Mater.*, **8** (1996) 2499.

[17] Y. Zhou and J. A. Switzer, *Mat. Res. Innovat.*, **2** (1998) 22.

[18] L. Wang, PhD thesis, University of Texas at Arlington, December 2006, Pg. 58.

[19] B. D. Cullity, *"Elements of X-ray Diffraction"*, 2nd edition (1978).

[20] Y. Chen, H. Yan, B. Yang, Y. Lv, M. Wen, J. Xu, M. Wu, X. Zhu, Z. Fu, *Appl. Phys. A: Mater. Sci. Process.*, **98** (2010) 467.

[21] A. G. Milnes and D. L. Feucht, "*Heterojunctions and Metal-Semiconductor Junctions*", *Academic*, New York, 1972.

[22] W. Siripala, A. Ivanovskaya, T. F. Jaramillo, S. H. Baeck, E.W. McFarland, *Sol. Energ. Mater. Sol. Cells*, **77** (2003) 229.

[23] H. Kobayashi, H. Mori, T. Ishida, Y. Nakato, *J. Appl. Phys.* **77** (1995) 1301.

Chapter 5

Electrochemical deposition of $Cu_2O^+/Cu_2O/ZnO$ trilayer device to improve the light absorption in p-Cu_2O/n-ZnO

Chapter 5: Electrochemical deposition of $Cu_2O^+/Cu_2O/ZnO$ trilayer device to improve the light absorption in p-Cu_2O/n-ZnO

5.1 Introduction

It is well known that the Cu_2O deposited at low-temperature has a low holes concentration [1-3] and short electron transport length mainly due to the low mobility (1.2 $cm^2.V^{-1}.S^{-1}$) [4-6]. This creates recombination region far from the Cu_2O/ZnO heterojunction interface (> 1.0 µm). Therefore, the conversion efficiency of the low temperature grown Cu_2O/ZnO heterojunction decreases due to the recombination of minority carrier before reaching the heterojunction interface.

To overcome this problem, Marin et al. [7] have engineering Cu_2O^+/Cu_2O/ZnO back surface field device to improve the charge collection in Cu_2O/ZnO solar cells. This new design was fabricated using an atmospheric atomic layer deposition (AALD) printing method, to grow 200 nm high doped copper oxide (Cu_2O^+) overlayer (has a carrier concentration around two orders of magnitude higher than the electrodeposited Cu_2O layer) on thick Cu_2O layer prepared by electrodeposition. Which reduce Cu_2O layer thickness from 3.0 µm to the approximate charge collection length (1.0 µm) while still allowing a high potential to be built into the solar cell. The conversion efficiency of this device was 28 % higher than the conversion efficiency of Cu_2O/ZnO device. In a recent study, Y. Liu et al. [3] reported a correction of the transport length of the minority carrier in the electrodeposited Cu_2O layer. Where the transport length consistent with the crystallite size of electrodeposited Cu_2O is found to be ~430 nm, significantly shorter than what other researchers have estimated in the past (1.0 µm). Thus, to achieve a higher conversion efficiency of Cu_2O^+/Cu_2O/ZnO back surface field device. The thickness of Cu_2O layer in this device should be reduced from 1.0 µm to ~430 nm to meet the real transport length of Cu_2O. Actually, to our knowledge, the fabrication of Cu_2O^+/Cu_2O/ZnO by electrochemical deposition has not yet been reported.

Based on those studies, to improve the light absorbance and carrier collection length in our samples, the Cu_2O^+/Cu_2O/ZnO back surface field device prepared by three steps ECD is reported in this chapter. Copper oxide (Cu_2O^+) layer of carrier concentration two orders higher than Cu_2O was deposited from strong alkaline solution (pH 12) on Cu_2O layer (pH 11). The ZnO thickness was fixed at 100 nm for all samples, while a different thickness of Cu_2O (300 and 500 nm) and Cu_2O^+ (100 and 150 nm) was employed. The effect of Cu_2O and Cu_2O^+

thickness on the structural, morphological optical and electrical properties of $Cu_2O^+/Cu_2O/ZnO$ heterojunction was investigated in details.

5.2 Electrodeposition of $Cu_2O^+/Cu_2O/ZnO$ heterojunctions

All the samples were deposited by electrochemical deposition in a potentiostatic mode, using a computer-controlled Potentiostat/Galvanostat (Voltalab 40) as a potential source relied to a three-electrode cell. The fluorine-doped tin oxide substrate (FTO, 10–20 Ω/cm^2 sheet resistance) is used as working electrode, a platinum wire as a counter electrode and saturated calomel electrode (SCE, + 0.241 V vs. SHE) as a reference electrode. Prior to the ECD, the FTO substrates were degreased ultrasonically in acetone and ethanol for 10 minutes to remove the organic contamination on the surface then well rinsed with distilled water.

The $Cu_2O^+/Cu_2O/ZnO$ heterojunctions were formed by three steps electrodeposition process on FTO substrate. Firstly, we deposited ZnO layer on FTO coated glass substrate followed by the deposition of two type of Cu_2O layers. The obtained samples are presented in figure 5.1.

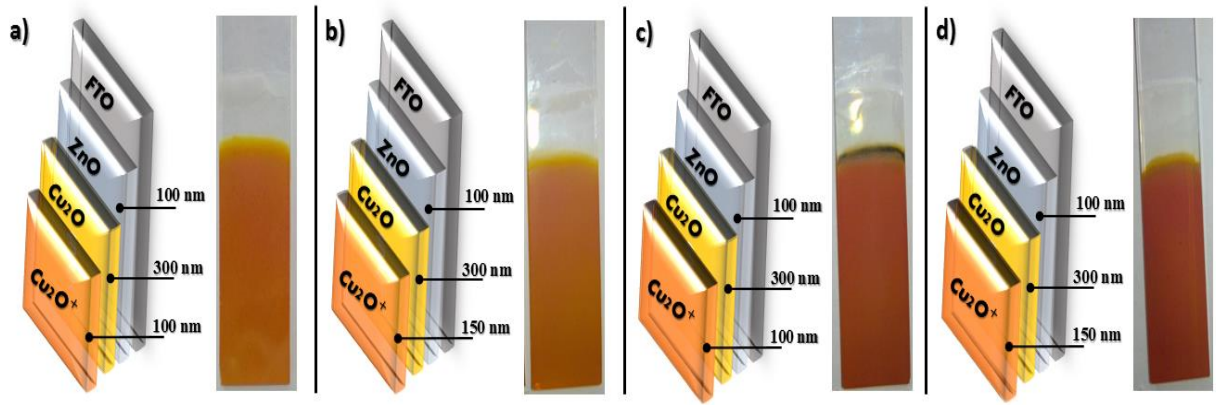

Fig. 5.1. *Schematic diagram and photographs of:* ***a)*** *100 nm Cu_2O^+/300 nm Cu_2O/ZnO,* ***b)*** *150 nm Cu_2O^+/300 nm Cu_2O/ZnO,* ***c)*** *100 nm Cu_2O^+/500 nm Cu_2O/ZnO/AZO and* ***d)****150 nm Cu_2O^+/500 nm Cu_2O/ZnO heterojunctions deposited on FTO.*

The ZnO layer (100 nm) is deposited from nitrate bath under the same deposition parameter for all samples. However, the Cu_2O layers were deposited under different ECD conditions. The first layer of Cu_2O is deposited from an alkaline solution of pH 11 and the second one is deposited from the same solution but at pH 12. To avoid any confusion in the notation, we kept the same one used in chapter 4; i.e. the copper oxide deposited at pH 11 is noted as "Cu_2O", while that deposited at pH 12 is noted as "Cu_2O^+". The ECD conditions used for the layers deposition are summarized in table 5.1.

Table 5.1. *The electrochemical deposition parameters of ZnO, Cu_2O and Cu_2O^+ layers.*

Layer thickness	Bath composition	pH	Temperature (°C)	Potential (V/SCE)
100 nm ZnO	1M KNO_3 0.08M $Zn(NO_3)_2$	6.5	70	-1.7
300-500 nm Cu_2O	0.05 M $CuSO_4$ 0.05M $C_6H_8O_7$ 4 M NaOH	11	60	-0.5
100-150 nm Cu_2O^+	0.05 M $CuSO_4$ 0.06 M $C_6H_8O_7$ 4 M NaOH	12	70	-0.65

The structural, optical, morphological and electrical properties of the deposited samples were characterized by the same techniques described in the previous chapters.

5.3 Results and discussion

5.3.1 Structural characterization

The crystallinity of the obtained $Cu_2O^+/Cu_2O/ZnO$ heterojunctions was confirmed by XRD analysis. Figure 5.2 presents the XRD patterns of $Cu_2O^+/Cu_2O/ZnO$ heterojunctions with different thickness of Cu_2O (300 and 500 nm) and Cu_2O^+ (100 and 150 nm). For all samples, besides the diffraction peak of the FTO substrate (marked by asterisks), all other diffraction peaks can be ascribed to ZnO wurtzite structure (JCPDS card n° 00-036-1451) and cubic Cu_2O structure (JCPDS card n° 00-034-1354) which proves the purity of the samples. The noted peaks at 29.54, 42.31, 61.36, and 73.57 were indexed to (110), (200), (220) and (311) orientations of Cu_2O, respectively. While the weak peak at 31.6 was indexed to (100) orientations of ZnO. The overlapped peaks at 36.31° correspond to both ZnO (101) and Cu_2O (111) orientations. Moreover, the (111) direction of Cu_2O and (101) of ZnO are very intense, indicating that the obtained heterojunctions are preferentially oriented along (111) and (101), respectively. The sharp and narrow peaks show that the electrodeposited heterostructures are highly crystallized. It is important to note that the peaks intensity increases with increasing the thickness of Cu_2O and Cu_2O^+ due to the augmentation of the Cu_2O amount with increasing the thickness.

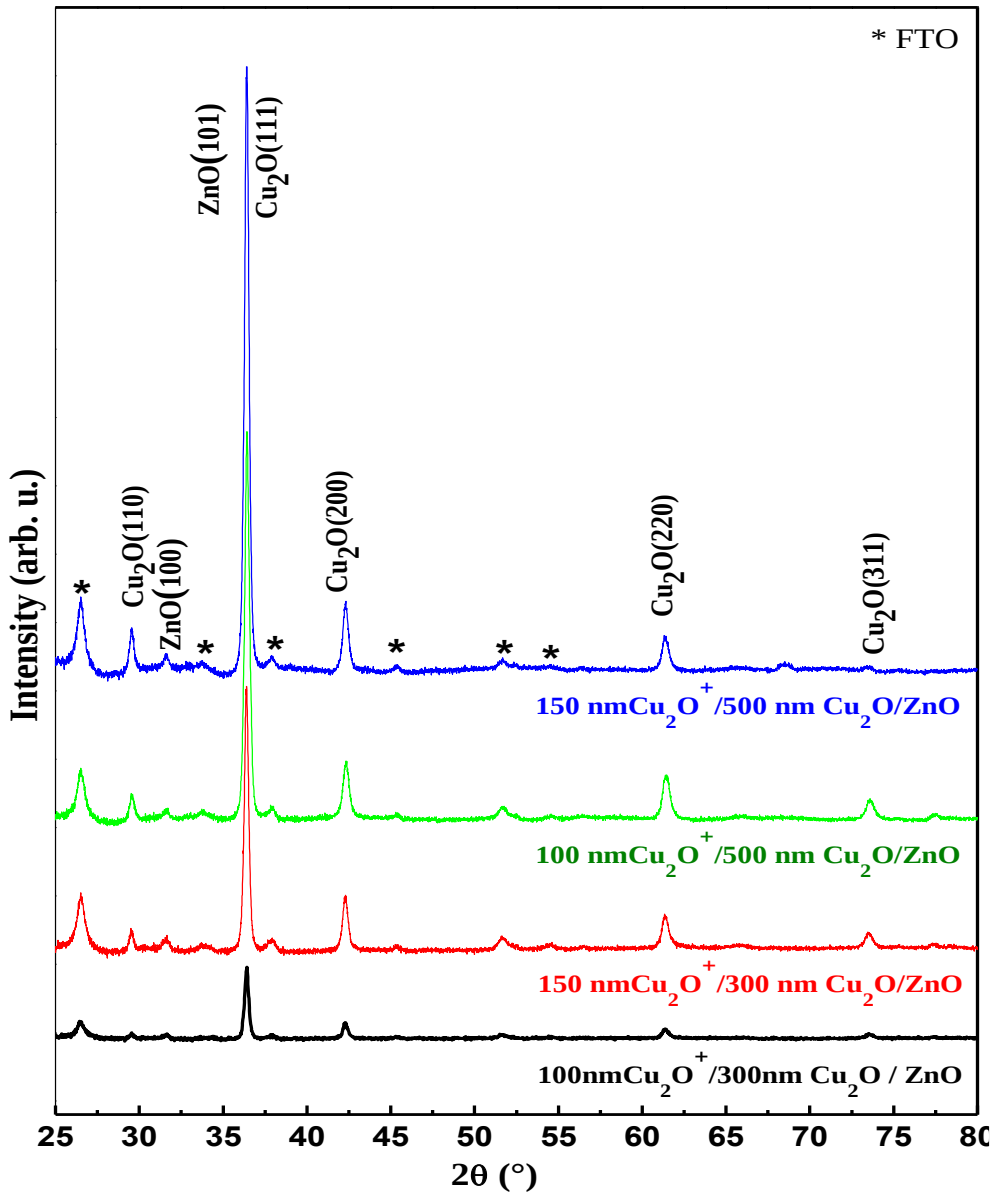

Fig. 5.2. *XRD patterns of samples* $Cu_2O^+/Cu_2O/ZnO$ *with different thicknesses of* Cu_2O *(300 and 500 nm) and* Cu_2O^+ *(100 and 150 nm) layers.*

The average crystallite size (D) of the deposited heterojunctions can be estimated using the Scherrer formula [8]:

$$D = \frac{0.94\lambda}{\beta \cos \theta} \tag{5.1}$$

where D is the crystallite size (nm), λ=1.54056 Å is the wavelength of the incident radiation, β is the full width at half maximum [FWHM] (rad), and θ is the Bragg angle (rad). The FWHMs have been determined by fitting Gaussian profile peaks to the experimental data.

The crystallites size estimated from the XRD spectra of $Cu_2O^+/Cu_2O/ZnO$ heterojunction with 300 nm of Cu_2O were 45.0 and 42.2 nm for 100 and 150 nm Cu_2O^+, respectively. While

the crystallites sizes estimated from the XRD spectra of $Cu_2O^+/Cu_2O/ZnO$ heterojunction with 500 nm of Cu_2O nm were 53.0 and 50.6 nm for100 and 150 nm Cu_2O^+, respectively. Comparing the results, $Cu_2O^+/Cu_2O/ZnO$ shows higher crystallites size with increasing the Cu_2O thickness from 300 to 500 nm. It is well known that a different crystallite sizes contain different dislocation defects, which have a great effect on the charge transport mechanism in the heterojunction [9].

5.3.2 Morphological analysis

The morphology of the deposited samples was examined by field emission scanning electron microscopy (FE-SEM) analysis and the grains size was estimated using Visiometre software. Before presenting the FE-SEM images of $Cu_2O^+/Cu_2O/ZnO$ heterojunctions, it is necessary to present FE-SEM images of the Cu_2O/ZnO heterojunction (i.e. the sample before depositing Cu_2O^+). Figure 5.3a,b presents top-view FE-SEM images of Cu_2O/100 nm ZnO heterojunctions with 300 and 500 nm thickness of Cu_2O layers, respectively. These images were studied in details in chapter 4, here; we presented them as reference samples to identify the effect of the Cu_2O^+ layer on the surface morphology. As shown in fig.5.3a, the 300 nm layer of Cu_2O, deposited on ZnO layer, is constituted of pyramidal grains (of size between 100 and 286 nm) contains large holes of average size about 30 nm. It is clear that the deposition of 150 nm Cu_2O^+ on 300 nm Cu_2O/ZnO improved greatly the surface morphology by filling the holes, as shown in figure 5.3c. In addition, the size of Cu_2O^+ grains increased to vary between 200 and 480 nm (Fig. 5.3c'), which is two times higher than that of Cu_2O grains.

Turning to Cu_2O/ZnO heterojunction with 500 nm Cu_2O layer, the top view FE-SEM image in fig. 5.3b reveals a dense film with well-defined pyramidal grains of Cu_2O with grains size vary between 100 and 360 nm spread all over the top surface of ZnO layer. The deposition of 150 nm Cu_2O^+ layer on 500 nm Cu_2O ameliorate the pyramidal morphology as presented in fig. 5.3d. The higher magnification image (fig.5.3d') shows an increase in the pyramidal grains size to range between 340 and 630nm.

It is important to note that the deposition of 150 nm Cu_2O^+ on Cu_2O layer (of 300 or 500 nm) did not change the film morphology, only the grains size increased. This means that the deposited Cu_2O^+ formed a flat and homogenous layer on the pyramidal grains of Cu_2O layer.

Let us now compare the FE-SEM images of $Cu_2O^+/Cu_2O/ZnO$ heterojunctions with 300 and 500 nm Cu_2O presented in fig. 5.3c' and fig. 5.3d', respectively. Since the thickness of ZnO layer and Cu_2O^+ layer is fixed at 100 and 150 nm, respectively, any changes in the morphology

of $Cu_2O^+/Cu_2O/ZnO$ heterojunction is due to Cu_2O layer properties. It is clear that higher grains size was obtained for 500 nm Cu_2O.

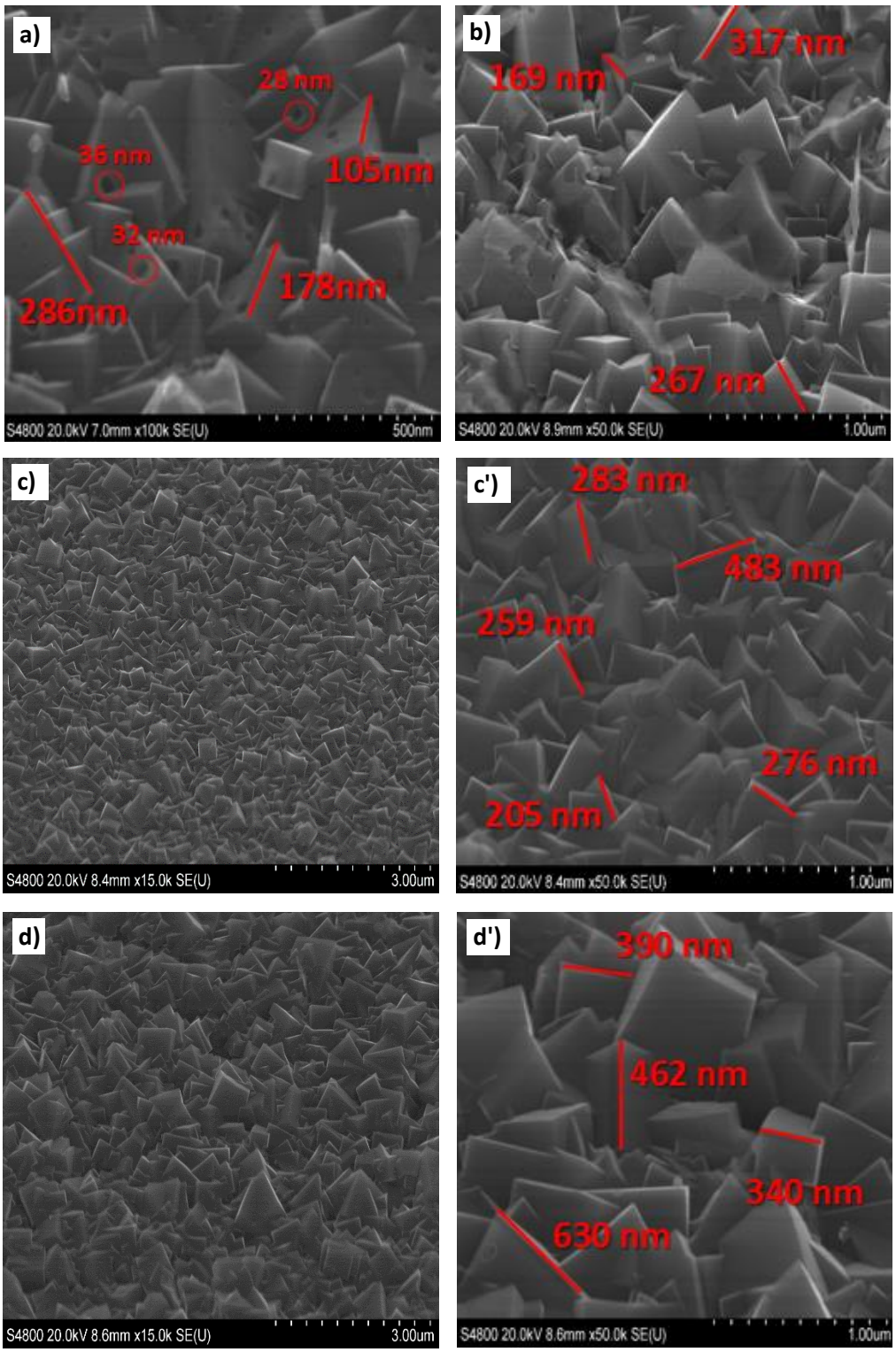

Fig. 5.3. *Typical top view FE-SEM images of* ***a)*** *300 nm Cu_2O/ZnO* ***b)*** *500 nm Cu_2O/ZnO* ***c)*** 150 nm *Cu_2O^+/300 nm Cu_2O/ZnO* and ***d)*** 150 nm *Cu_2O^+/500 nm Cu_2O/ZnO heterojunctions. c')-d') the higher magnification images.*

Overall, the deposition of 150 nm Cu_2O^+ on Cu_2O improved greatly the surface morphology of $Cu_2O^+/Cu_2O/ZnO$ heterojunction, which is expected to affect the electrical properties and consequently enhance the device performance.

5.3.3 Optical characterization

The light absorption–transmission ability is an important property that defines the performance of the heterojunction. In this section, we investigated the absorbance and transmittance property of the absorber layer Cu_2O^+/Cu_2O deposited on FTO substrate with different thickness of Cu_2O (300 and 500nm) and Cu_2O^+ (100 and 150 nm); Then compared it with $Cu_2O^+/Cu_2O/ZnO$ heterojunctions with different thickness of Cu_2O (300 and 500nm) and Cu_2O^+ (100 and 150 nm).

The UV-Vis transmittance and absorbance spectra of the Cu_2O^+/Cu_2O structure with different thicknesses of Cu_2O and Cu_2O^+ layers, recorded in the wavelength range from 200 to 800 nm, are shown in fig. 5.4. From the spectra in figure 5.4a, we can see that the transmittance of the samples significantly decreases from 60 to 40% with increasing the Cu_2O thickness from 300 to 500 nm. This due to the change of the sample's color from light orange to dark orange with increasing the Cu_2O thickness, which prevents the light transmission. It is important to note that increasing the Cu_2O^+ thickness from 100 to 150 nm has no significant influence on the transmission of Cu_2O^+/Cu_2O structure, thus, any change in Cu_2O^+/Cu_2O transmission depend on Cu_2O layer performance.

Moving on to the absorbance spectra in figure 5.4b, the absorbance spectra of the 500 nm Cu_2O layer deposited on FTO was used as a reference to investigate the effect of the Cu_2O^+ on the performance of the absorbent layer. All the Cu_2O^+/Cu_2O structures show stronger and larger absorbance peak than that of Cu_2O layer, in the visible region. Hence, the absorption improved greatly after the deposition of Cu_2O^+ on Cu_2O layer. Comparing the absorbance peaks of Cu_2O^+/Cu_2O structures, no significant increase in the absorption was detected when varying the Cu_2O^+ thickness from 100 to 150nm. However, a red shift of the absorption edge, into the visible region, was observed with increasing the thickness of Cu_2O layer from 300 to 500 nm. In addition, the Cu_2O^+/Cu_2O structures with 500 nm reveal a higher absorption peak intensity compared to Cu_2O^+/Cu_2O structures with 300 nm Cu_2O. This improvement offers to the absorber layer a better benefit of the solar light.

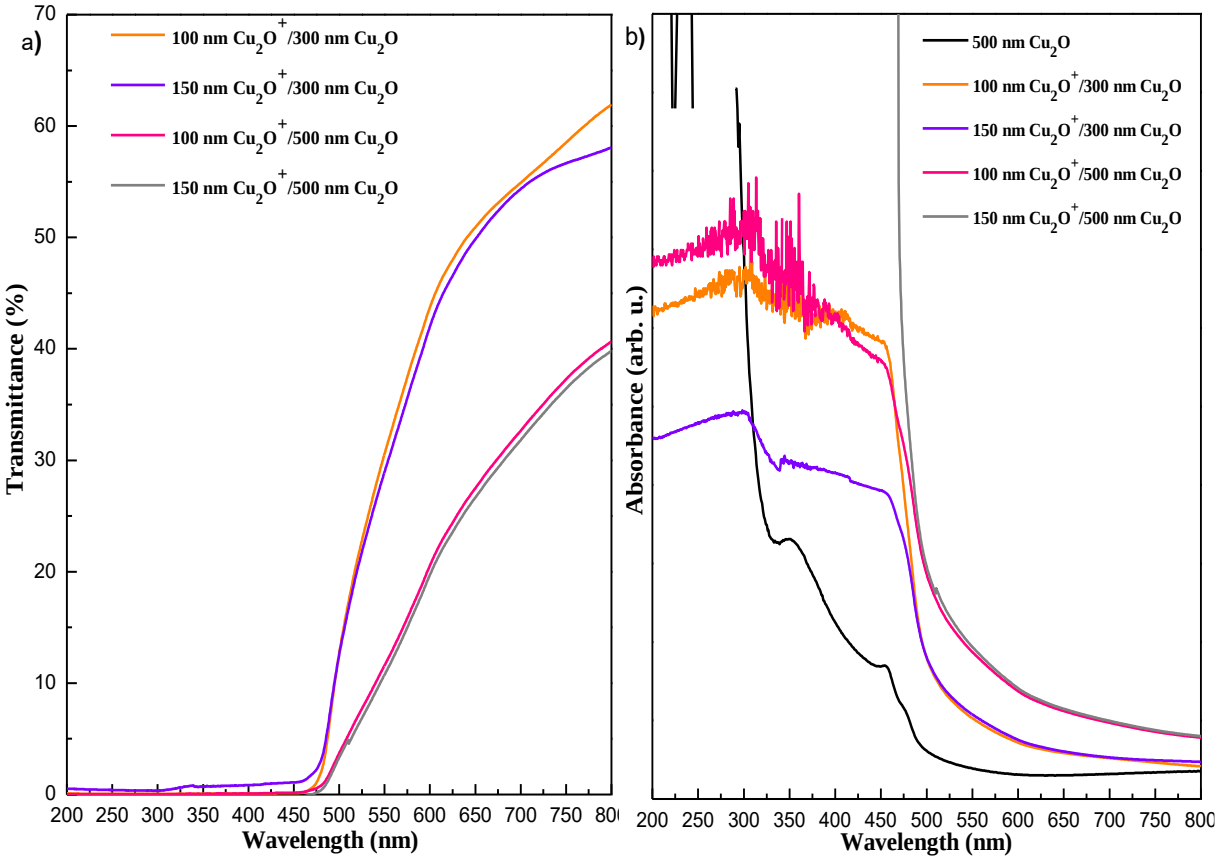

Fig. 5.4. a) *UV-vis transmittance spectras of Cu_2O^+/Cu_2O structures with different thickness of Cu_2O (300 and 500nm) and Cu_2O^+ (100 and 150 nm).* ***b)*** *UV–vis absorbance spectras of the respective samples plus 500 nm Cu_2O layer.*

In order to find the effect of Cu_2O and Cu_2O^+ layers thickness on the absorption edge, the optical band gap energies of our samples were determined using Tauc relation [10]:

$$(\alpha h\nu)^2 = A(h\nu - E_g) \qquad (5.2)$$

where α is the absorption coefficient and hν is the photon energy, A is a constant, Eg is the band gap energy of the material. Accordingly, the optical band gap can be obtained by extrapolating the corresponding straight lines downwards to the photon energy axis in the Tauc plot [11].

Figure 5.5 presents the Tauc's plots of Cu_2O^+/Cu_2O structures with a different thickness of Cu_2O and Cu_2O^+. All the samples revealed a large bandgap energy, for Cu_2O^+/Cu_2O structures with 300 nm Cu_2O layer, the Eg values were 2.47 and 2.45 eV for 100 and 150 nm Cu_2O^+ layer, respectively. Those values are intermediate, larger than that of 300 nm Cu_2O layer (2.20 eV) and lower than that of Cu_2O^+ (2.50 eV; reported in chapter 4). On the other hand, Cu_2O^+/Cu_2O structures with 500 nm Cu_2O layer shows Eg values of 2.38 and 2.36 eV for 100 and 150 nm of Cu_2O^+ layer, respectively. These values are larger than that of 500 nm Cu_2O layer (2.30 eV) and lower than that of Cu_2O^+ (2.50 eV). Therefore, the Cu_2O^+/Cu_2O structure with high Cu_2O thickness has a larger absorbance in the visible region.

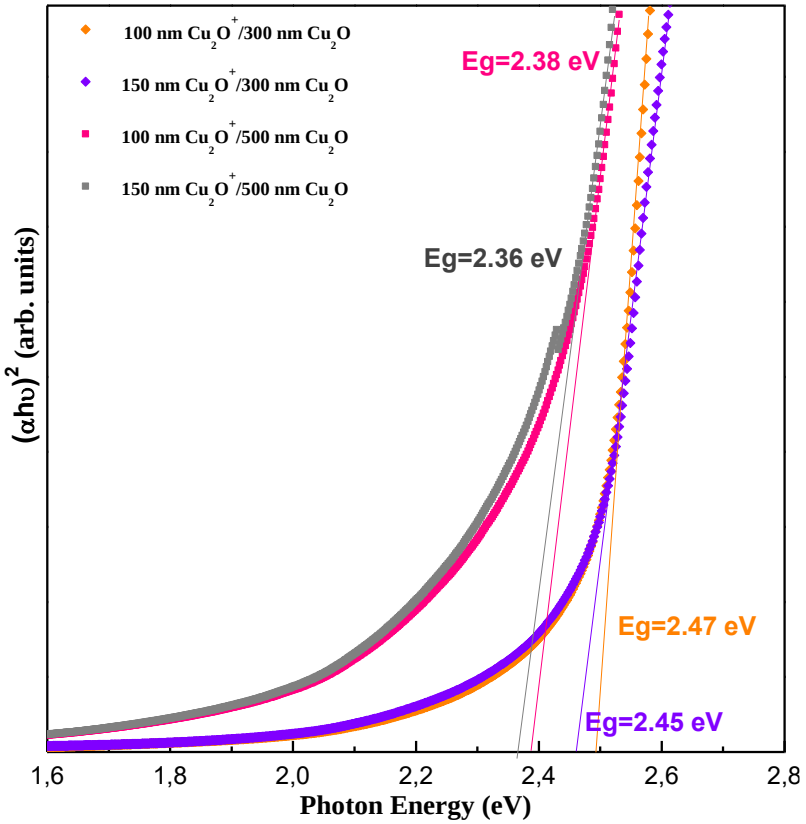

Fig. 5.5. *Tauc's plot of Cu_2O^+/Cu_2O structures with different thickness of Cu_2O (300 and 500 nm) and Cu_2O^+ (100 and 150 nm).*

The optical properties of the Cu_2O^+/Cu_2O/ZnO heterojunctions will be investigated in the following section. The UV-Vis transmittance and absorbance spectra of Cu_2O^+/Cu_2O/ZnO heterojunctions with different thickness of Cu_2O (300 and 500 nm) and Cu_2O^+ (100 and 150 nm) layers, recorded in a wavelength range from 200 to 1100 nm, are presented in figure 5.6. It can be seen from fig. 5.6a that Cu_2O^+/Cu_2O/ZnO heterojunctions with 300 nm Cu_2O have high transmittance of 56 and 60 % for 100 and 150 nm Cu_2O^+, respectively. While the Cu_2O^+/Cu_2O/ZnO heterojunctions with 500 nm Cu_2O show low transmittance of 22 and 28% for 100 and 150 nm Cu_2O^+, respectively. Those values are lower than that of Cu_2O^+/Cu_2O structures reported earlier (fig. 5.4a). Which is due to the difference in the conductivity between ZnO and FTO. Baek et al. reported that the conductivity of the working electrode determines the electrical and crystallographic properties of the Cu_2O layers [12]. The comparison of chronocoulometry curves (Q vs. t) confirmed that the deposition of Cu_2O was faster on FTO substrate (not shown here), due to the high resistivity of the ZnO layer compared to FTO substrate. Thus, the Cu_2O^+/Cu_2O structures deposited on FTO have high crystallinity (DRX patterns not shown here), as a result, better optical properties than Cu_2O^+/Cu_2O deposited on ZnO.

The $Cu_2O^+/Cu_2O/ZnO$ heterojunctions present a large absorption peak extends from the UV to the visible region, as illustrated in figure 5.6a. This may be ascribed to the combination of the narrow bandgap of Cu_2O (approximately 2.17 eV) and the wide band gap of ZnO (approximately 3.37 eV) [13]. In addition, the absorption edge shifted from 500 to 600 nm with increasing the Cu_2O thickness from 300 to 500 nm. It is well established that the high absorption in the visible range is important for Cu_2O^+/Cu_2O structures as an absorber layer in $Cu_2O^+/Cu_2O/ZnO$ heterojunction.

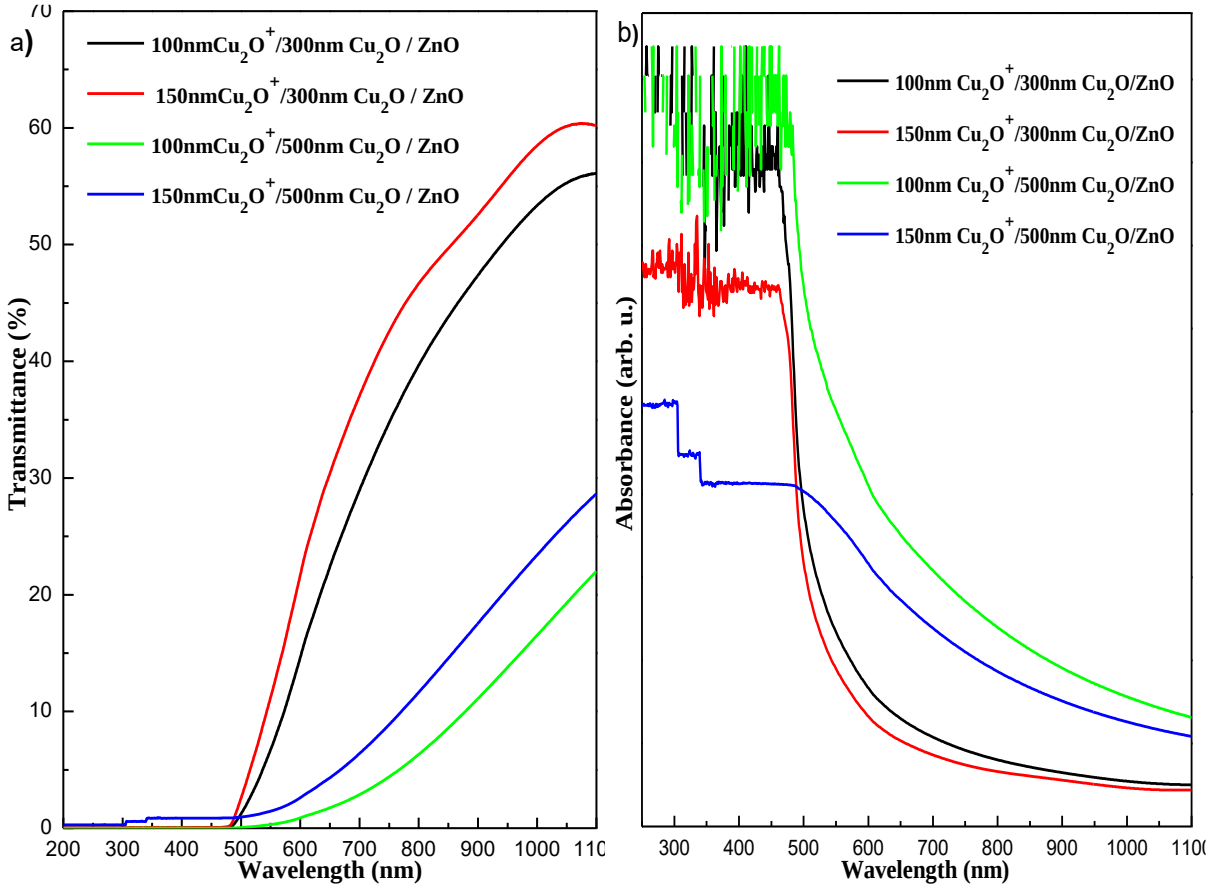

Fig. 5.6. a) *UV-vis transmittance spectras of $Cu_2O^+/Cu_2O/ZnO$ heterojunctions with different thickness of Cu_2O (300 and 500 nm) and Cu_2O^+ (100 and 150 nm).* ***b)*** *UV–vis absorbance spectras of the respective samples.*

The optical band gap energies of $Cu_2O^+/Cu_2O/ZnO$ heterojunctions were estimated from the plot of Tauc relation (eq. 5.2) by extrapolating the straight lines in Tauc's plot as explained in the previous section. Figure 5.7 presents the Tauc's plots of $Cu_2O^+/Cu_2O/ZnO$ structures with a different thickness of Cu_2O (300 and 500 nm) and Cu_2O^+ (100 and 150 nm). The obtained values of the band gap energies of $Cu_2O^+/Cu_2O/ZnO$ heterojunctions with 300 nm Cu_2O were 2.45 and 2.46 eV for 100 and 150 nm Cu_2O^+, respectively. Whereas, $Cu_2O^+/Cu_2O/ZnO$

heterojunctions with 300 nm Cu_2O show lower band gap energies of 2.38 and 2.24 eV for 100 and 150 nm Cu_2O^+, respectively.

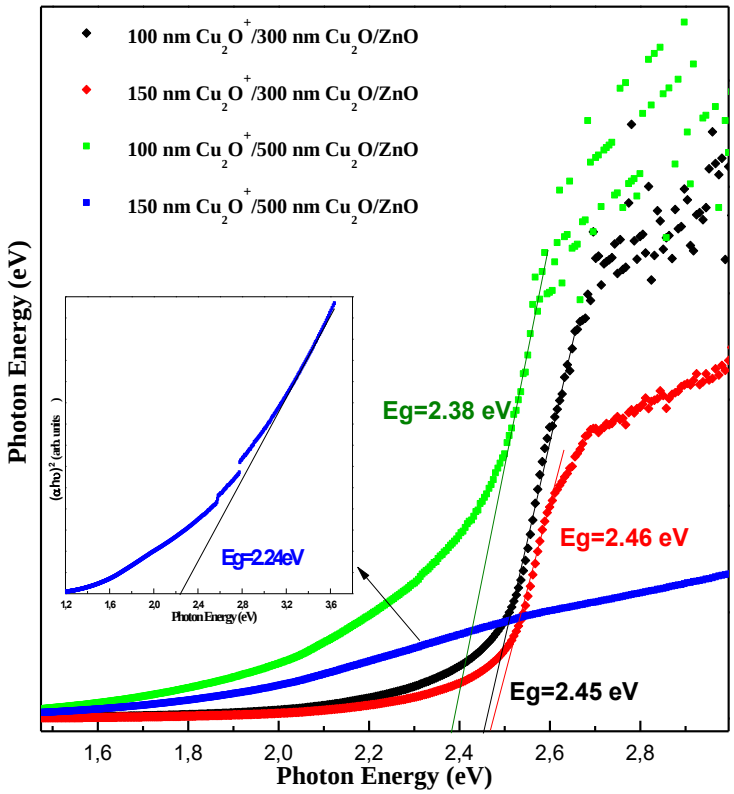

Fig. 5.7. *Tauc's plot of $Cu_2O^+/Cu_2O/ZnO$ heterojunctions with different thickness of Cu_2O (300 and 500 nm) and Cu_2O^+ (100 and 150 nm).*

5.3.4 Electrical characterization

The performance of the deposited heterojunctions was investigated by current-voltage measurements. Figure 5.8 presents the I-V curves recorded in the dark for $Au/Cu_2O^+/Cu_2O/ZnO/FTO$ device with a different thickness of Cu_2O (300 and 500 nm) and Cu_2O^+ (100 and 150 nm).

As can be seen from figure 5.8a-b, for $Cu_2O^+/Cu_2O/ZnO$ heterojunctions with 300 nm Cu_2O, increasing the thickness of Cu_2O^+ layer from 100 to 150 nm improved significantly the device performance. A near perfect response with a low leakage current of -0.9×10^{-7}A at a reverse bias of - 0.6 V was obtained for 150 nm Cu_2O^+ layer (Fig. 5.8b). Comparable results were observed for the $Cu_2O^+/Cu_2O/ZnO$ heterojunctions with 500 nm Cu_2O. Where increasing the thickness of Cu_2O^+ layer from 100 to 150 nm improved considerably the device performance as shown in figure 5.8c-d. Therefore, 150 nm of Cu_2O^+ layer shows better performance for $Cu_2O^+/Cu_2O/ZnO$ heterojunctions with 300 or 500 nm of the Cu_2O layer. Comparing the I-V

curves of this two heterojunctions (Fig. 5.8b,c), it is clear that reveals that 150 nm Cu_2O^+/300 nm Cu_2O/ZnO device shows the best performance, with built-in-potential of 0.64 V.

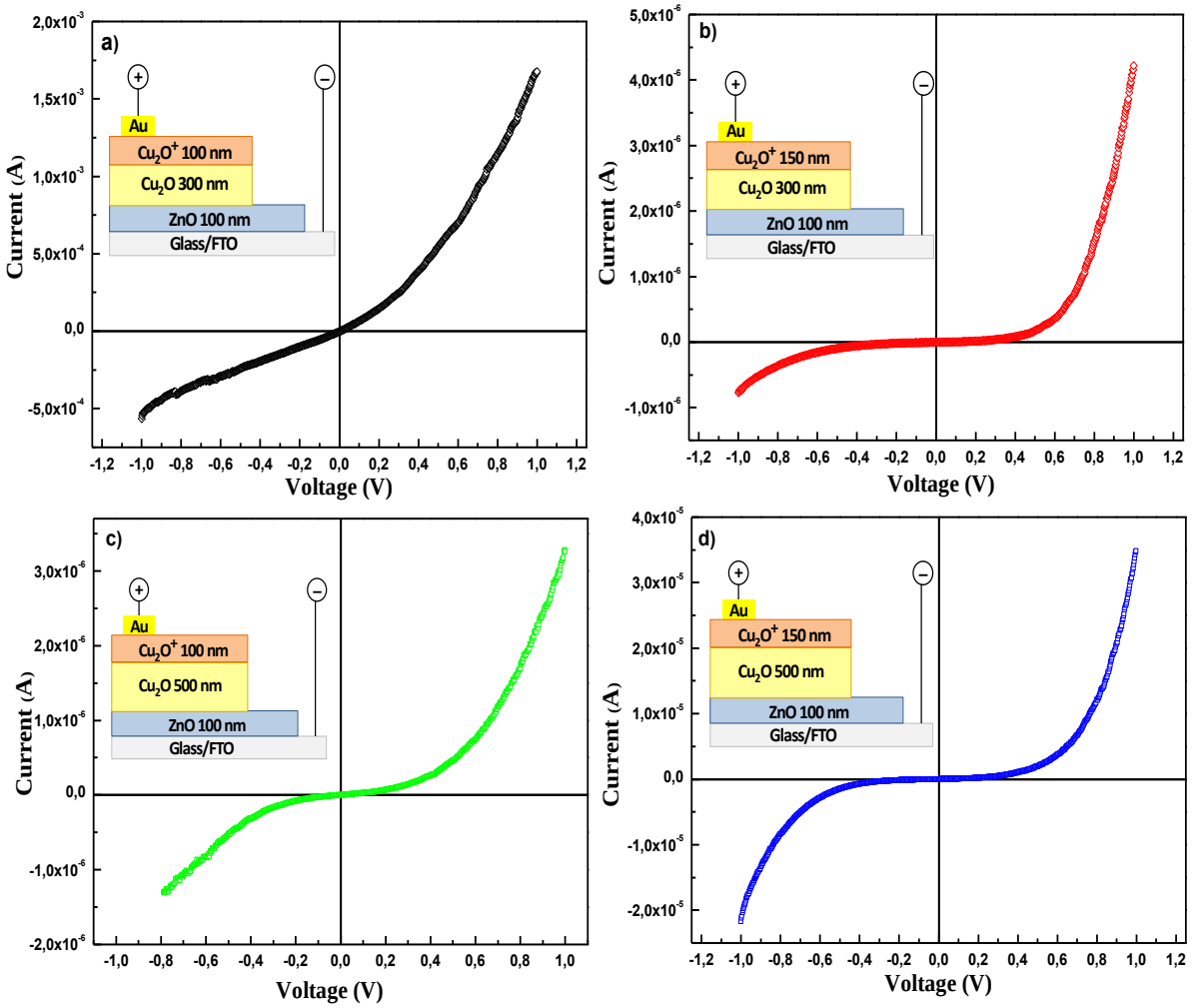

Fig. 5.8. *Current–voltage measurements of:* ***a)*** *100 nm Cu_2O^+/300 nm Cu_2O/ZnO,* ***b)*** *150 nm Cu_2O^+/300 nm Cu_2O/ZnO,* ***c)*** *100 nm Cu_2O^+/500 nm Cu_2O/ZnO and* ***d)****150 nm Cu_2O^+/500 nm Cu_2O/ZnO heterojunctions deposited on FTO.*

Based on Anderson model [14], the energy band diagrams of Cu_2O^+/Cu_2O/ZnO heterojunctions with 150 nm Cu_2O^+ layer were constructed. The conduction band offset (ΔE_c) and the valence band offset (ΔE_v) of the heterojunction are calculated using the following equation:

$$\Delta E_c = \chi_2 - \chi_1 \quad (4.5)$$

$$\Delta E_v = Eg_2 - Eg_1 + \Delta E_c \quad (4.6)$$

The electron affinity (χ) values of ZnO and Cu_2O are 4.2 and 3.2 eV, respectively [15, 16]. The band gap energy of Cu_2O layer did not change with increasing the layer thickness from 300 to

500 nm. Thus, we used the Eg values of Cu_2O^+/Cu_2O structures (Fig.5.5), instead of the Eg of the individual layers.

Figure 5.9 shows the energy band diagrams of 150 nm Cu_2O^+/Cu_2O/100 nm ZnO heterojunctions with 300 and 500 nm of Cu_2O layer.

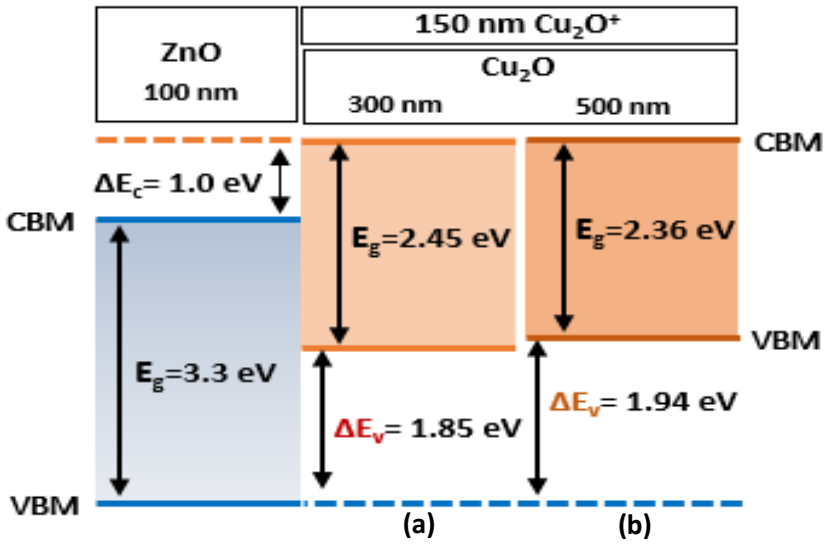

Fig. 5.9. *Band diagrams of 150 nm Cu_2O^+/Cu_2O/100 nm ZnO heterojunctions with* ***a)*** *300 nm Cu_2O (pH 11),* ***b)*** *500 nm Cu_2O (pH 11). For the simplicity, the two Cu_2O/ZnO heterojunctions were drown with one ZnO in the left side.*

The calculated conduction band offset (ΔE_c) was 1.0 eV for the two samples. While the valence band offset (ΔE_v) increased from 1.85 to 1.94 eV with increasing Cu_2O layer thickness from 300 to 500 nm (Fig. 5.9a-b). This confirms that the transport of electrons between the p-Cu_2O^+ and the n-ZnO layers is easier for Cu_2O^+/Cu_2O/ZnO device with 300 nm Cu_2O layer. Which explains the high performance of this device compared to the other samples (Fig. 5.8).

5.4 Conclusion

In this Chapter, Cu_2O^+/Cu_2O/ZnO heterojunction was prepared by simple potentiostatic electrochemical deposition under optimal conditions. In this structure, the Cu_2O layer (pH 11) was coated by Cu_2O^+ layer (of a carrier concentration two orders higher than Cu_2O) deposited from strongly alkaline solution (pH 12). The effect of Cu_2O and Cu_2O^+ layers thickness on the structural, morphological, optical and electrical properties of the heterojunction was studied. The structural characterization confirms high crystallinity for Cu_2O^+/Cu_2O/ZnO heterojunctions following cubic (111) and wurtzite (101) structures, respectively. The cross-section FE-SEM images indicate the formation of a flat and continuous layer of Cu_2O^+ onto the pyramidal shaped grain of Cu_2O layer. High optical transmittance was noted for

$Cu_2O^+/Cu_2O/ZnO$ with a low thickness of Cu_2O layer (300 nm). The current-voltage (I–V) curves confirm the formation of the junction in all samples. The best response was noted for $Cu_2O^+/Cu_2O/ZnO$ heterojunction with 150 nm Cu_2O^+ and 300 nm Cu_2O due to the low band valence offset (ΔE_v) in this device.

References

[1] T. Gershon, K .P. Musselman, A. Marin, R. H. Friend, J. L. MacManus-Driscoll, *Sol. Energ. Mater. Sol. Cells,* **96** (2012) 148.

[2] K. P. Musselman , A. Marin , L. Schmidt-Mende , J. L. MacManus-Driscoll , *Adv. Funct. Mater.*, **22** (2012) 2202.

[3]Y. Liu , H. K. Turley , J. R. Tumbleston , E. T. Samulski , R. Lopez , *Appl. Phys. Lett.*, **98** (2011) 162105.

[4] T. Shinagawa, M. Onoda, B. M Fariza, J. Sasano, M. Izaki, *J. Mater. Chem. A*, **1** (2013) 9182.

[5] K. P. Musselman, A. Wisnet, D.C. Iza, H. C. Hesse, C. Scheu, J. L. MacManus-Driscoll, L. Schmidt-Mende, *Adv. Mater.* **22** (2010) E254.

[6] Y. Liu, H. K. Turley, J. R. Tumbleston, E. T. Samulski, R. Lopez, *Appl. Phys. Lett.* **98** (2011) 162105.

[7] A.T Marin, D. Munoz-Rojas, D. C. Iza, T. Gershon, K. P. Musselman, J. L. MacManus-Driscoll *Adv. Functional Mater.*, **23** (2013) 3413.

[8] B. D. Cullity, *Elements of X-ray Diffraction*, 2nd edition (1978)

[9] D. Zhang, Y. Liu, Y. Liu, H. Yang, *Phys. B: Condens. Matter.*, **351** (2004) 178.

[10] S. Hussain, C. Cao, G. Nabi, W. S. Khan, Z. Usman, T. Mahmood, *Electrochim. Acta,* **56** (2011) 8342.

[11] J. Tauc, Optical Properties of Solids, Course 22, in: F. Abeles (Ed.), North Holland Pub, Amsterdam, 1970.

[12] S. K. Baek, J. H. Shin, S. W. Cho, H. K. Cho, *J Vacuum Sci: Tech.,* **B 33** (2015) 02B104.

[13] X. Jiang, Q. Lin, M. Zhang, G. He, Z. Sun, *Nanoscale Research Lett.,* **10** (2015) 30.

[15] A. G. Milnes and D. L. Feucht, "*Heterojunctions and Metal-Semiconductor Junctions*", *Academic*, New York, 1972.

[16] W. Siripala, A. Ivanovskaya, T. F. Jaramillo, S. H. Baeck, E.W. McFarland, *Sol. Energ. Mater. Sol. Cells*, **77** (2003) 229.

[17] H. Kobayashi, H. Mori, T. Ishida, Y. Nakato, *J. Appl. Phys.* **77** (1995) 1301.

General conclusion

The present thesis was designed to study the Cu_2O/ZnO heterojunction photovoltaic device fabricated by electrochemical deposition. The main goal was to improve the performance of the electrodeposited Cu_2O/ZnO heterojunction device by applying many strategies, such as the insertion of ZnO buffer layer, adjusting the pH of Cu_2O deposition bath and engineering a back surface field architecture. The major findings of this research are summarized below.

In chapter 2, the Cu_2O/ZnO and Cu_2O/Al:ZnO (AZO) devices were prepared by two steps electrodeposition, on FTO substrates, to investigate the effect of the window layer (ZnO, AZO) on the device performance. The electrochemical, structural, morphological, optical and electrical characterizations were carried out by Mott–Schottky measurement, field emission scanning electron microscope (FE-SEM), X-ray diffraction (XRD), UV–Vis analysis. The Cu_2O/AZO heterojunction shows high crystallinity following cubic (111) and wurtzite (101) structures and large crystallite sizes of 67.7 nm and 72.2 nm for AZO and Cu_2O, respectively. Moreover, a dense film of pyramidal shaped Cu_2O grins was covering the continuous and flat layer of AZO. In addition, the optical transmission of the device reached 70 % in the visible region. However, the performance of Cu_2O/AZO device was lower than that of Cu_2O/ZnO device. Due to the high mismatch between AZO and Cu_2O that creates more recombination sites at the interface of p-Cu_2O/n-AZO heterojunction. Thus, the interface of this device needs more improvement.

In chapter 3, we investigated the effect of the insertion of ZnO buffer layer on the performance of the electrodeposited Cu_2O/AZO device. The ZnO layer of different thickness was deposited between Cu_2O and AZO layers to reduce the recombination sites in the interface of Cu_2O/AZO. The electrochemical, structural, morphological, optical and electrical characterizations were performed by Mott–Schottky (M-S) and electrochemical impedance spectroscopy (EIS) measurements, field emission scanning electron microscope (FE-SEM), X-ray diffraction (XRD) and UV–Vis analysis. We have found that ZnO conductivity increases with increasing ZnO layer thickness from 50 to 200 nm. In addition, the insertion of 200 nm ZnO buffer layer between Cu_2O and AZO layers (Cu_2O/200 nm ZnO/AZO heterojunction) tuned the band alignment between AZO and Cu_2O layers. In this new device, the band offsets become smoother, which facilitate the electrons passage. Thus, the performance of Cu_2O/AZO was greatly improved by the insertion of ZnO buffer layer (200 nm).

In order to improve the absorber layer (Cu_2O) properties, in chapter 4, we deposited Cu_2O layer from a strongly alkaline solution of two different pH values and for different thickness. The effect of the bath pH on the electrical, structural and optical properties of Cu_2O was investigated by M-S and photocurrent measurements, X-ray diffraction and UV–Vis analysis. Increasing the pH to 12 enhanced the carrier concentration and improved the photo-response of Cu_2O layer. Moreover, a high-quality Cu_2O layer of the cubic structure following (111) orientation with large crystallite size was obtained at this pH. Then, those Cu_2O layers were used as an absorber layer in Cu_2O/ZnO heterojunction. The effect of Cu_2O layer properties on the structural, morphological, optical and electrical properties of Cu_2O/ZnO heterojunction was carefully examined. The Cu_2O/ZnO heterojunction with 500 nm Cu_2O deposited at pH 12 shows good crystallinity following the cubic (111) and the wurtzite (101) structures, respectively. Moreover, the formation of a textured film of Cu_2O pyramidal grains deposited on continuous flat ZnO was confirmed by the cross-section FE-SEM images. Therefore, this device gives the best performance due to the low valence band offset of 1.8 eV.

In chapter 5, the Cu_2O^+/Cu_2O/ZnO device was prepared by three steps electrodeposition to improve the light absorbance and carrier collection length. To construct this device, the Cu_2O layer was coated with thin Cu_2O^+ layer (of carrier concentration two orders higher than Cu_2O) deposited from strong alkaline solution (pH 12). The ZnO thickness was fixed at 100 nm for all samples, while a different thickness of Cu_2O (300 and 500 nm) and Cu_2O^+ (100 and 150 nm) was employed. The effect of Cu_2O and Cu_2O^+ layers thickness on the structural, morphological, optical and electrical properties of the heterojunction was studied in details. Overall, the deposition of the Cu_2O^+ layer on Cu_2O layer tuned the absorption and improved the morphology of the absorber layer especially the 150 nm Cu_2O^+/300 nm Cu_2O structure that reveals a high band gap energy of 2.45 eV. Consequently, 150 nm Cu_2O^+/300 nm Cu_2O/ZnO heterojunction shows high crystallinity and large absorption in the visible region. The cross-section FE-SEM images indicate the formation of a flat and continuous layer of Cu_2O^+ onto the pyramidal shaped grain of Cu_2O layer and the I-V measurements confirmed the best performance to this device due to the low band valence offset (ΔE_v) between 150 nm Cu_2O^+/300 nm Cu_2O structure and ZnO layer.

In this work, the Cu_2O/ZnO device was deposited by two steps electrochemical deposition and we attempted various strategies to improve

the Cu_2O/ZnO heterointerface properties. These approaches can be used to improve photovoltaic devices based on other materials combination such as Cu_2O/ZnS or Cu_2O/TiO_2.

RESUME

Dans la société moderne, la consommation d'énergie augmente énormément année par année, en raison des exigences de confort et de la croissance de la population mondiale et de l'économie. Les sources conventionnelles d'énergie ont malheureusement des problèmes, à savoir la disponibilité et la pollution. Par conséquent, nous devons développer et utiliser des ressources énergétiques alternatives, en particulier notre ressource naturelle énorme, le soleil. Puisque l'énergie solaire est illimitée, la conversion directe de l'énergie solaire en énergie électrique à l'aide de dispositifs photovoltaïques est considérée comme une solution idéale à la demande croissante de l'alimentation énergétique.

Récemment, il y a eu un intérêt croissant pour des cellules solaires composé de matériaux à faible coût, non toxique, abondant en terre comme une énergie propre alternative. Les hétérojonctions à base de semi-conducteurs nanostructurés, constituées de deux ou plusieurs composants, ont attiré une attention considérable à cause de leurs nombreuses applications optoélectroniques telles que les lasers, les photo-détecteurs et les cellules solaires. Le choix des matériaux ayant des propriétés proportionnées est un paramètre primordial pour obtenir une excellente performance de ces structures. Jusqu'à présent, l'oxyde de zinc (ZnO) et l'oxyde de cuivre (Cu_2O) sont considérés comme des candidats très intéressants, car ils ont les qualités précédemment mentionnées, en plus des propriétés optiques et électroniques exceptionnelles. En effet, la jonction de Cu_2O (type-p) avec le ZnO (type-n) a été fabriquée et a présenté une excellente performance dans les applications photovoltaïques. Une étude récente, a comparé plusieurs hétérojonctions TCO-Cu_2O, où plusieurs semi-conducteurs de type-n, tels que, In_2O_3, ZnO, In_2O_3:Sn (ITO), ZnO:Al (AZO) ont été déposés par Laser pulsé (DLP) sur une couche de Cu_2O, il a été confirmé alors que l'hétérojonction ZnO/Cu_2O présente la meilleure propriété photovoltaïque. Dans cette hétérojonction, le n-ZnO agit comme un transporteur des électrons et une couche fenêtre, en raison de sa grande mobilité électronique, large bande interdite de 3.3 eV et sa transparence optique dans la région visible. D'autre part, le Cu_2O, qu'est l'un des quelques oxydes qui montre naturellement la conductivité du type-p, agit comme une couche absorbante de cellule solaire grâce à son grand coefficient d'absorption optique (10^5 cm^{-1}) dans la région visible, sa bande interdite de 2.1 eV et une longueur de diffusion du porteur minoritaire appropriée.

L'efficacité de conversion la plus élevée rapportée à ce jour était de 8,1% pour un dispositif de MgF_2/ZnO:Al/$Zn_{0.38}Ge_{0.62}O$/Cu_2O:Na déposé sous vide par laser pulsé (DLP).

Cependant, cette efficacité est faible par rapport à la valeur théorique ; qui est principalement due à la mauvaise qualité de l'interface ZnO/Cu_2O et au faible transport des porteurs minoritaires. Ainsi, pour améliorer la performance de l'hétérojonction ZnO/Cu_2O, il est nécessaire de surmonter ces deux défis. Plusieurs méthodes ont été utilisées comme solutions pour ces problèmes, tels que la sensibilisation au colorant, le dopage et l'ingénierie de l'heterostructure.

Les méthodes les plus couramment utilisées pour déposer l'hétérojonction Cu_2O/ZnO n'étaient pas seulement compliquées et impliquent un traitement couteux mais utilisent également des températures élevées. Il est bien connu que interface métal/semi-conducteur est très réactif et instable au stade initial de la déposition à haute température. Ainsi, l'interface des hétérojonctions ZnO/Cu_2O déposées à haute température est riche en cuivre métallique, ce qui réduire la performance. Par conséquence, il est important de choisir une méthode de déposition de faible coût et d'un procédé simple pour former une interface de haute qualité. L'électrodéposition est une procédure de fabrication à faible coût et à basse température, qui offre un contrôle direct de l'épaisseur du film, la simplicité du processus et le potentiel de production à grande échelle. Malgré ce grand spectre des avantages, il existe peu de rapports sur les hétérojonctions de ZnO/Cu_2O déposé entièrement par electrodeposition.

Dans cette recherche de doctorat, nous nous concentrons sur l'amélioration de la performance du Cu_2O/ZnO formé par dépôt électrochimique. Afin d'atteindre cet objectif, nous avons mis en œuvre de nombreuses stratégies ; Dans un premier temps, nous avons utilisé deux couches fenêtres différentes (ZnO et Al dopées ZnO (AZO)), où les hétérojonctions Cu_2O/ZnO et Cu_2O/Al:ZnO ont été déposées sur FTO dans des conditions optimales de par deux étapes d'électrodéposition. Les propriétés structurelles, optiques, morphologiques et électriques des deux jonctions ont été étudiées en détail. Le dispositif Cu_2O/ZnO présente de meilleure performance que l'hétérojonction Cu_2O/AZO en raison du fort désaccord entre AZO et Cu_2O qui crée plus de sites de recombinaison dans l'interface de l'hétérojonction p-Cu_2O/n-AZO.

Deuxièmement, nous avons élargi la recherche sur l'hétérojonction Cu_2O/AZO, nous avons introduit une couche tampon ZnO de différente épaisseur entre la couche de Cu_2O et celle d'AZO pour l'ingénierie de l'heterointerface. L'hétérojonction Cu_2O/ZnO/AZO a été formée par électrodéposition en trois étapes. Nous avons démontré que la performance de l'hétérojonction Cu_2O/ZnO/AZO est améliorée en augmentant l'épaisseur de ZnO. La meilleure performance a été obtenue pour une couche tampon ZnO de 200 nm comme épaisseur optimale. Cette couche

tampon diminue le décalage de bande entre les couches AZO et Cu_2O, ce qui facilite le transport des électrons dans la jonction.

Troisièmement, nous avons optimisé les propriétés du Cu_2O en augmentant le pH de deposition pour améliorer le transport de porteurs de charges dans la couche absorbante. Le Cu_2O a été déposé à partir d'une solution fortement alcaline de deux valeurs de pH différentes et d'épaisseur différente. La modification du pH de deposition a augmenté la concentration du porteur et a amélioré la photo-réponse de la couche du Cu_2O. L'effet des propriétés de la couche du Cu_2O sur les propriétés structurelles, morphologiques, optiques et électriques de l'hétérojonction Cu_2O/ZnO a été soigneusement examiné. L'hétérojonction Cu_2O/ZnO avec 500 nm de Cu_2O déposée à pH 12 montre la meilleure performance due au faible décalage de bande de valence de 1,8 eV dans ce dispositif.

Enfin, nous avons appliqué l'architecture du champ de surface arrière pour améliorer l'absorbance de la lumière et la longueur de collection du porteurs. Le dispositif Cu_2O^+/Cu_2O/ZnO a été préparé par électrodéposition en trois étapes, où la couche Cu_2O a été revêtue d'une fine couche de Cu_2O^+ (d'une concentration de porteurs supérieure, de deux orders, à Cu_2O) déposée à partir d'une solution fortement alcaline (pH 12). L'effet de l'épaisseur des couches Cu_2O et Cu_2O^+ sur les propriétés structurelles, morphologiques, optiques et électriques de l'hétérojonction a été étudié en détail. Nous avons confirmé que le dépôt de la couche de Cu_2O^+ sur la couche de Cu_2O améliorait l'absorption et la morphologie de la couche absorbante, en particulier la structure 150 nm Cu_2O^+/300 nm Cu_2O. De plus, le dispositif Cu_2O^+/Cu_2O/ZnO avec une structure de 150 nm Cu_2O^+/300 nm Cu_2O, en tant qu'absorbeur, présente la meilleure performance, en raison du faible décalage de bande de valence (ΔE_v) entre la structure 150 nm Cu_2O^+ /300 nm Cu_2O et la couche de ZnO.

Les résultats de cette étude fournissent de nombreuses stratégies pour améliorer les performances des dispositifs photovoltaïques ZnO/Cu_2O préparés par dépôt électrochimique.

الملخص

في بحث الدكتوراه هذا، نركز على تحسين أداء Cu_2O / ZnO التي تشكلت بالترسيب الكهروكيميائي وذلك بتنفيذ العديد من الاستراتيجيات مثل ادراج طبقة عازلة من ZnO و تحسين خصائص Cu_2O عن طريق زيادة درجة حموضة الترسيب وتطبيق بنية حقل السطح الخلفي.

في البداية استخدمنا طبقتين نافذتين مختلفتين (ZnO (AZO) ملدن ZnO et Al) حيث Cu_2O/ZnO et Cu_2O/Al:ZnO رسبت على FTO في ظل شروط أفضل بطريقة الترسيب الكهروالكتروني في مرحلتين. تمت دراسة الخصائص الهيكلية والبصرية والمورفولوجية والكهربائية لمتماثل القطبين بالتفصيل. التركيب Cu_2O/ZnO يعرض كفاءة أفضل Cu_2O / AZO بسبب الخلاف القوي بين Cu_2O AZO مما يخلق المزيد من مواقع إعادة التركيب في واجهة p- Cu_2O/n-AZO.

ثانيا، لقد قمنا بتوسيع نطاق البحث على Cu_2O/AZO، قدمنا طبقة عازلة ZnO ذات سماكة مختلفة بين طبقة Cu_2O وطبقة AZO للهندسة من متغاير الواجهة. Cu_2O/ZnO/AZO يشكل على طريقة الترسيب الكهروالكتروني من ثلاث مراحل. لقد أثبتنا أنه تم تحسين أداء Cu_2O/ZnO/AZO بزيادة سماكة ZnO. تم الحصول على أفضل أداء لطبقة عازلة ZnOمن 200 نم كسماكة مثلى .هذه الطبقة العازلة تقلل من فجوة النطاق بين طبقات AZO وCu_2O ، مما يسهل نقل الإلكترونات في متماثل الاقطاب.

ثالثا، قمنا بتحسين خصائص Cu_2O عن طريق زيادة درجة حموضة الترسيب لتحسين نقل ناقلات الشحنة في الطبقة الماصة. تم ترسيب Cu_2O من محلول قلوي قوي من قيم pH مختلفة وسمك مختلف. أدى تعديل pH الترسيب الي زيادة تركيز الناقل وتحسين الاستجابة الضوئية لطبقة Cu_2O ، كما تم فحص تأثير خواص طبقة Cu_2O على الخواص التركيبية والمورفولوجية والضوئية والكهربائية بعناية كبيرة للخلية Cu_2O/ZnO. يُظهر Cu_2O/ZnO مع 500 نم للمركب Cu_2O المرسب في pH 12 أفضل أداء بسبب انخفاض فارق نطاق التكافؤ بمقدار 1.8 فولت في هذه الخلية.

وأخيرًا، طبقنا بنية حقل السطح الخلفي لتحسين امتصاص الضوء وطول فترة تجميع الموجات الحاملة. تم إعداد Cu_2O^+/Cu_2O/ZnO بواسطة الترسيب الكهروالكتروني في ثلاث مراحل ، حيث تم طلاء طبقة Cu_2O بطبقة رقيقة من Cu_2O^+ (من تركيز أعلى من الناقلين) المرسبة من محلول قلوي قوي (pH12). تأثير سماكة الطبقتين Cu_2O و Cu_2O^+ على الخصائص الهيكلية والمورفولوجية والبصرية والكهربائية تمت دراستها بالتفصيل .لقد أكدنا أن ترسب $Cu2O^+$ على طبقة Cu_2O تحسن امتصاص ومورفولوجية الطبقة الماصة، لا سيما بنية Cu_2O 300 nm/Cu_2O^+ 150nm. بالإضافة إلى ذلك، Cu_2O/ZnO/Cu_2O^+ مع بنية Cu_2O 300 nm/Cu_2O^+ 150 nm، كممتص، تُظهر أداء أفضل، نظرًا لانخفاض في نطاق التكافؤ (ΔEv) بين بنية Cu_2O 300nm/Cu_2O^+ بمقدار 150 nm وطبقة ZnO .

نتائج هذه الدراسة توفر العديد من الاستراتيجيات لتحسين أداء الأجهزة الكهروضوئية Cu_2O / ZnO التي أعدت بطريقة الترسيب الكهروكيميائية .

الكلمات المفتاحية: الترسيب الكهروكيميائي, Cu_2O/ZnO, متماثل القطبين, فرق نطاق التكافؤ

Abstract

The main goal of this thesis was to improve the performance of the electrodeposited Cu_2O/ZnO heterojunction device by applying many strategies, such as the insertion of ZnO buffer layer, adjusting the pH of Cu_2O deposition bath and engineering a back surface field architecture. At first, we deposited a p-Cu_2O layer on n-ZnO (or AZO) layer by two steps electrodeposition. The properties of Cu_2O/ZnO and Cu_2O/Al:ZnO heterojunctions were investigated and we confirmed a good performance for Cu_2O/ZnO device. To improve the performance for of this latter we deposited Cu_2O/ZnO/Al:ZnO device by inserting ZnO layer, with different thickness, between Al: ZnO and Cu_2O to enhance the mismatch and reduce the band offset. The device with 200nm ZnO show improvement of the performance compared to Cu_2O/ZnO and Cu_2O/Al: ZnO. Then, we improved the quality of Cu_2O by increasing the deposition pH values and used it as an absorber layer. The Cu_2O/ZnO heterojunction with 500 nm Cu_2O deposited at pH 12 shows the best performance due to the low valence band offset of 1.8 eV. Finally, we fabrication Cu_2O^+/Cu_2O/ZnO to enhance the light absorbance and the carrier collection length by the creation of back surface field devices. The 150 nm Cu_2O^+/300 nm Cu_2O/ZnO heterojunction shows the best performance due to the low band valence offset (ΔE_v) between 150 nm Cu_2O^+/300 nm Cu_2O structure and ZnO layer.

Keywords: Electrodeposition, ZnO/Cu_2O, heterojunctions, band offset

Résumé

L'objectif principal de cette thèse est d'améliorer la performance du dispositif d'hétérojonction Cu_2O/ZnO préparé par électrodéposition en appliquant de nombreuses stratégies, comme l'insertion d'une couche tampon de ZnO, l'ajustement du pH de déposition de Cu_2O et l'ingénierie d'une architecture de champ de surface arrière. Dans un premier temps, nous avons déposé une couche de p-Cu_2O sur une couche de n-ZnO (ou n-AZO) par électrodéposition en deux étapes. Les propriétés des hétérojonctions Cu_2O / ZnO et Cu_2O/Al: ZnO ont été étudiées et nous avons confirmé une bonne performance pour le dispositif Cu_2O/ ZnO. Pour améliorer la performance de ces derniers, nous avons déposé le dispositif Cu_2O/ ZnO/Al:ZnO en insérant une couche de ZnO, de différentes épaisseurs, entre Al:ZnO et Cu_2O pour améliorer la discordance et réduire le décalage de la bande. Le dispositif à 200 nm ZnO montre une amélioration de la performance par rapport à Cu_2O / ZnO et Cu_2O/Al:ZnO. Ensuite, nous avons amélioré la qualité de Cu_2O en augmentant les valeurs de pH de déposition, et l'avons utilisé comme une couche absorbante. L'hétérojonction Cu_2O/ZnO avec 500 nm de Cu_2O déposée à pH 12 montre la meilleure performance en raison du faible décalage de bande de valence de 1,8 eV. Enfin, nous avons déposé Cu_2O^+/Cu_2O/ZnO pour améliorer l'absorbance de la lumière et la longueur de collecte du porteur. L'hétérojonction 150 nm Cu_2O^+/300 nm Cu_2O/ZnO présente la meilleure performance du fait du faible décalage de bande de valence entre la structure150 nm Cu_2O^+/300 nm Cu_2O et la couche de ZnO.

Mots clés : Electrodéposition, ZnO/Cu_2O, Hétérojonctions, Décalage de Bande